

CORONA OF MAGNETARS

Andrei M. Beloborodov¹

Physics Department and Columbia Astrophysics Laboratory, Columbia University, 538 West 120th Street New York, NY 10027; amb@phys.columbia.edu

Christopher Thompson

Canadian Institute for Theoretical Astrophysics, University of Toronto, 60 St. George Street, Toronto, ON M5S 3H8, Canada; thompson@cita.utoronto.ca

ABSTRACT

We develop a theoretical model that explains the formation of hot coronae around strongly magnetized neutron stars — magnetars. The starquakes of a magnetar shear its external magnetic field, which becomes non-potential and is threaded by an electric current. Once twisted, the magnetosphere cannot untwist immediately because of its self-induction. The induced electric field lifts particles from the stellar surface, accelerates them, and initiates avalanches of pair creation in the magnetosphere. The created plasma corona maintains the electric current demanded by $\text{curl } \mathbf{B}$ and regulates the self-induction e.m.f. by screening. This corona persists in dynamic equilibrium: it is continually lost to the stellar surface on the light-crossing time $\sim 10^{-4}$ s and replenished with new particles. In essence, the twisted magnetosphere acts as an accelerator that converts the toroidal field energy to particle kinetic energy. Using a direct numerical experiment, we show that the corona self-organizes quickly (on a millisecond timescale) into a quasi-steady state, with voltage $e\Phi_e \sim 1$ GeV along the magnetic lines. The voltage is maintained near threshold for ignition of pair production, and pair production occurs at a rate just enough to feed the electric current. The heating rate of the corona is $\sim 10^{36} - 10^{37}$ erg/s, in agreement with the observed persistent, high-energy output of magnetars. We deduce that a static twist that is suddenly implanted into the magnetosphere will decay on a timescale of 1-10 yrs. The particles accelerated in the corona impact the solid crust, knock out protons, and regulate the column density of the hydrostatic atmosphere of the star. The transition layer between the atmosphere and the corona may be hot enough to create additional e^\pm pairs. This layer is the likely source of the observed 100 keV emission from magnetars. The corona emits curvature radiation above 10^{14} Hz and can supply the observed IR-optical luminosity. We outline the implications of our results for the non-thermal radiation in other bands, and for the post-burst evolution of magnetars.

¹Also at Astro-Space Center of Lebedev Physical Institute, Profsojuznaja 84/32, Moscow 117810, Russia

Subject headings: plasmas — stars: coronae, magnetic fields, neutron — X-rays: stars

1. INTRODUCTION

At least 10% of all neutron stars are born as magnetars, with magnetic fields $B > 10^{14}$ G. Their activity is powered by the decay of the ultrastrong field and lasts about 10^4 years. They are observed at this active stage as either Soft Gamma Repeaters (SGRs) or Anomalous X-ray Pulsars (AXPs) (see Woods & Thompson 2006 for a recent review). Twelve active magnetars are currently known, and all of them have similar parameters: spin period $P \sim 10$ s, persistent X-ray luminosity $L \sim 10^{35} - 10^{36}$ erg/s, and surface temperature $k_B T \sim 0.5$ keV. The large-scale (dipole) component of the magnetic field $B_{\text{dipole}} > 10^{14}$ G has been inferred from the measurement of rapid spindown in several AXPs, and more recently in two SGRs (Kouveliotou et al. 1998, 1999). However, there is evidence for even stronger magnetic field inside the star, as was originally deduced from considerations of magnetic field transport (Thompson & Duncan 1996). In particular, the occurrence of enormously energetic X-ray flares in SGRs points to internal magnetic fields approaching $\sim 10^{16}$ G (Hurley et al. 2005). Bursting activity has also been detected in two AXPs (Kaspi et al. 2003), which strongly supports the hypothesis that active rearrangement of the magnetic field takes place in AXPs as well as SGRs, although at differing rates.

Besides the sporadic X-ray outbursts, a second, persistent, form of activity has been discovered by studying the emission spectra of magnetars. Until recently, the spectrum was known to have a thermal component with temperature $k_B T \sim 0.5$ keV, interpreted as blackbody emission from the star’s surface. The soft X-ray spectrum also showed a tail at 2 – 10 keV with photon index $\Gamma = 2 - 3.5$. Intriguingly, the hardness of the 2 – 10 keV spectrum correlates with long-term activity as a transient burst source (Marsden & White 2001). This deviation from pure surface emission already suggested that energy is partially released above the star’s surface. Recently, observations by RXTE and INTEGRAL have revealed even more intriguing feature: magnetars are bright, persistent sources of 100 keV X-rays (Kuiper et al. 2004; Molkov et al. 2005; Mereghetti et al. 2005; den Hartog et al. 2006). This high-energy emission forms a separate component of the magnetar spectrum, distinct from the soft X-ray component that was known before. The new component becomes dominant above 10 keV, has a very hard spectrum, $\Gamma \simeq 1$, and peaks above 100 keV where the spectrum is unknown. The luminosity in this band, $L \sim 10^{36}$ erg s $^{-1}$, even exceeds the thermal luminosity from the star’s surface. These hard X-rays can be emitted only in the exterior of the star and demonstrate the presence of an active plasma corona.

Our goal in this paper is to understand the origin and composition of the magnetar corona. The starting point of our analysis is the fact that an evolving magnetar experiences strong deformations of its crust, due to a shifting configuration of the internal magnetic field. These “starquakes” shear the magnetic field that is anchored in the crust, thereby injecting an electric current into the stellar magnetosphere. This process bears some resemblance to the formation of current-carrying structures in the Solar corona, although there are important differences which shall be discussed

below. We investigate how the starquakes and twisting of the magnetosphere can lead to the formation of a plasma corona around a magnetar.

The persistence of magnetospheric twists can explain several observed properties of the AXPs and SGRs (Thompson, Lyutikov, & Kulkarni 2002; hereafter TLK). TLK investigated the observational consequences using a static, force-free model, idealizing the magnetosphere as a globally twisted dipole. They showed that the stellar radiation is significantly modified by multiple scattering off the current-carrying particles in the exterior of the star, which can explain the soft tail of the surface emission that is observed at $2 - 10$ keV. A twist also affects the spindown rate of the neutron star: it causes the poloidal field lines to flare out slightly from a pure dipole configuration, thereby increasing the braking torque acting on the star.

Our work is driven by two questions, which are closely related. First, how is the magnetosphere populated with plasma? The neutron star surface has a temperature $k_B T \lesssim 1$ keV and the scale-height of its atmospheric layer is only a few cm. How is the plasma supplied above this layer and what type of particles populate the corona? What are the typical energies of the particles? Second, electric currents in the corona are subject to dissipation and hence the twist of the magnetic field must decay with time. How quick is this decay? Does this decay imply the disappearance of corona?

Plasma near a neutron star is strongly constrained compared with many other forms of plasma encountered in laboratory and space, and therefore easier to model. The relative simplicity is due to the fact that the magnetic field is extremely strong and fixed — its evolution timescale is much longer than the residence time of particles in the corona. Furthermore, particles are at the lowest Landau level and move strictly along the magnetic field lines, which makes the problem effectively one-dimensional. Finally, the magnetic lines under consideration are closed, with both ends anchored in the highly conducting stellar material. As we explain in § 2, this leads to an essential simplification compared with the long-standing problem of plasma dynamics in radio pulsars.

In this paper we propose a mechanism for the formation of the corona and show that a simple solution exists for the plasma dynamics in the magnetosphere. An outline of the model is as follows. The key agent in corona formation is an electric field E_{\parallel} parallel to the magnetic field. E_{\parallel} is generated by the self-induction of the gradually decaying magnetic twist and measures the rate of the decay. It determines the rate of energy release in the corona via Joule dissipation.

A plasma corona cannot exist if $E_{\parallel} = 0$ — then the corona is not heated and, being in contact with the cool stellar surface, it will have to condense to a thin surface layer with $k_B T \lesssim 1$ keV. In addition, the magnetospheric electric current cannot flow upward against gravity unless a force eE_{\parallel} drives it. On the other hand, when E_{\parallel} exceeds a critical value, e^{\pm} avalanches are triggered in the magnetosphere, and the created pairs screen the electric field. This leads to a “bottleneck” for the decay of a magnetic twist, which implies a slow decay.

The maintenance of the corona and the slow decay of the magnetic twist are intimately related because both are governed by E_{\parallel} . In order to find E_{\parallel} , one can use Gauss’ law $\nabla \cdot \mathbf{E} = 4\pi\rho$, where

ρ is the net charge density of the coronal plasma. This constraint implies that \mathbf{E} and ρ must be found self-consistently. We formulate the problem of plasma dynamics in a twisted magnetic field and the self-consistent electric field, and investigate its basic properties. The problem turns out to be similar to the classical double-layer problem of plasma physics (Langmuir 1929) with a new essential ingredient: e^\pm pair creation.

We design a numerical experiment that simulates the behavior of the 1-D plasma in the magnetosphere. The experiment shows how the plasma and electric field self-organize to maintain the time-average magnetospheric current $\bar{\mathbf{j}}$ demanded by the magnetic field, $(4\pi/c)\bar{\mathbf{j}} = \nabla \times \mathbf{B}$. The electric current admits no steady state on short timescales and keeps fluctuating, producing e^\pm avalanches. This state may be described as a self-organized criticality. Pair creation is found to provide a robust mechanism for limiting the voltage along the magnetic lines to $e\Phi_e \lesssim 1$ GeV and regulate the observed luminosity of the corona.

The paper is organized as follows. We start with a qualitative description of the mechanism of corona formation, and show that it can be thought of as an electric-circuit problem (§ 2). A careful formulation of the circuit problem and the set up of numerical experiment are described in § 3. In § 4 we study the circuit without pair creation and find that it does not provide a self-consistent model. Pair creation is found to be inevitable and described in detail in § 5. In § 6 we discuss the transition region between the corona and the relatively cold surface layer of the star. The maintenance of a dense plasma layer on the stellar surface is addressed in § 7. Observational implications and further developments of the corona model are discussed in § 8.

2. MECHANISM OF CORONA FORMATION

2.1. Ejection of Magnetic Helicity from a Neutron Star

A tightly wound-up magnetic field is assumed to exist inside magnetars (e.g. Thompson & Duncan 2001). The internal toroidal field can be much stronger than the external large-scale dipole component.¹ The essence of magnetar activity is the transfer of magnetic helicity from the interior of the star to its exterior, where it dissipates. This involves rotational motions of the crust, which inevitably twist the external magnetosphere that is anchored to the stellar surface. The magnetosphere is probably twisted in a catastrophic way, when the internal magnetic field breaks the crust and rotates it. Such starquakes are associated with observed X-ray bursts (Thompson & Duncan 1995). The most interesting effect of a starquake for us here is the partial release of the winding of the internal magnetic field into the exterior, i.e., the injection of magnetic helicity into the magnetosphere.

¹Existing calculations of the relaxation to magnetostatic equilibrium in a fluid star (e.g., a nascent magnetar) assume that the initial toroidal and poloidal fluxes are comparable (Braithwaite & Spruit 2004). The initial toroidal flux can, in fact, be substantially stronger due to the presence of rapid differential rotation in the newly formed star.

Since the magnetic field is energetically dominant in the magnetosphere, it must relax there to a force-free configuration with $\mathbf{j} \times \mathbf{B} = 0$. The effective footpoints of the force-free field lines sit in the inner crust of the neutron star. At this depth currents may flow across the magnetic lines because the deep crust can sustain a significant Ampère force $\mathbf{j} \times \mathbf{B}/c \neq 0$: this force is balanced by elastic forces of the deformed crust. The ability of the crust to sustain $\mathbf{j} \nparallel \mathbf{B}$ quickly decreases toward the surface, and it is nearly force-free where² $\rho \lesssim 10^{13} B_{15}^{2.5} \text{ g/cm}^3$ (Thompson & Duncan 2001). The build-up of these stresses in the crust from an initial magnetostatic equilibrium has been studied recently by Braithwaite & Spruit (2006).

The ejection of helicity may be thought of as directing an interior current (which previously flowed across the field and applied a $\mathbf{j} \times \mathbf{B}/c$ force) into the force-free magnetosphere. The ejected current flows along the magnetic lines to the exterior of the star, reaches the top of the line and comes back to the star at the other footpoint. The electric circuit closes at the base of the force-free region. The currents emerging during the starquake may percolate through a network of fractures in the crust. Then large gradients in the field are initially present which can be quickly erased. A relatively smooth magnetospheric twist of scale $\sim R_{\text{NS}}$ will have the longest lifetime.

Globally twisted magnetic fields are observed to persist in the Solar corona over many Alfvén crossing times. Twisted magnetic configurations have also been studied in laboratory experiments. In particular, the toroidal pinch configuration has been studied in detail and is well explained as a relaxed plasma state in which the imparted magnetic helicity has been nearly conserved (Taylor 1986). The toroidal pinch relaxes to the minimum-energy state which has a uniform helicity density: $\nabla \times \mathbf{B} = \mu \mathbf{B}$ with $\mu = \text{const.}$ This state is achieved because the experiment has toroidal geometry and the current is isolated from an external conductor. The relaxation process is then free to redistribute the current between neighboring magnetic flux tubes via small-scale reconnection, which leads to a uniform μ . The geometry is different in the case of a magnetar (or the sun) — the field lines are anchored to the star and their configuration depends on the footpoint motion (for related calculations of the relaxed state of a driven plasma see, e.g., Tang & Boozer [2005]). The long lifetime ($\gtrsim 1$ year) of a twisted configuration around magnetars is supported by observations of long-lived changes in the spindown rate and X-ray pulse profiles (Woods & Thompson 2006; TLK) as well as persistent nonthermal X-ray emission.

The shape of a twisted force-free magnetosphere may be calculated given the boundary conditions at the footpoints. An illustrative model of a globally twisted dipole field was considered by TLK. It has one parameter — twist angle $\Delta\phi$ — and allows one to see the qualitative effects of increasing twist on the magnetic configuration. The current density in this configuration is

$$\mathbf{j}(r, \theta) = \frac{c}{4\pi} \nabla \times \mathbf{B} \simeq \frac{c\mathbf{B}}{4\pi r} \sin^2 \theta \Delta\phi \quad (r > R_{\text{NS}}), \quad (1)$$

where r, θ, ϕ are spherical coordinates with the polar axis chosen along the axis of the dipole. Even

²Throughout this paper we use the shorthand notation $X = X_n \times 10^n$, where quantity X is measured in c.g.s. units.

for strong twists, $\Delta\phi \sim 1$, the poloidal components B_r and B_θ are found to be close to the normal dipole configuration, although the magnetosphere is somewhat inflated. The main difference is the appearance of a toroidal field B_ϕ .

The emerging currents are easily maintained during the X-ray outburst accompanying a star-quake. A dense, thermalized plasma is then present in the magnetosphere, which easily conducts the current. Plasma remains suspended for some time after the starquake because of the transient thermal afterglow with a high blackbody temperature, up to ~ 4 keV. The cyclotron resonance of the ions is $\hbar e B / m_p c = 6.3 B_{15}$ keV and, during the afterglow, the radiative flux at the resonance is high enough to lift ions from the surface against the force of gravity (Ibrahim et al. 2001).

Eventually the afterglow extinguishes and the radiative flux becomes unable to support the plasma outside the star. The decreasing density then threatens the capability of the magnetosphere to conduct the current of the magnetic twist. A minimal “corotation” charge density $\rho_{co} = -\mathbf{\Omega} \cdot \mathbf{B} / 2\pi c$ is always maintained because of rotation of the star with frequency Ω (Goldreich & Julian 1969), but it is far smaller than the minimal density that is needed to supply the current \mathbf{j} (eq. 1):

$$\frac{|\rho_{co}|}{|\mathbf{j}|/c} \sim \frac{1}{\Delta\phi} \left(\frac{\Omega R_{\max}}{c} \right) \ll 1. \quad (2)$$

Here $R_{\max}(r, \theta) = r / \sin^2 \theta$ is the maximum radius of a dipolar field line that passes through coordinates (r, θ) . The current, however, will be forced to continue to flow by its self-induction, and the magnetosphere finds a way to re-generate the plasma that can carry the current (see § 2.2). So, the twisted force-free configuration persists.

The stored energy of non-potential (toroidal) magnetic field associated with the ejected current is subject to gradual dissipation. In our model, this dissipation feeds the observed activity of the corona. The stored energy is concentrated near the star and carried by closed magnetic lines with a maximum extension radius $R_{\max} \sim 2R_{NS}$. Thus, most of the twist energy will be released if these lines untwist, and we focus in this paper on the near magnetosphere $R_{\max} \sim 2R_{NS}$.

2.2. Bottleneck for the Twist Decay and Plasma Supply to the Corona

Consider a magnetic flux tube³ with cross section $S \lesssim R_{NS}^2$ and length $L \sim R_{NS}$ which carries a current $I = Sj$. The stored magnetic energy of the current per unit length of the tube is

$$\frac{\mathcal{E}_{twist}}{L} \sim \frac{I^2}{c^2} S. \quad (3)$$

The decay of this energy is associated with an electric field parallel to the magnetic lines \mathbf{E}_\parallel : this field can accelerate particles and convert the magnetic energy into plasma energy. Conservation of

³In an axisymmetric magnetosphere, we could equally well focus on a flux surface of revolution which sits within a range $\Delta\theta$ of polar angle θ and has a cross section $S = 2\pi r^2 \sin \theta \Delta\theta$.

energy can be expressed as

$$\frac{\partial}{\partial t} \left(\frac{B^2}{8\pi} \right) = -\mathbf{E} \cdot \mathbf{j} - \nabla \cdot \left(c \frac{\mathbf{E} \times \mathbf{B}}{4\pi} \right), \quad (4)$$

as follows from Maxwell’s equations with $E \ll B$ (e.g. Landau & Lifshitz 1975). The first term on the right-hand side is the Joule dissipation caused by \mathbf{E}_{\parallel} . The second term — the divergence of the Poynting flux — describes the redistribution of magnetic energy in space.

The decay of the twist on a single magnetic line can be related to the net voltage between the footpoints of the line,

$$\Phi_e = \int_A^C \mathbf{E} \cdot d\mathbf{l}. \quad (5)$$

Here A and C are the anode and cathode footpoints and $d\mathbf{l}$ is the line element; the integral is taken along the magnetic line outside the star (Fig. 1). The product $\Phi_e I$ approximately represents the dissipation rate $\dot{\mathcal{E}}$ in the tube. (The two quantities are not exactly equal in a time-dependent circuit.) The instantaneous dissipation rate is given by

$$\dot{\mathcal{E}} = \int_A^C \mathbf{E} \cdot \mathbf{I}(l) d\mathbf{l}, \quad (6)$$

where $\mathbf{I}(l) = S\mathbf{j}$ is the instantaneous current at position l in the tube. The current is fixed at the footpoints A and C, $I = I_0$; it may, however, fluctuate between the footpoints.

Note that the true 4D potential Φ is different from Φ_e and not related to the dissipation rate. Φ is the 0-component of the 4-potential $\Phi^\mu = (\Phi, \mathbf{A})$ which is related to the electric field by

$$\mathbf{E} = -\nabla\Phi - \frac{1}{c} \frac{\partial \mathbf{A}}{\partial t}. \quad (7)$$

If anode and cathode are connected by an ideal conductor then $\Phi(C) - \Phi(A) = 0$ while the voltage Φ_e may not vanish.

The voltage Φ_e is entirely maintained by the self-induction that accompanies the gradual untwisting of the magnetic field. Thus, Φ_e reflects the gradual decrease of the magnetic helicity in the tube,

$$\dot{\mathcal{H}} = \frac{\partial}{\partial t} \int_A^C \mathbf{A} \cdot \mathbf{B} dV = - \int_A^C \mathbf{E} \cdot \mathbf{B} S(l) dl. \quad (8)$$

(Here $dV = S(l)dl$ is the volume element.) It also determines the effective resistivity of the tube: $\mathcal{R} = \Phi_e/I$. The self-induction voltage passes the released magnetic energy to charged particles, and a higher rate of untwisting implies a higher energy $e\Phi_e$ gained per particle. A huge magnetic energy is stored in the twisted tube, and a quick untwisting would lead to extremely high Lorentz factors of the accelerated particles.

There is, however, a bottleneck that prevents a fast decay of the twist: the tube responds to high voltages through the copious production of e^\pm pairs. Runaway pair creation is ignited when

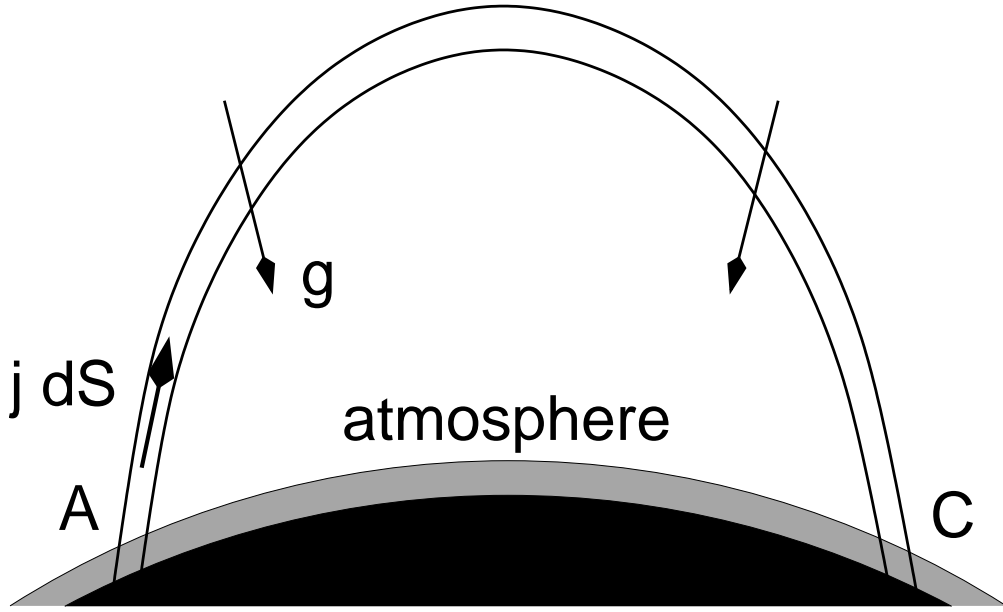


Fig. 1.— Schematic picture of a twisted current-carrying magnetic tube. The electric circuit closes to the highly conducting atmospheric layer on the stellar surface and flows down to the footpoints in the deep crust (see the text). The current has a tendency to become charge-starved above the atmospheric layer whose scale-height $h = k_B T / g m_p$ is a few cm.

electrons are accelerated to a certain Lorentz factor $\gamma_{\pm} \sim 10^3$. (We describe the microphysics of pair creation in § 5.) The created e^{\pm} plasma does not tolerate large E_{\parallel} — the plasma is immediately polarized, screening the electric field. This provides a negative feedback that limits the magnitude of Φ_e and buffers the decay of the twist.

There is a minimum Φ_e needed to supply plasma to the corona and to maintain the current. There are two possible sources of plasma: (1) ions and electrons stripped from the stellar surface, and (2) pairs created in the magnetosphere (or in the heated surface layer discussed in § 6). Correspondingly there are two characteristic voltages in the problem: first,

$$e\Phi_e \sim gm_i R_{\text{NS}} \sim 200 \text{ MeV}, \quad (9)$$

corresponding to an electric field that is strong enough to lift ions (of mass m_i) from the anode end of the circuit into the magnetosphere, and electrons from the opposite end; and, second,

$$e\Phi_e \sim \gamma_{\pm} mc^2 = 0.5\gamma_{\pm} \text{ MeV}, \quad (10)$$

which can accelerate particles to the Lorentz factor γ_{\pm} sufficient to ignite e^{\pm} creation.

If Φ_e is too low and the plasma is not supplied, a flux tube is guaranteed to generate a stronger electric field. The current becomes slightly charge-starved: that is, the net density of free charges becomes smaller than $|\nabla \times \mathbf{B}|/4\pi e$. The magnetic twist $\nabla \times \mathbf{B}$ does not respond to this because of the enormous self-induction, and a small reduction of the conduction current \mathbf{j} induces a displacement current $(1/4\pi)\partial\mathbf{E}/\partial t = (c/4\pi)\nabla \times \mathbf{B} - \mathbf{j}$. The longitudinal electric field E_{\parallel} then quickly grows until it can pull particles away from the stellar surface and ignite pair creation.

The limiting cases $E_{\parallel} \rightarrow 0$ (no decay of the twist) and $E_{\parallel} \rightarrow \infty$ (fast decay) both imply a contradiction. The electric field and the plasma content of the corona must regulate each other toward a self-consistent state, and the gradual decay of the twist proceeds through a delicate balance: E_{\parallel} must be strong enough to supply plasma and to maintain the quasi-steady current in the corona; however, if plasma is oversupplied then E_{\parallel} will be reduced by screening. A cyclic behavior is possible, in which plasma is periodically oversupplied and E_{\parallel} is screened. Our numerical experiment described below will show that such a cyclic behavior indeed takes place.

2.3. Comparison with Rotation-Powered Pulsars

Canonical radio pulsars are usually assumed to have a magnetosphere that is almost everywhere potential, $\nabla \times \mathbf{B} = 0$, except for narrow bundles of open field lines that connect the polar caps of the star to its light cylinder. The plasma content of the magnetosphere then depends on its rotation: the charge density $\rho_{\text{co}} = -\mathbf{\Omega} \cdot \mathbf{B}/2\pi c$ must be maintained to screen the electric field induced by rotation (Goldreich & Julian 1969). In this picture, the persistent current of a canonical pulsar only flows along the open field lines out to the light cylinder.

The sign of this current I_{open} is determined by the corotation charge density. In the case of a centered dipole, ρ_{co} has the same sign near the two magnetic poles, and so the outgoing (radial) component of the current has the same sign in the two hemispheres. (The same conclusion holds for a more complicated magnetic field beyond a certain distance from the star: the magnetic field rapidly approaches a dipole at $r \gg R_{\text{NS}}$.) The closure of the electric circuit back to the star remains poorly understood.

Since an electric field can pull out charges of one sign from the stellar surface, it can supply only a charge-separated current to the open lines. In radio pulsars, this leads to a large potential drop near the polar cap and the acceleration of particles to high Lorentz factors so that pair creation becomes possible. For example, when the polar magnetic field is $\sim 10^{12}$ G, pair breakdown requires $\gamma_{\pm} \sim 10^6 - 10^7$, above which curvature photons have enough energy to convert to electron-positron pairs directly off the magnetic field (Ruderman & Sutherland 1975). The pulsar magnetosphere is thought to be filled by the created e^+ , e^- and possibly ions pulled out from the stellar surface, which maintain the required ρ_{co} .

Magnetars rotate slowly, and the boundary of the rigidly corotating magnetosphere sits at a large radius $R_{\text{lc}} = c/\Omega \sim 3 \times 10^4 R_{\text{NS}}$. The polar caps are correspondingly tiny. Nearly the entire plasma corona of interest is immersed in a magnetic field that closes back to the star well inside the light cylinder.⁴ The radial component of the current therefore has the *opposite* sign at the two ends of the circuit. In contrast to the open-field current, charges of both signs can be supplied from the stellar surface: opposite charges can flow in the circuit from opposite ends of the magnetic lines (see Fig. 1). So, the charge-separated flow does not develop on the closed lines and strong, localized gaps with runaway pair creation may not form.

The corotation density ρ_{co} is small in the near magnetosphere of magnetars (see eq. [2]), and we will neglect the rotation of the star. The small ρ_{co} can be maintained by a slight polarization of the coronal plasma, $e(n_{e+} + Zn_i - n_{e-}) = \rho_{\text{co}} \ll en_{e-}$.

One may also compare the magnitude of the twist at the poles of the star, as sustained by the rotation, with the twist that is applied elsewhere in the magnetosphere by sub-surface stresses. The conserved current flowing along a bundle of magnetic field lines of radius a is

$$I = \frac{c}{2} a B_{\phi} = \frac{c}{2} a^2 B_P \frac{d\phi}{dl}. \quad (11)$$

Since the current I and the poloidal magnetic flux $\pi a^2 B_P$ are constants along the tube, the twist $d\phi/dl$ must also be constant and can be estimated as

$$\frac{d\phi}{dl} \sim \frac{\Delta\phi}{R_{\text{max}}}. \quad (12)$$

⁴The spindown rate is mainly determined by the current I_{open} . The details of plasma dynamics along the open field lines are less important for our purposes because I_{open} carries a tiny energy compared with the current on closed lines. For spindown calculations it is sufficient to know the value of I_{open} which may be found from the force-free model (TLK).

Here R_{\max} is the maximum radius to which the tube extends and $\Delta\phi$ is the net twist angle integrated along the tube. The net twist angle is limited by the global stability of magnetosphere to $\Delta\phi \lesssim 1$. Therefore, $d\phi/dl$ can be much larger on the field lines with $R_{\max} \sim 2R_{\text{NS}}$ than it is at the magnetic poles ($R_{\max} \sim R_{\text{lc}}$).

3. ELECTRIC CIRCUIT

3.1. Basic Properties

Three facts facilitate our analysis of the plasma dynamics in the electric circuit of magnetars:

1. The ultrastrong magnetic field makes the particle dynamics one-dimensional (1-D). The rest-energy density of the coronal plasma is $\sim mcj/e$, where m is the mass of a plasma particle. It is much smaller than the magnetic energy density $B^2/8\pi$: their ratio is $\sim mc^2/eBR_{\text{NS}} \sim 10^{-15}(m/m_p) B_{15}^{-1}$. The magnetic field lines are not perturbed significantly by the plasma inertia, and they can be thought of as fixed “rails” along which the particles move. The motion of the charges is confined to their lowest Landau levels and is strictly parallel to the field.

2. The particle motion is collisionless in the magnetosphere. It is governed by two forces only: the component of gravity projected onto the magnetic field and a collective electric field E_{\parallel} which is determined by the charge density distribution and must be found self-consistently.

3. The star possesses a dense and thin atmospheric layer.⁵ Near the base of the atmosphere, the required current $\mathbf{j} = (c/4\pi)\nabla \times \mathbf{B}$ is easily conducted, with almost no electric field. Therefore the problem has simple boundary conditions: $E_{\parallel} = 0$ and fixed current. The atmosphere screens the magnetospheric electric field from the star.

Our goal is to understand the plasma behavior above the screening layer, where the atmospheric density is exponentially reduced and an electric field E_{\parallel} must develop. The induced electric field \mathbf{E} and conduction current \mathbf{j} satisfy the Maxwell equation,

$$\nabla \times \mathbf{B} = \frac{4\pi}{c} \mathbf{j} + \frac{1}{c} \frac{\partial \mathbf{E}}{\partial t}. \quad (13)$$

Here \mathbf{j} is parallel to the direction of the magnetic field. Projection of equation (13) onto the magnetic field gives

$$\frac{\partial E_{\parallel}}{\partial t} = 4\pi(j_B - j), \quad j_B \equiv \frac{c}{4\pi} |\nabla \times \mathbf{B}|, \quad (14)$$

where we have taken into account the force-free condition $\nabla \times \mathbf{B} \parallel \mathbf{B}$. If the conduction current j is smaller than j_B , then $\partial E_{\parallel}/\partial t > 0$ and an electric field appears that tends to increase the current. Alternatively, if $j > j_B$ then an electric field of the opposite sign develops which tends to reduce the current. Thus, j is always regulated toward j_B . This is the standard self-induction effect.

⁵Such a layer initially exists on the surface of a young neutron star. Its maintenance is discussed in § 7 below.

The timescale of this regulation, τ , is very short. Consider a deviation $|j - j_B| \sim j_B$; then equation (14) gives

$$\frac{E_{\parallel}}{\tau} \sim 4\pi j_B. \quad (15)$$

The current $j = env$ (carried by particles with charge e and mass m) responds to the induced E_{\parallel} by changing v ,

$$\frac{v}{\tau} \sim \frac{eE_{\parallel}}{m}. \quad (16)$$

From equations (15) and (16) we get

$$\frac{1}{\tau^2} \sim \frac{4\pi e^2 n}{m} = \omega_P^2. \quad (17)$$

Thus the timescale of the current response to deviations of j from j_B is simply the Langmuir plasma timescale ω_P^{-1} , which is very short. Taking the characteristic density of the corona,

$$n \sim n_c \equiv \frac{j_B}{ec}, \quad (18)$$

and $j_B \sim (c/4\pi)(B/r)$ ([eq. 1]), we estimate $n \sim 10^{17} B_{15} r_6^{-1} \text{cm}^{-3}$. The corresponding electron plasma frequency ($m = m_e$) is $\omega_P \sim 10^{13} \text{ Hz}$. The timescale for the current to relax to j_B is $\tau \sim 10^{-13} \text{ s}$, which is tiny compared with the light crossing timescale of the circuit, $R_{\text{NS}}/c \sim 3 \times 10^{-5} \text{ s}$. Local deviations from charge neutrality tend to be erased on the same plasma timescale.

Since the particles in the corona have the characteristic velocity $v \sim c$, the Debye length of the plasma $\lambda_D = v/\omega_P$ can be taken equal to the plasma skin depth c/ω_P . An important physical parameter of the corona is the ratio of the Debye length to the circuit size $L \sim R_{\text{NS}}$.

$$\zeta = \frac{\lambda_D}{L} = \frac{c}{L\omega_P}. \quad (19)$$

In the case of the twisted dipolar magnetosphere (eq. [1]), this becomes

$$\zeta = 3 \times 10^{-9} B_{15}^{-1/2} (\Delta\phi \sin^2 \theta)^{-1/2}. \quad (20)$$

The same parameter may be expressed using a dimensionless current $j_B/j_* \sim 10^{17} B_{15} \Delta\phi \sin^2 \theta$. Here j_* corresponds to the plasma density $n_* = j_*/ec$ such that $\lambda_D = L$,

$$\frac{j_B}{j_*} = \zeta^{-2}, \quad j_* = \frac{m_e c^3}{4\pi e L^2}. \quad (21)$$

3.2. Quasi-Neutral Steady State?

Suppose for now that no e^{\pm} are created in the corona, so that the circuit must be fed by charges lifted from the stellar surface. May one expect that a steady current $j = j_B$ is maintained

in the neutral corona by a steady electric force $eE_{\parallel} \sim gm_i$ or $eE_{\parallel} \sim gm_e$? It turns out that such a balance between gravitational and electric forces is impossible in the circuit for the following reason: E_{\parallel} exerts opposite forces on positive and negative charges while the force of gravity has the same sign. This precludes a steady state where E_{\parallel} lifts particles into the magnetosphere without a significant deviation from neutrality appearing somewhere in the circuit. The point is illustrated by the following toy model.

Suppose positive charges e (mass m_+) flow with velocity $v_+ > 0$ and negative charges $-e$ (mass m_-) flow with velocity $v_- < 0$. The flow of each species is assumed to be cold in this illustration, with a vanishing velocity dispersion at each point, and the total current is $j = j_+ + j_-$ where $j_{\pm} = \pm en_{\pm}v_{\pm}$. The continuity equation for positive/negative charges reads

$$\frac{\partial(\pm en_{\pm}/B)}{\partial t} + \frac{\partial(j_{\pm}/B)}{\partial l} = 0, \quad (22)$$

where l is the coordinate along the field line. Suppose the circuit is steady, $\partial/\partial t = 0$, and no strong deviation from neutrality occurs, i.e. $n_+ \simeq n_-$ everywhere. Then one finds

$$\frac{j_+}{j_-} = -\frac{v_+}{v_-} = \text{const}. \quad (23)$$

That is, the ratio of velocities must remain constant along the field line. Hence v_+ and v_- must *both* vanish at the footpoints. This cannot be: for example, at the anode E_{\parallel} must lift ions against gravity, and hence it cooperates with gravity to accelerate the falling electrons rather than stops them.⁶

So, if the current-carrying particles are supplied by the star, we expect either a significant charge separation at some places in the circuit, or a time-dependent behavior (or both). One must also allow for the creation of e^{\pm} pairs if the light charges are accelerated to high enough energies, which will be discussed in § 5. Our approach to this problem is a direct numerical experiment that simulates the time-dependent behavior of plasma particles in the circuit.

3.3. Numerical Simulation of a One-Dimensional Circuit

We shall describe below a time-dependent simulation of a circuit operating in a thin magnetic tube with $j_B = (c/4\pi)|\nabla \times \mathbf{B}|$ fixed in time. Strictly speaking, j_B is *quasi*-steady: it will be found to decay on a long resistive timescale (\sim yrs), much longer than the dynamic time of the current $t_{dyn} = L/c \sim 10^{-4}$ s. The purpose of the simulation is to understand how plasma is supplied above the surface layer, and to find the electric field that develops along the tube.

⁶A static plasma configuration is possible with the electric and gravitational forces balancing each other at each point of the circuit. However, $j = 0$ in this configuration and it is not relevant to our circuit problem. Besides, such a configuration would be unstable.

The electric field may be decomposed as $\mathbf{E} = \mathbf{E}_{\parallel} + \mathbf{E}_{\perp}$ where \mathbf{E}_{\parallel} is parallel to the magnetic field. It is \mathbf{E}_{\parallel} that governs the plasma motion and determines the release of magnetic energy. We will focus on this component and assume $\nabla \cdot \mathbf{E}_{\perp} = 0$; then Gauss' law reads

$$4\pi\rho = \nabla \cdot \mathbf{E}_{\parallel} = \frac{dE_{\parallel}}{dl}, \quad (24)$$

where l is length measured along the magnetic tube. The assumption $\nabla \cdot \mathbf{E}_{\perp} = 0$ significantly simplifies the problem: it becomes strictly one-dimensional since \mathbf{E}_{\perp} has no relation to charge density and falls out from the problem. In a real magnetosphere, \mathbf{E}_{\perp} may exist, possibly with a non-zero divergence. Then the plasma charge density in the tube would have to maintain $\nabla \cdot \mathbf{E}_{\perp}$ in addition to dE_{\parallel}/dl . Hereafter we assume $\mathbf{E} = \mathbf{E}_{\parallel}$ and drop the subscript \parallel .

We note that the conditions $j_B(t) = \text{const}$ and $\nabla \cdot \mathbf{E}_{\perp} = 0$ exclude the excitation of transverse waves in the magnetosphere. These waves are described by the coupled fluctuations δj_B and \mathbf{E}_{\perp} on scales much smaller than the circuit size L . (Wavelengths $\lambda \sim c/\omega_P$ can be excited by plasma oscillations.) These fluctuations may be expected to have a negligible effect on the circuit solution unless δj_B becomes comparable to j_B .

The force-free condition $\mathbf{j}_B \times \mathbf{B}$ together with $\nabla \cdot \mathbf{j}_B = 0$ requires that $j_B(l) \propto B(l)$ along the magnetic line. We can scale out this variation simply dividing all local quantities (charge density, current density, and electric field) by B . This reduces the problem to an equivalent problem where $j_B(l) = \text{const}$.

Only forces along magnetic lines control the plasma dynamics, and the curvature of magnetic lines falls out from the problem. Therefore, we can set up the experiment so that plasma particles move along a straight line connecting anode and cathode (Fig. 2). We designated this line as the z -axis.

Furthermore, since j_B is fixed constant in time, the particle motions on different magnetic lines are decoupled. Indeed, the particle dynamics is controlled by electric field E which is related to the instantaneous charge distribution by Gauss' law (24).⁷ Thus, $E(z)$ on a given magnetic line is fully determined by charge density $\rho(z)$ *on the same line*. The plasma and electric field evolve along the line as if the world were 1-D.

This one-dimensional system may be simulated numerically. Consider N particles moving along the z -axis ($N \sim 10^6$ in our simulations). Their positions z_i and velocities v_i evolve in time according to

$$\frac{dz_i}{dt} = v_i, \quad \frac{dp_i}{dt} = g\gamma_i m_i + e_i E, \quad i = 1, \dots, N, \quad (25)$$

where e_i and m_i are charge and mass of the i -th particle, $p_i = \gamma_i m_i v_i$, and $\gamma_i = (1 - v_i^2/c^2)^{-1/2}$. Also, $g(z)$ is the projection of the gravitational acceleration onto the magnetic line. In the simulations,

⁷The Maxwell equation (14) and Gauss' law (24) are equivalent when charge conservation $\partial j/\partial z = -\partial \rho/\partial t$ is taken into account.

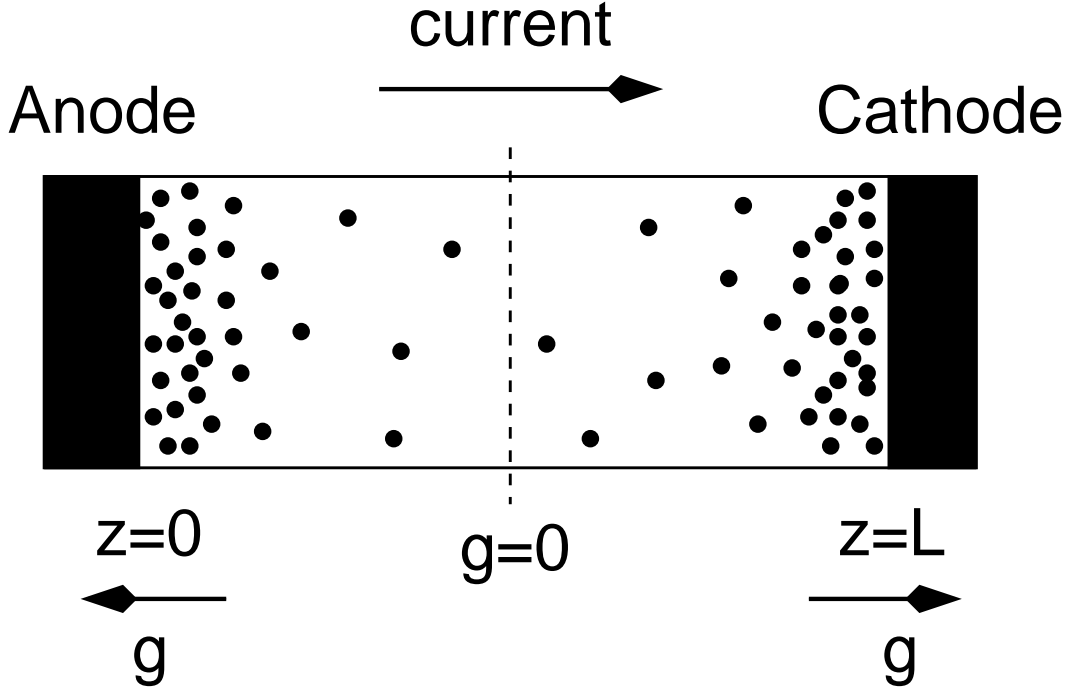


Fig. 2.— Set up of numerical experiment. Thin and dense plasma layers are maintained near the cathode and anode by injecting cold particles through the boundaries of the tube (footpoints of the magnetospheric field). The electric current is kept constant at the boundaries and the system is allowed to evolve in time until a quasi-steady state is reached.

we assume $g = g_0(2z/L - 1)$ where L is the distance between the anode and cathode; then $g = \pm g_0$ at the cathode/anode surfaces and $g = 0$ in the middle $z = L/2$. The electric field appearing in equation (25) is given by

$$E(z) = 4\pi \int_0^z \rho dz, \quad (26)$$

where $E(0) = 0$ is determined by the boundary condition discussed above. Since the current $j = j_B$ is fixed at both ends, the net charge between anode and cathode does not change with time and remains zero (in agreement with conditions $E[L] = E[0] = 0$).

Given the instantaneous positions z_i of charges e_i we immediately find $E(z)$ from Gauss's law (eq. [26]). Thus, we have a well-defined 1-D problem of particle motion in a self-consistent electric field and the fixed gravitational field. To find a quasi-steady state of such a system we start with an initial state and let it relax by following the particle motion.

Note that the evolution of the system may be followed without calculating ρ or j : the equations contain only integrated charge $Q(z) = \int_0^z \rho dz$. In contrast with usual particle-in-cell simulations, no grid or cells are needed. One finds the *exact* E at any point z simply by counting the net charge of particles between z and anode. The only source of numerical error is caused by the finite timestep of the particle dynamics, and we keep it small in the simulations, $\Delta t = 10^{-5} - 10^{-4}(L/c)$.

The main dimensionless parameter of the problem is $\zeta = c/\omega_P L \sim 3 \times 10^{-9}$ (see § 3.1). Although it is not possible to simulate circuits with such a low value of ζ , we can experiment with a similar system with $\zeta \simeq 10^{-2}$. This allows one to understand the mechanism of the circuit and find plasma parameters that will be easy to scale to a real magnetosphere.

A large number of particles $N \gtrsim 10^6$ may be followed with modern computers in a reasonable time, and $\zeta \ll 1$ may be achieved by choosing an appropriate charge per particle. Two other basic requirements must be satisfied in the simulations: (1) the number of particles within the Debye length is much larger than one; and (2) the timestep is much smaller than ω_P^{-1} and small enough to follow accurately the particle dynamics. Finally, we require the particle charge e to be sufficiently small, so that its electric field in our 1-D problem satisfies $eE = 4\pi e^2 \ll m_e g$. Given a number of particles N , this last condition constrains ζ from below. The minimum ζ achieved in our numerical experiment is $\sim 5 \times 10^{-3}$.

The ions and electrons in the simulated circuit have different masses m_i and m_e . The ratio m_i/m_e is smaller than it would be in a real magnetosphere. Below we will show models with $m_i/m_e = 10$ and 30. Hereafter subscripts i and e refer to ions and electrons, respectively, and subscript p will refer to positrons.

The neutral atmospheric layers near the boundaries of the computational box $z = 0, L$ are created by injecting a flux of positive and negative charges with small temperatures T_e and T_i . Although most charges are bound to the star, a few must drift to the top of the atmosphere and get lifted by the electric field into the magnetosphere. The numerical simulation will show precisely how this happens.

The boundary conditions $E = 0$ and $j = j_B$ are imposed *beneath* the atmospheric layers. The condition $j = j_B$ implies keeping track of the flux of leaving charges, and injecting new particles with the correct imbalance between the positive and negative charges. Thus the required current is fed at a constant rate at the conducting boundaries. If net charge escaping through the cathode boundary during timestep dt is smaller than $j_B dt$, we inject electrons to maintain the required j_B , otherwise we inject the needed number of ions. Similarly, $j = j_B$ is enforced at the anode boundary. This maintains the current, but does not determine the contributions to j_B from different types of particles. The plasma self-organizes during the experiment and decides itself what the contributions must be.

The forced injection of net positive charge at anode and net negative charge at cathode would immediately create a long range electric field if the current were not flowing in the system. A deviation of j from j_B at any point of the circuit leads to appearance of an electric field at that point. Thus, the boundary conditions $j(0) = j(L) = j_B$ are equivalent to equation (14).

The electric field does a net positive work on the current-carrying particles. In our experiment, the deposited kinetic energy sinks through the boundaries and never comes back. We envision dense radiatively efficient layers just outside the simulation box and assume that the lost energy is emitted there. The surface layers maintained in the experiment have density only $\sim 20 - 100$ times $n_0 = j_B / ce$, which is just sufficient to screen the electric field and avoid interference of the boundaries in the circuit solution. A future full simulation may include radiative losses *in situ* in the tube and allow one to track the fate of released energy and the spectrum of produced radiation.

Our final choice regards the initial plasma state in the tube. We tried different initial states and got same results. In the runs shown below we take as initial conditions $j(z) = j_B$, a mildly relativistic bulk velocity $v_e = v_i = 0.4c$ and Maxwellian momentum distribution with temperature equal to the bulk kinetic energy.

The problem has four scales: tube length L , electron plasma scale $\lambda_{De} = c/\omega_{Pe}$, ion plasma scale $\lambda_{Di} = (m_i/m_e)^{1/2}\lambda_{De}$, and scale-height of the atmospheric layer $h = k(T_e + T_i)/g(m_i + m_e)$. For a real magnetosphere, $\lambda_{De} < \lambda_{Di} < h < L$. We choose the parameters of the experiment so that these relations are satisfied. The inclusion of pair production in the simulation brings a new scale: mean free path l (see § 3.5 below).

A numerical code implementing the described method was developed and first tested on simple plasma problems without gravity, $g = 0$. For example, we calculated the two-stream instability starting with two oppositely directed cold beams of positive and negative charges, and found the correct development of Langmuir oscillations on the plasma timescale. Various technical tests have been done, e.g. independence of the results of timestep and charge of individual particles e . The main parameter of the problem is ζ , and circuits with equal ζ and different N , e , dt gave the same result. Another test passed is the agreement of the linear-accelerator state obtained by the code (§ 5) with the analytical solution of Carlqvist (1982).

As we shall see below, e^\pm creation is inevitable in the magnetospheric circuit, and it will be

discussed in detail in § 5. However, first we investigate what happens in the circuit with pair creation “switched-off,” when the current-carrying charges must be supplied by the atmospheric layers.

4. CIRCUIT WITHOUT PAIR CREATION

The circuit model has the following parameters: (1) dimensionless current $j_B/j_* = \zeta^{-2}$ (see § 3.1), (2) gravitational potential barrier Φ_g (we will assume $\Phi_g = c^2/4$ in numerical examples), (3) density of the hydrostatic boundary layer n_{atm} (which is regulated in the numerical experiment by the particle injection rate at the boundaries), and (4) injection temperatures of ions, T_i , and electrons, T_e .

Note that T_i and T_e may exceed the surface temperature of the star because the atmosphere below the screening layer is heated from above by the corona. The vertical temperature profile that is established below the screening layer is a separate problem which we do not attempt to solve in this paper. So, T_i and T_e serve as parameters of our model, and we explore first how the mechanism of the circuit depends on these parameters.

4.1. Thermally-Fed Circuit

If the hydrostatic atmosphere is sufficiently hot, its Boltzmann tail at large heights may be able to conduct the current without the need to lift particles by an electric field. The plasma must remain quasi-neutral in the Boltzmann tail. One may think of the neutral atmosphere as a gas of composite particles $m = m_i + m_e$ with effective temperature $T = T_i + T_e$. Its scale-height is given by

$$h = \frac{k_B T}{g_0 m} = \frac{k(T_i + T_e)}{g_0(m_i + m_e)}. \quad (27)$$

The plasma density is reduced exponentially on scale h . The reduced density remains high enough to conduct the current j_B all the way to the top of the gravitational barrier if

$$n_{\text{atm}} \exp\left(-\frac{m\Phi_g}{k_B T}\right) > n_c = \frac{j_B}{ec}. \quad (28)$$

One example of a circuit that satisfies condition (28) is shown in Figure 3. The electrons and ions are injected at the boundaries with $k_B T_i = k_B T_e = 0.5 m_e c^2$ and $m_i = 10 m_e$. This gives a scale-height $h = 0.09 L$. After several light-crossing times L/c , the circuit develops the Boltzmann atmosphere that conducts the required current $j_B = 10^3 j_*$. The electric field remains small and dynamically unimportant, $eE < g_0 m_i$.

The thermally-fed regime requires too high a temperature for the pure ion-electron circuit. Indeed, $mc^2 = (m_i + m_e)c^2 \simeq 1 \text{ GeV}$ and then $k_B T > 1 \text{ GeV} / \log(n_{\text{atm}}/n_c)$ would be required.

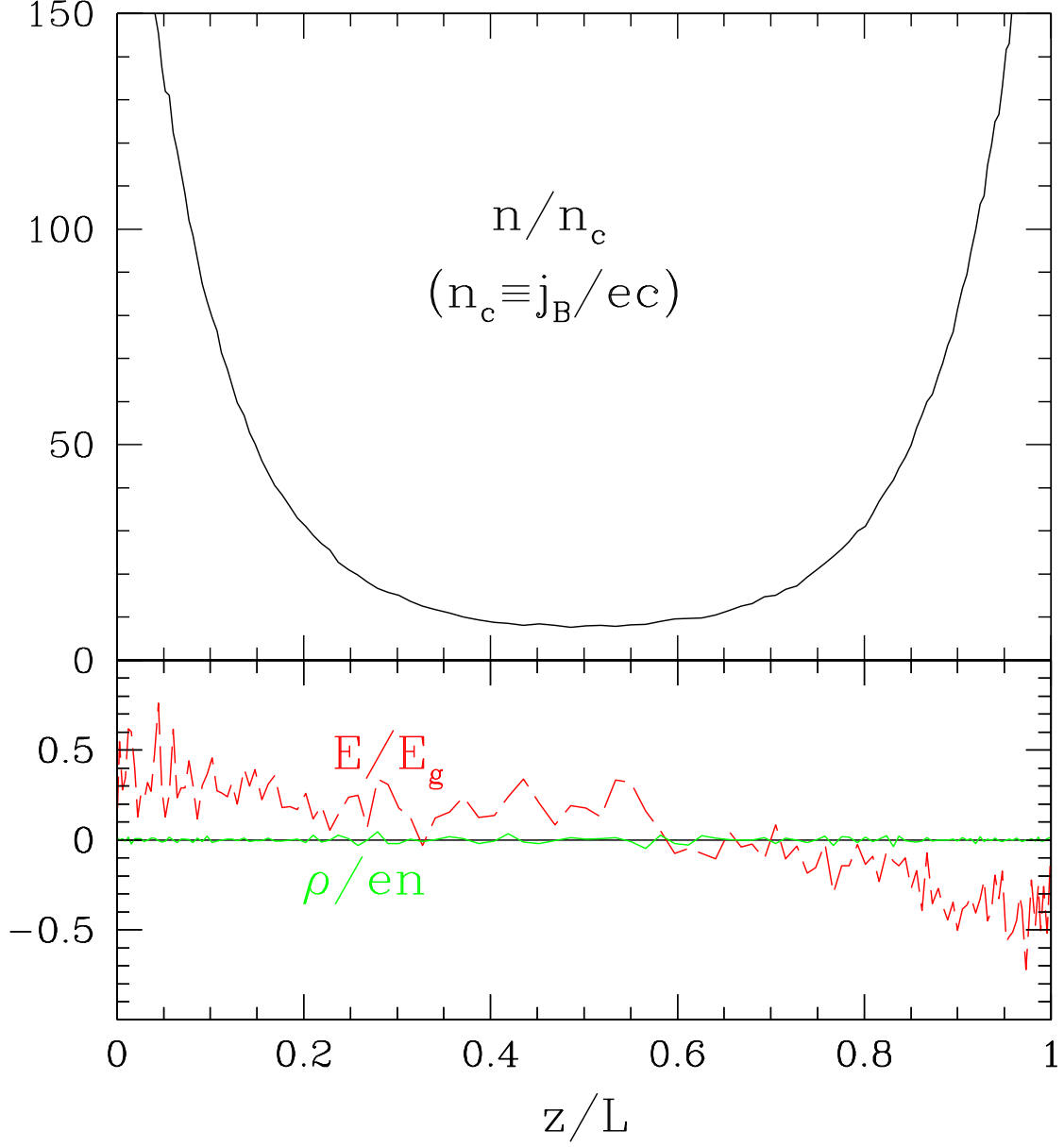


Fig. 3.— Thermally-fed circuit without e^\pm production. Upper panel: the plasma density $n = n_e + n_i$ in units of $n_c = j_B/ec$. Lower panel: deviation from neutrality ρ/en , and electric field in units of E_g defined by $eE_g = m_i g_0$. In this simulation, $m_i = 10m_e$ and $\zeta = c/\omega_P L \simeq 0.03$. The snapshot is taken at $t = 20L/c$, after the system has reached the quasi-steady state.

Pair creation would take place at much lower temperatures (a pair-dominated thermal circuit will be considered in § 5). Therefore, the thermally-fed pair-free circuit solution cannot apply to a real magnetosphere. The rest of this section focuses on circuits that do not satisfy condition (28).

4.2. Linear Accelerator

When the condition (28) is not satisfied, the circuit becomes plasma-starved and an electric field develops that lifts particles from the dense surface layer. We find that such a circuit quickly relaxes to a state where it acts as an ultra-relativistic linear accelerator.

One example is shown Figure 4. The parameters of this particular model are $j_B/j_* = 10^4$, $k_B T_e = 0.1 k_B T_i = 0.04 m_e c^2$, and $n_{\text{atm}}/n_c \simeq 20$. We obtained similar solutions for various combinations of T_e , T_i , and n_{atm}/n_0 that do not satisfy condition (28) of a thermally-fed regime. In all cases, the circuit reached the quasi-steady state at $t \lesssim 5L/c$.

In this state, oscillations of electric field (on the plasma timescale ω_P^{-1}) are confined to the thin atmospheric layers. A static accelerating electric field is created above the layers where the atmosphere density is exponentially reduced. The striking result is that on top of each layer, a large charge builds up, which is positive ($+Q$) at the anode and negative ($-Q$) at the cathode. The two charges create a long-range electric field $E = 4\pi Q$.

This configuration is a relativistic double layer (Carlqvist 1982). It is well described by Carlqvist’s solution, which has no gravity in the circuit and assumes zero temperature at the boundaries, so that particles are injected with zero velocity. According to this solution, the potential drop between anode and cathode, in the limit $e\Phi_e \gg m_i c^2$, is given by

$$e\Phi_e = \frac{1}{2} \left[\left(\frac{m_i}{Zm_e} \right)^{1/2} + 1 \right] L\omega_P m_e c, \quad \omega_P \equiv \left(\frac{4\pi j_e}{m_e c} \right)^{1/2}. \quad (29)$$

where Z is the charge number of the ions (in our experiment $Z = 1$ was assumed). In the limit $m_i \gg Zm_e$, this expression depends only on the ion and not the electron mass.

The established voltage is much larger than is needed to overcome the gravitational barrier Φ_g . It does not even depend on Φ_g as long as Φ_g is large enough to prohibit the thermally-fed regime. Gravity causes the transition to the linear-accelerator state, but the state itself does not depend on Φ_g . The asymmetry of the double-layer solution (Fig. 4) is caused by the difference between the electron and ion masses. A similar but symmetric configuration is obtained for $m_i = m_e$.

The symmetric double layer with $m_e = m_i$ is especially simple and can be qualitatively understood as follows. The currents carried by ions and electrons are equal by symmetry, $j_i = j_e = \frac{1}{2} j$, and hence plasma is approximately neutral between the anode and cathode where $v_i \simeq v_e \simeq c$. A significant deviation from neutrality $|n_e - n_i| \sim n_i + n_e$ takes place in the acceleration regions Δz near anode and cathode because here v_i differs from v_e . For instance, near the anode the ions are

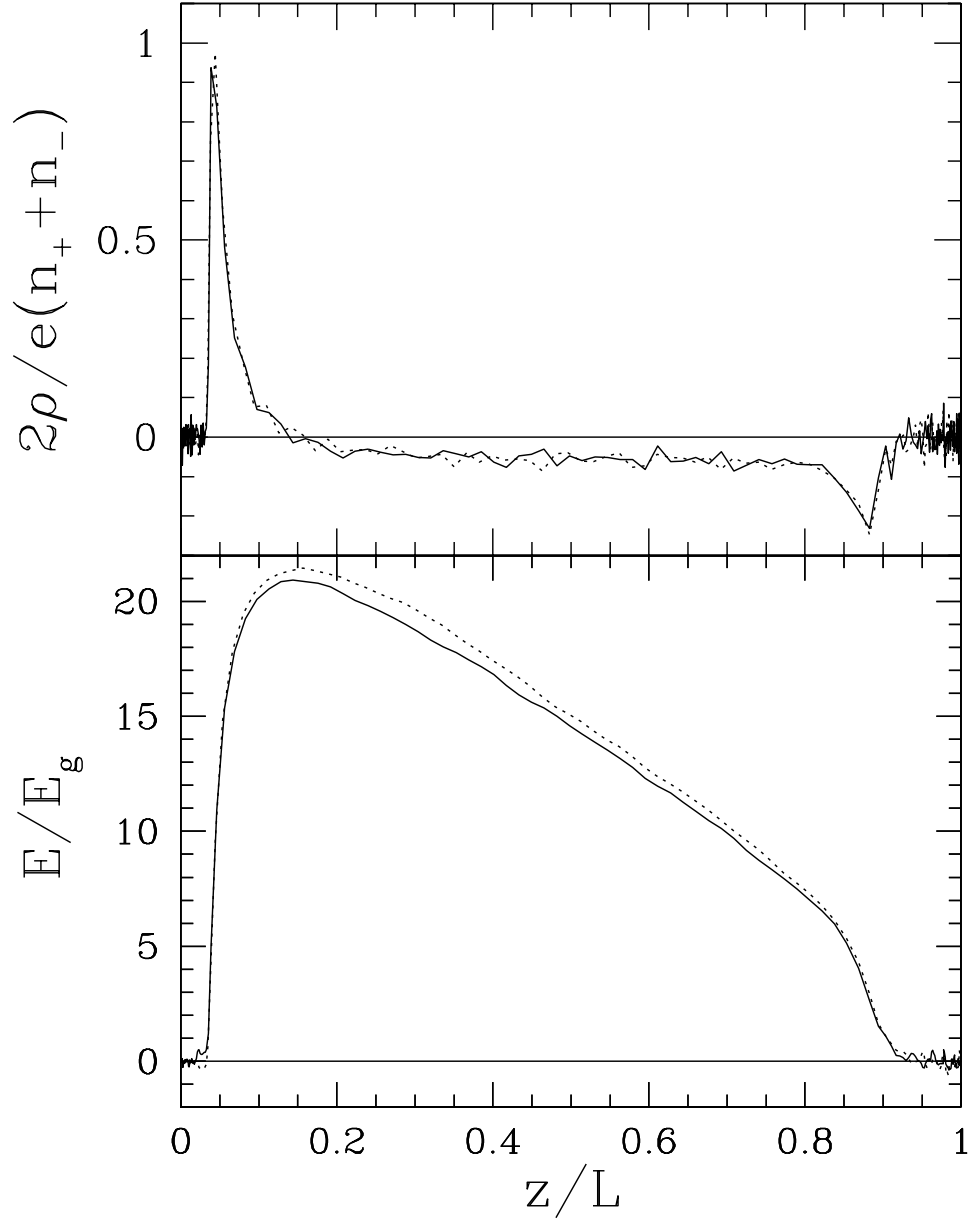


Fig. 4.— Circuit without e^\pm production. Upper panel shows the normalized charge density and lower panel shows the electric field in units of E_g defined by $eE_g = m_i g_0$. Solid and dotted curves correspond to two different moments of time, demonstrating that a quasi-steady state has been reached. In this simulation, $m_i = 10m_e$ and $\zeta = c/\omega_P L \simeq 0.01$. The final state is the relativistic double layer described analytically by Carlqvist (1982).

not accelerated yet to c , and their charge density $\rho_i = j_i/v_i$ is larger than that of the incoming electron beam, $\rho_e = j_e/v_e \simeq j_e/c$, so the net charge density is positive. One can show that the anode charge $Q(z) = \int_0^z (j_i/v_i - j_e/v_e) dz$ peaks at height $z \sim \Delta z$ where ions move with a mildly relativistic velocity $v_i \sim c/2$. Similarly, at cathode end, where the emitted electron flow is still slow, the net charge density is negative, and the charge $-Q$ peaks at the distance Δz from the cathode. The thickness Δz and the characteristic electric field E in the mildly relativistic region are related by $eE\Delta z \sim m_e c^2$.

Combining the condition $eE\Delta z \sim m_e c^2$ with $E = 4\pi Q \sim 4\pi en_c \Delta z$, one finds $\Delta z \sim \lambda_D$ and $Q \sim en_c \lambda_D$. This is the only possible self-consistent static solution for a double layer (besides the trivial solution $E = 0$ which is prohibited in our case by gravity). $E = 4\pi Q$ must be this large in a static double layer because a smaller E would accelerate the particles more slowly, which would imply larger non-neutral regions Δz near the ends of the circuit and larger Q . Gauss' law would then imply a larger E , leading to inconsistency with the assumed smaller E .

Similar estimates may be made for the asymmetric double layer with $m_i > m_e$. In the limit $e\Phi_e \gg m_i c^2$, one again finds $j_i \simeq j_e$ from the Langmuir condition (see Carlqvist 1982),

$$\frac{j_i}{j_e} = \left(\frac{e\Phi_e + 2m_e c^2}{e\Phi_e + 2m_i c^2/Z} \right)^{1/2} \simeq 1. \quad (30)$$

There is only one qualitative difference from the symmetric case. Now the mildly relativistic region near the anode, $v_i \sim c/2$, has a thickness $\Delta z_A \sim \lambda_{Di}$, and near the cathode, $v_e \sim c/2$, — $\Delta z_C \sim \lambda_{De}$. The spikes of charge near anode and cathode are now different: the cathode spike is smaller by a factor of $\lambda_{De}/\lambda_{Di} = Z(m_e/m_i)^{1/2}$. The net charge of a double layer, however, must vanish to satisfy the boundary conditions $E = 0$. The “missing” negative charge is distributed between the two spikes, throughout the circuit. This behavior is observed in Fig. 4 and derived analytically by Carlqvist (1982).

The static double-layer solution has been much studied previously, but its possible astrophysical applications remained unclear. Our numerical experiment shows that an ion-electron circuit in a gravitational field relaxes to the double layer of the macroscopic size L and huge voltage Φ_e . The system does not find any state with a lower Φ_e , even though it is allowed to be time-dependent. The experiment shows that, regardless the initial state, the charges $\pm Q$ near the anode/cathode build up with time in spite of the strong fluctuations that persist in the atmospheric layers (reversing the sign of E), and Q grows until the Carlqvist solution is reached.

The effective boundaries of the double layer in our experiment are not exactly at $z = 0, L$ because the atmosphere has a finite temperature, and the current is maintained without significant deviations from neutrality up to height z_* where the circuit becomes plasma-starved. The z_* may be estimated from the condition $n_{\text{atm}} \exp(-z_*/h) \sim n_c$, which gives $z_* \sim \ln(n_{\text{atm}}/h) h$.

If the linear accelerator were maintained in the twisted magnetosphere, the twist would be immediately killed off. The huge voltage implies a large untwisting rate and a fast dissipation of

the toroidal magnetic energy (§ 2). The electron Lorentz factor developed in the linear accelerator is (taking the real $m_i/m_e = 1836$ and $\zeta \sim 3 \times 10^{-9}$),

$$\gamma_e = \frac{e\Phi_e}{m_e c^2} \simeq \frac{20}{\zeta} \sim 6 \times 10^9. \quad (31)$$

However, new processes will become important before the particles could acquire such high energies: production of e^\pm pairs will take place. Therefore, the linear-accelerator solution cannot describe a real magnetosphere. We conclude that pair creation is an important ingredient of the circuit that will regulate the voltage to a smaller value.

5. PAIR CREATION IN THE CORONA

5.1. Resonant Channel of Pair Creation

In the magnetospheres of normal radio pulsars with $\sim 10^{12}$ G dipole magnetic fields, e^\pm pairs are created when seed electrons are accelerated to large Lorentz factors $\gamma_e \sim 10^7$ and emit curvature gamma rays. By contrast, e^\pm creation in a magnetar magnetosphere can occur at much lower γ_e because the ultra-strong magnetic field opens a new channel of pair creation. This channel involves resonant scattering of X-rays by accelerated particles and immediate conversion of the upscattered photons to e^\pm pairs.⁸

Consider an electron moving along a magnetic line with Lorentz factor $\gamma_e \gg 1$. In the rest frame of the electron, an ambient X-ray photon moves nearly parallel to the magnetic field with an energy $\hbar\omega'_X = \gamma_e(1 - \cos\theta_{kB})\hbar\omega_X$, where $\hbar\omega_X$ and θ_{kB} are the photon energy and pitch angle with respect to the magnetic field as measured in the frame of the star. The scattering may be viewed as a two-step process: the excitation of the electron into the first Landau state with energy

$$E_B = \left(\frac{2B}{B_{\text{QED}}} + 1 \right)^{1/2} m_e c^2, \quad (32)$$

followed rapidly by a de-excitation. Notice that E_B is significantly larger than $m_e c^2$ in a super-QED magnetic field, which means that the photon imparts a significant recoil to the electron. As a result, the electron decelerates in the lab frame, and its new Lorentz factor parallel to the field is

$$\gamma_{\parallel} \simeq \gamma_{\text{res}} \left(\frac{2B}{B_{\text{QED}}} + 1 \right)^{-1/2}. \quad (33)$$

⁸A similar process can operate in radio pulsars in a non-local manner. When a high-energy photon is created by resonant upscattering in a sub-QED field it cannot create a pair at the same location — it needs to propagate a sufficient distance to build up a sufficient angle with respect to the (curved) magnetic lines (e.g. Hibschan & Arons 2001). A detailed treatment of the competition between splitting and pair creation in the open-field line region of pulsars with surface magnetic fields near B_{QED} has been given by Baring & Harding (2001). In this case, the bulk of the pair creation occurs close to the threshold energy.

The emission of the de-excitation photon does not change γ_{\parallel} on the average. So, the average Lorentz factor of the electron after the resonant scattering is $\langle \gamma_{sc} \rangle = \gamma_{\parallel}$.

The condition for resonant scattering is $\hbar\omega'_X \simeq (B/B_{\text{QED}})m_e c^2$, or equivalently

$$\gamma_{res} = \frac{B/B_{\text{QED}}}{1 - \cos \theta_{kB}} \left(\frac{\hbar\omega_X}{m_e c^2} \right)^{-1} \simeq 10^3 B_{15} \left(\frac{\hbar\omega_X}{10 \text{keV}} \right)^{-1}. \quad (34)$$

An electron with $\gamma_e \sim 10^3$ will be in resonance with 10 keV photons, and an electron with $\gamma_e \sim 6 \times 10^3$ with the blackbody peak of the stellar radiation $\hbar\omega_X \sim 3k_B T \sim 1.5 \text{ keV}$.

The upscattered photon gets beamed along the local magnetic line, within a cone of opening angle $\theta \simeq \langle \gamma_{sc} \rangle^{-1}$. Its mean energy is

$$\langle \hbar\omega_X \rangle = (\gamma_{res} - \langle \gamma_{sc} \rangle) m_e c^2 \simeq \gamma_{res} m_e c^2. \quad (35)$$

This energy is limited by the recoil effect, as it is in Klein-Nishina scattering.

In the frame of the de-exciting electron (Lorentz factor γ_{\parallel}), the scattered photon has a random direction and its characteristic energy is E_B . In the inner magnetosphere, the photon typically converts immediately to an e^{\pm} pair. One can see that, in general, the processes of resonant scattering or cyclotron emission in a super-QED field give photons that cannot escape — they convert to pairs practically at the same location. Further details of the pair creation process, including the dependence on polarization of the de-excitation photon are discussed in § 6.4.

Thus, there is a characteristic $\gamma_e \sim 10^3$ at which the electron efficiently upscatters the ambient X-rays and produces e^{\pm} pairs. The rate of pair creation by an accelerated electron depends on the cross section of resonant scattering and the number density of the target photons.

The cross section for resonant scattering (electron excitation) can be written in the rest frame of the electron as

$$\sigma_{res}(\omega, \theta'_{kB}) = \sigma_{res0} \omega \delta \left(\omega - \frac{eB}{m_e c} \right), \quad (36)$$

where θ'_{kB} is the angle of propagation of the final photon with respect to \mathbf{B} as measured in the frame of de-exciting electron (Lorentz factor γ_{\parallel}). Here it is taken into account that the photon is incident almost parallel to \mathbf{B} as a result of relativistic aberration. The coefficient $\sigma_{res0} = (\pi^2 e/B)(1 + \cos^2 \theta'_{kB})$ in the non-relativistic regime ($B \ll B_{\text{QED}}$) where the recoil effect is negligible (e.g. Canuto, Lodenquai, & Ruderman 1971). The cross sections for scattering into the O-mode and E-mode in the final state are related by $\sigma_{res}(O) = \cos^2 \theta'_{kB} \sigma_{res}(E)$. The normalization of the cross section changes when $B \gtrsim B_{\text{QED}}$, and at large $B \gg B_{\text{QED}}$ it simplifies to⁹

$$\sigma_{res0} \simeq \frac{\pi^2 e}{2B} \quad (B \gg B_{\text{QED}}). \quad (37)$$

⁹This expression may be derived from the more general expressions presented by Herold (1979).

In this regime, there are equal probabilities for the photon to end up in the E-mode or O-mode in the final state, independent of θ'_{kB} ,

$$\sigma_{\text{res}}(E) = \sigma_{\text{res}}(O) = \frac{1}{2} \sigma_{\text{res}0} \delta \left(\omega - \frac{eB}{m_e c} \right). \quad (38)$$

The number density of target photons for resonant scattering is

$$n_X \simeq \frac{L_X}{4\pi R_{\text{NS}}^2 \hbar \omega_X c} = 2 \times 10^{20} L_{X35} \left(\frac{\hbar \omega_X}{\text{keV}} \right)^{-1} \text{ cm}^{-3}.$$

The mean free path of an electron to scattering a photon is then

$$l_{\text{res}} = \frac{1}{n_X \sigma_{\text{res}0}} \left| \frac{d \ln B}{d \ln l} \right| \sim \frac{3}{n_X \sigma_{\text{res}0}} \sim 6 \times 10^3 \frac{B_{15}}{L_{X35}} \left(\frac{\hbar \omega_X}{\text{keV}} \right) \text{ cm}. \quad (39)$$

The upscattered photon immediately converts to an e^\pm pair, at a small distance from the scattering site compared with l_{res} . So, the distance over which an accelerated electron creates a pair is practically equal to the free path to scattering. In a given field B , it depends only on the spectrum of target photons. While being accelerated, an electron with initially low γ_e may first experience a resonance with a high-energy photon, so it is important to know the radiation spectrum at high energies, above the blackbody peak.

It is possible that the transition region between the corona and the star emits 100 keV photons (Thompson & Beloborodov 2005; see §§6 and 8.4 below), which may be targets for resonant scattering by electrons with relatively low $\gamma_e \sim 100$. Photons with energy much above ~ 100 keV are not good targets for resonant scattering in the strong- B region near the star; then l_{res} becomes comparable to R_{NS} .

5.2. Inconsistency of the Linear Accelerator

Now we can show that the linear accelerator discussed in § 4.2 becomes inconsistent in the presence of pair creation and cannot be established in the magnetosphere.

Suppose it is established. Electrons in the accelerator will be in resonance with photons at the peak of the stellar blackbody spectrum, $\hbar \omega_X \sim 1$ keV, when they have Lorentz factors $\gamma_{\text{res}} \sim 10^4 B_{15}$. Using the Carlqvist solution for the electron Lorentz factor $\gamma_e(z)$, we find the characteristic distance from cathode where electrons reach γ_{res} . This distance is given by

$$a_{\text{res}} \simeq \gamma_{\text{res}} \lambda_{\text{De}}. \quad (40)$$

Here we have used $\lambda_{\text{De}} \ll a_{\text{res}} \ll (m_i/m_e)^{1/2} L$; the electric field of the double layer varies little across this region and equals $E = 4\pi(j/c)\lambda_{\text{De}}$, where j is the current flowing through the circuit. The resonance region is at the distance $a_{\text{res}} \sim 30$ cm from cathode and its thickness is $\sim a_{\text{res}}$. The

mean free path of electrons in this region is $l_{\text{res}} \sim 6 \times 10^3$ cm (see eq. [39]), which is much larger than a_{res} . This means that only a small fraction $f = a_{\text{res}}/l_{\text{res}}$ of the flowing electrons will create a pair and the bulk of them pass through the resonance region without any interactions with photons.

In sum, $f \ll 1$ positrons are created per unit electron flowing through the circuit. The created positrons will flow from the resonance region to the cathode. This backflow carries a current fj . The charge density created by the positron backflow is fj/c , which is

$$\rho_+ = \frac{a_{\text{res}}}{l_{\text{res}}} \frac{j}{c}. \quad (41)$$

This charge density creates a potential drop,

$$\Delta\Phi = 2\pi \frac{a_{\text{res}}^3}{l_{\text{res}}} \frac{j}{c}. \quad (42)$$

The linear-accelerator configuration becomes inconsistent if $e\Delta\Phi > \gamma_{\text{res}}m_e c^2$ — then the created positrons will screen the initially assumed potential drop between the resonance region and cathode. This condition may be written as

$$l_{\text{res}} < \frac{1}{2} \gamma_{\text{res}}^2 \zeta L. \quad (43)$$

We can evaluate it by substituting $L = R_{\text{NS}} = 10$ km and expressing l_{res} in terms of a luminosity $dL_X/d\ln\omega = \hbar\omega_X n_X$. Using the idealized example of a twisted dipole magnetosphere with the corresponding expression (20) for ζ , one finds

$$\frac{dL_X}{d\ln\omega_X} > 4 \times 10^{33} B_{15}^{-1/2} (\Delta\phi)^{1/2} \sin\theta \left(\frac{\hbar\omega_X}{1 \text{ keV}} \right)^3 \text{ ergs s}^{-1}. \quad (44)$$

The linear accelerator configuration is inconsistent if this condition is satisfied at some $\hbar\omega_X$. One can see that it is most easily satisfied at the blackbody peak $\hbar\omega_X \sim 1$ (the observed blackbody luminosity is $\sim 10^{35}$ erg/s).

Note that even if the linear-accelerator state were formally allowed as a self-consistent solution, the coronal circuit would not have to evolve to this state. Indeed, if the voltage in the circuit evolves gradually to higher and higher values, an e^\pm discharge occurs well before the linear accelerator could be established. We now consider the circuit that operates on e^\pm discharge, at a much lower voltage compared to the linear accelerator.

5.3. Discharge via Pair Breakdown

The development of pair breakdown may be illustrated with the following toy model. Suppose a uniform electric field E is fixed in the tube of size L . To start, we introduce one seed electron at the cathode with zero velocity. The electron accelerates toward the anode and its Lorentz factor γ_e grows. The toy model assumes that the electron creates a pair when it reaches a certain threshold

γ_{res} . At this point, the electron energy is shared between three particles, so the energy of the original electron is reduced. In this illustration we use a random energy distribution between the three particles with the mean values of $1/2$, $1/4$, and $1/4$ of $\gamma_{\text{res}}m_e c^2$. This introduces stochasticity in the pair breakdown.¹⁰

The key parameter is a_{res}/L where

$$a_{\text{res}} = \frac{(\gamma_{\text{res}} - 1)m_e c^2}{eE}$$

is the length of electron (or positron) acceleration to the energy $\gamma_{\text{res}}m_e c^2$, starting from rest. The necessary condition for breakdown is $a_{\text{res}}/L < 1$ — otherwise the seed electron reaches the anode before gaining enough energy for pair creation.

The development of the pair breakdown is shown in a spacetime diagram in Figure 5. Each pair-creation event gives two new particles of opposite charge, which initially move in the same direction. One of them is accelerated by the electric field and lost at the boundary after a time $< L/c$, while the other is decelerated and can reverse direction before reaching the boundary. After the reversal, the particle is accelerated toward the opposite boundary and creates at least two new particles, one of which can reverse direction etc. This reversal of particles in the tube allows the e^\pm plasma to be continually replenished. In the super-critical state (left panel in Fig. 5) more than one reversing particle is created per passage time L/c and an avalanche develops exponentially on a timescale $\sim a_{\text{res}}/c$. In the near-critical regime shown in the right panel of Fig. 5, just one reversing particle is created per passage time L/c . This critical state is unstable: sooner or later the avalanche will be extinguished.

This toy model is very idealized because it assumes a fixed electric field E . In reality, the behavior of E is coupled to the charge density in the tube, which is determined by the particle dynamics and the boundary conditions $j = j_B$. E changes on a timescale much shorter than L/c and the behavior of the coupled plasma and electric field is complicated.

The toy model, however, shows an essential property of the e^\pm breakdown: it is a critical stochastic phenomenon. Above a critical voltage pair creation proceeds in a runaway manner, and the current and the dissipation rate would run away if the voltage were fixed. Below the critical voltage pairs creation does not ignite. The criticality parameter is $L/a_{\text{res}} = e\Phi_e/(\gamma_{\text{res}} - 1)m_e c^2$. The tube with enforced current at the boundaries must self-organize to create pairs in the near-critical regime $e\Phi_e \sim \gamma_{\text{res}}m_e c^2$ and maintain the current.

If the current demanded by $\nabla \times \mathbf{B}$ is not maintained, the induction voltage will grow until it exceeds the critical value $e\Phi_e \sim \gamma_{\text{res}}m_e c^2$ (corresponding to $a_{\text{res}} \sim L$) and a pair breakdown

¹⁰In reality there are other sources of stochasticity, in particular, the random free-path to resonant scattering with a mean value $l_{\text{res}}(\gamma_e)$. It is taken into account in the numerical experiment described below (§ 5.3). For the illustrative purposes of this section, it is sufficient to introduce any random element in the pair creation process to make it stochastic.

develops. Avalanches of e^\pm then supply plasma that tends to screen the electric field by conducting the necessary current, and the voltage in the tube is reduced. The discharging tube is similar to other phenomena that show self-organized criticality, e.g., a pile of sand on a table (Bak, Tang, & Weisenfeld 1987). If sand is steadily added, a quasi-steady state is established with a characteristic mean slope of the pile. The sand is lost (falls from the table) intermittently, through avalanches — a sort of “sand discharge.” In our case, charges of the opposite signs are added steadily instead of sand (fixed j at the boundaries), and voltage $\Phi_e = EL$ plays the role of the mean slope of a pile. The behavior of the discharging system is expected to be time-dependent, with stochastic avalanches.

A steady state is not expected for a pair-creating circuit for two reasons: (1) The created pairs may not maintain a static electric field. Like the Carlqvist double layer, a self-consistent static voltage must be huge, much above the critical value tolerated by pair discharges. No static solution exists at modest voltages because it implies a slow particle acceleration and a large charge imbalance in a broad region, leading to inconsistency (see the end of § 4.3). (2) The near-critical behavior is unstable: either a runaway is ignited or pair creation extinguishes soon after a seed particle is injected.

Breakdown discharges are well known in tubes with low-temperature plasma, which is weakly ionized. In that case, the critical voltage accelerates electrons to the ionization threshold and avalanches of ionization develop. Charge carriers are then supplied by ionization rather than pair creation. Another difference is that the fast electrons are lost to the cylindrical wall of the tube, so the problem is not 1-D, and coherent waves of ionization can develop.

5.4. Numerical Simulations

5.4.1. Setup

We implement the pair-creation process in our numerical experiment in a simple way: electrons (or positrons) can create pairs if their Lorentz factors are in a specified range $\gamma_1 < \gamma_e < \gamma_2$. The mean free-path for e^\pm emission by an accelerated electron in this window, l_{res} , is a parameter of the experiment. It determines the probability of pair creation by the electron during a timestep dt : this probability is cdt/l_{res} . Note that $\lambda_{De} \ll l_{\text{res}} \ll R_{\text{NS}}$.

In a real magnetosphere, the resonance window $\gamma_1 < \gamma_e < \gamma_2$ is shaped by the spectrum of target photons F_ω and the local magnetic field B . In our simplified model, this window is constant along the magnetic line. It is possible to use a more realistic resonance condition that takes into account variations in B and F_ω along a magnetospheric field line. However, our major goal is to see whether e^\pm creation leads to a qualitatively different state of the circuit. We shall see that the new state weakly depends on the details of the resonance condition when $B > B_{\text{QED}}$ and $\gamma_{\text{res}} \gg 1$ everywhere in the circuit.

We consider here only circuits with boundary temperatures too low for plasma to be supplied thermally. Then the circuit solution weakly depends on the chosen values of T_i and T_e . In this section, we show a sequence of models with $k_B T_e = 0.04 m_e c^2$ and $k_B T_i = 0.04 m_i c^2$. The corresponding scale height of the surface layers is $h = 0.04 L$.

To illustrate the weak dependence on details of the pair creation process we consider the two extreme cases of very efficient and very inefficient e^\pm creation. Pair creation is less efficient if the resonant window (γ_1, γ_2) is narrow and the mean free-path l is large even in this window. We therefore focus on two models: Model A: an infinitely wide resonance window $(\gamma_{\text{res}}, \infty)$ with free path $l = 0$ and Model B: a narrow resonance window $(\gamma_{\text{res}}, 2\gamma_{\text{res}})$ with a large mean free path $l = L/3$. The inclusion of pair creation brings two new parameters into the experiment: γ_{res} and l . We are especially interested in values of γ_{res} that are comparable to or below m_i/m_e , which corresponds to a real magnetosphere.

5.4.2. Results

The results of the numerical experiments are shown in Figures 6-14. Figure 6 displays the relation between current j and voltage Φ_e in a circuit with $m_i = 10 m_e$ and $\gamma_{\text{res}} = 10$. The current is normalized to a minimum current j_* for which the characteristic Debye length $\lambda_{De} = c/\omega_P$ equals the size of the system L (see eq. [21]). At small j_B , the double layer configuration is established in the circuit; its voltage is not sufficient to ignite e^\pm production. With increasing j_B , the voltage of the double layer increases as $(j_B/j_*)^{1/2}$ and reaches $\gamma_{\text{res}} m_e c^2$ at $j_1 \simeq j_* \gamma_{\text{res}}^2$; then it stops growing. At $j_B > j_1$ the voltage saturates at the characteristic $e\Phi_e \sim \gamma_{\text{res}} m_e c^2$ in both Models A and B. This asymptotic regime $j_B \gg j_1$ is of interest to us because magnetars are in this regime. All subsequent figures show the asymptotic behavior at $j_B \gg j_1$.

Each point in Fig. 6 is obtained by running a time-dependent simulation that relaxes to a quasi-steady state. Figures 7 and 8 show the relaxation history in two simulations with $j_B = 10^4 j_*$. The voltage Φ_e is zero in the initial state and grows on the dynamical timescale $t_{\text{dyn}} = L/c$ while the plasma and electric field self-organize to maintain the required current. The voltage grows until electrons in the circuit get accelerated to Lorentz factors $\gamma_e \sim \gamma_{\text{res}}$ and pair production begins. One can see that after a few dynamical times the voltage Φ_e stops growing and the circuit enters an oscillatory regime. During each oscillation, an increased voltage leads to a higher e^\pm production rate \dot{N}_+ , then too many e^\pm are produced which screen the voltage (discharge), \dot{N}_+ drops, and Φ_e begins to grow again. The oscillations persist until the end of the simulation ($40L/c$), with a constant amplitude.

We see that a quasi-steady state is reached after a few t_{dyn} . This state is time-dependent on short timescales, but it has a well-defined steady voltage when averaged over a few t_{dyn} . Models A and B have similar histories of Φ_e and \dot{N}_+ (cf. Figs. 7 and 8) except that Model A is noisier on short timescales and shows less coherent oscillations. (The quasi-periodic oscillations are, however,

pronounced in the Fourier spectra of $\Phi_e[t]$ and $\dot{N}_+[t]$.)

It is not surprising that Φ_e may vary on short timescales $t \ll t_{dyn}$. The voltage may change very quickly in the circuit simply by moving a modest number of charges across the boundaries. A characteristic voltage $e\Phi_e = m_e c^2$ that is able to accelerate electrons may be created on timescales as short as $t = m_e c^2 / 4\pi e L j_B = (j_B/j_*)^{-1} (L/c) \ll L/c$.

In all circuits of interest ($j_B \gg j_1$) we found the time-average voltage,

$$e\bar{\Phi}_e \sim \gamma_{res} m_e c^2. \quad (45)$$

This relation applies even to circuits with $\gamma_{res} m_e c^2 \gg m_i c^2$, where lifting of the ions is energetically preferable to pair creation. We conclude that *the voltage along the magnetic tube is self-regulated to a value just enough to maintain pair production and feed the current with e^\pm pairs*. The robustness of this result is illustrated in Figure 9, which shows circuits with $m_i/m_e = 10, 30$ and various γ_{res} . In all cases, $e\bar{\Phi}_e \sim \gamma_{res} m_e c^2$ is established, and the pair creation rate $2\dot{N}_+ \sim j_B/e$ is maintained. Thus, the near-critical state is self-organized as expected. Avalanches of e^\pm creation are observed to happen anywhere in the circuit between the dense boundary layers.

The current is carried largely by e^\pm everywhere in the tube. The ion fraction in the current depends on the ratio $e\bar{\Phi}_e/m_i c^2 \simeq \gamma_{res} m_e/m_i$ (Fig. 10). If this ratio is small, pairs are easily produced with a small electric field, too small to lift the ions, and the ion current is suppressed. In the opposite case, ions carry about 1/2 of the current. For typical parameters expected in the magnetosphere, $\gamma_{res} \lesssim m_i/m_e$, ions carry $\lesssim 10\%$ of the current.

The simulations also show that the released energy sinks through the anode and cathode boundaries at approximately equal rates, and that their sum is equal to $j_B \bar{\Phi}_e$. For magnetars, this implies that both footpoints of a twisted magnetic tube will radiate energy bolometrically at comparable rates.

5.4.3. Sample Model

We now describe in more detail the plasma behavior in one sample experiment. It assumes Model A for e^\pm creation and $\gamma_{res} = m_i/m_e = 10$.¹¹ The relaxation history of this experiment is shown in Figure 7, and a snapshot of the circuit is shown in Figure 11.

The charge density $\rho = e(n_i + n_p - n_e)$ and electric field are found to fluctuate significantly in time, while the densities n_i , n_p , and n_e are approximately steady. Deviations from charge neutrality are small: $\rho/e(n_i + n_p + n_i) \ll 1$ and $E^2/8\pi U_{pl} \ll 1$ where U_{pl} is the plasma kinetic energy density. The plasma turbulence is then linear to a first approximation and may be described

¹¹A similar solution is obtained for $\gamma_{res} = m_i/m_e = 30$. We expect the same circuit solution to apply to $\gamma_{res} = m_i/m_e = 1836$ or any other $\gamma_{res} = m_i/m_e \gg 1$.

as a superposition of Langmuir waves. We do not, however, attempt a development of analytical theory in this paper.

The anode current $j_e + j_i + j_p$ is dominated by electrons. The anode value of j_e even exceeds j_B by 17%. Together with ions ($j_i \simeq 0.13j_B$), electrons balance the negative current of positrons $j_p \simeq -0.3j_B$ so that the net current $j_e + j_i + j_p$ equals j_B . Positrons contribute negative j_p at the anode because energetic positrons moving in the “wrong” direction are created by accelerated electrons, and are able to leave the box against the mean electric field. The cathode current is dominated by positrons (64%); electrons contribute 23%, and ions 13%.

Bulk speeds of the three plasma components, v_e , v_i , v_p , and the dispersions of their dimensionless momenta $p/mc = \gamma\beta$ are shown in Figures 12 and 13. The dispersions are significant, which implies broad distribution functions.

The time-averaged distribution of pair creation over z is shown in Figure 14. It has two peaks: one is pair production by accelerated electrons and the other one is pair production by accelerated positrons. The net rate of pair-creation by e^- is about 2 times higher than that by e^+ .

A complicated kinetic state self-organizes in the phase space of electrons, ions, and positrons. The state keeps oscillating. The oscillations might be related to the fact that positrons move in a wrong direction at creation (negative current) and have to reverse direction to maintain the net $j = j_B$ without strong deviations from neutrality. This requires an extra voltage which leads to “overshooting” in the pair creation rate followed by a temporary screening of the electric field.

6. TRANSITION LAYER

The transition layer between the corona and the relatively cold atmosphere of the star is collisionless and optically thin. Its temperature can be much greater than the surface blackbody temperature $k_B T_{\text{bb}} \sim 0.5$ keV. This transition region may play a crucial role for two reasons.

1. It can radiate away the energy received from the corona because it is dense enough for efficient bremsstrahlung emission. The corona itself cannot radiate most of its dissipative power: two-body collisions are negligible there, and photons emitted by Landau de-excitation are too energetic and cannot get out — they are immediately converted to pairs in the ultra-strong magnetic field.
2. It may be hot enough to maintain thermal pair creation at an interesting rate. The pairs may expand above the surface and feed the charge flow in the coronal circuit (Thompson & Beloborodov 2005).

A detailed analysis of the transition layer is left for future work. Below we describe some key mechanisms by which energy is deposited and redistributed within the layer, and by which e^\pm pairs may be created.

6.1. Heating by Beam Instability

6.1.1. Formation of a plateau in the particle distribution function

The particles accelerated in the corona enter the hydrostatic atmosphere with high Lorentz factors $\gamma_b \sim e\Phi_e/m_e c^2$. This relativistic beam drives an electrostatic instability, which may be described by the standard quasi-linear theory of beam relaxation. The growth length for an electrostatic beam instability in the thermal atmosphere (density n_e) is (e.g. Godfrey, Shanahan, & Thode 1975)

$$l_b \sim \gamma_b \left(\frac{n_e}{n_b} \right)^{1/3} \frac{c}{\omega_{Pe}} = \frac{\gamma_b}{(4\pi n_b r_e)^{1/2}} \left(\frac{n_b}{n_e} \right)^{1/6}. \quad (46)$$

Here $\omega_{Pe} = (4\pi n_e e^2/m_e)^{1/2}$ is the electron plasma frequency in the atmosphere, and $r_e = e^2/m_e c^2 \simeq 2.8 \times 10^{-13}$ cm. The beam exponentially amplifies a seed Langmuir wave whose phase speed is in resonance with the beam. The exchange of energy with the atmospheric plasma occurs on a scale comparable to l_b . As the beam propagates a distance $\sim lb$ into the layer, the amplified Langmuir waves feed back on the beam and flatten its distribution function to a plateau. If the initial distribution function of the beam is idealized by δ -function, $f_b(\gamma_e) = \text{const} \delta(\gamma_e - \gamma_b)$, its relaxation to the plateau $1 < \gamma_e < \gamma_b$ implies the deposition of $\frac{1}{2}$ of the beam energy into plasma turbulence. Since the relaxation occurs in a strong magnetic field, the particle momentum distribution remains one-dimensional. This is different from beam relaxation in a normal plasma — in that case a large dispersion of perpendicular momenta develops before relaxing to the plateau in energy.

The coronal beam has a density $n_b \sim n_c = j_B/ec \sim 10^{16} \text{ cm}^{-3}$ and Lorentz factor $\gamma_b \simeq \gamma_{\text{res}} \sim 10^3$ (see § 5; this beam density corresponds to a total energy deposition rate of $10^{36} \gamma_{b,3} \text{ erg s}^{-1}$ over the surface of the star). Substituting these values to equation (46) one finds $l_b \sim 1$ cm. The beam relaxation occurs at a much larger depth than the skin depth of the atmospheric plasma, $l_b \gg c/\omega_P$. Therefore, the beam instability may heat the atmosphere only well below the screening layer in which particles are lifted to the magnetosphere by an induced electric field.

In our numerical experiments $l_b \sim 10(c/\omega_P) \sim 0.1L$ was larger than the scale height of the atmosphere, h , so heating by beam instability could not possibly operate. The possible atmospheric heating at larger depths was regulated in the experiment by hand, by setting the boundary temperatures T_e and T_i . Further investigation of beam heating is deferred to a future work.

Comparing the expected l_b and h , one has

$$\frac{l_b}{h} \sim \left(\frac{n_b}{n_e} \right)^{1/6} \left[\frac{k_B(T_e + T_i)}{\text{keV}} \right]^{-1}. \quad (47)$$

Note that l_b/h is reduced if the plasma temperature grows. It is possible that the atmosphere develops a hot layer with $l_b \ll h$, which absorbs a significant part of the beam energy. The excited Langmuir turbulence heats mostly electrons and T_e may grow to $k_B T_e \gtrsim 100$ keV. Then significant hard X-ray emission and thermal pair creation may set in as discussed below.

6.1.2. Comparison with Radio Pulsars

Observations of X-ray emission from radio pulsars provide evidence for thermally emitting hotspots with an area that is consistent with the surface area of the magnetic poles (De Luca et al 2005). Pair creation in the polar cap regions of a radio pulsar is thought to trigger a stochastic return current (Harding & Muslimov 2002). This return current is carried by charges of the opposite sign to ρ_{co} . Their density n_{down} can be referenced to the corotation charge density via a multiplicity \mathcal{M} ,

$$n = \mathcal{M}\rho_{\text{co}} = \mathcal{M}\frac{\Omega B_{\text{pole}}}{2\pi ec}, \quad (48)$$

where B_{pole} is the polar surface magnetic field. One finds that $\mathcal{M}_{\text{down}} \sim 1$ and that the mean kinetic energy $\gamma_{\text{down}} m_e c^2$ of the returning beam is comparable to the electrostatic potential energy at which the upward-moving beam creates pairs. Then one finds,

$$\frac{l_b}{h} = 0.02 \frac{\gamma_{\text{down}}}{\mathcal{M}_{\text{down}}^{1/2}} \left(\frac{k_B T_e}{\text{keV}} \right)^{-1} \left(\frac{g_{14} P_{-2}^{1/2}}{B_{\text{pole},12}^{1/2}} \right) \left(\frac{n_{\text{down}}}{n_e} \right)^{1/6}. \quad (49)$$

Substituting $\gamma_{\text{down}} \sim 10^6 - 10^7$ and $\mathcal{M}_{\text{down}} \sim 1$ for an ordinary radio pulsar ($B_{\text{pole}} \sim 10^{12}$ G) shows that the growth length is far too large to induce significant electrostatic heating in the atmosphere. The beam must therefore be stopped by Coulomb collisions and relativistic bremsstrahlung at a greater depth in the crust. The polar region of the pulsar surface can be expected to release the beam energy in the form of blackbody radiation.

The conclusion is different in the magnetar circuit. If we express the beam density in terms of ρ_{co} , which is small for magnetars, it will correspond to a large multiplicity $\mathcal{M}_{\text{down}} \sim R_{\text{lc}}/R_{\text{NS}} \sim 10^4$. The magnetic field is much stronger, $B_{\text{pole},12} \sim 10^2 - 10^3$, and, in common with strongly magnetic radio pulsars (Hibschman & Arons 2001), the acceleration of magnetospheric particles is limited by resonant upscattering of the thermal photons to an energy no larger than $\gamma_{\text{res}} m_e c^2$. All these three factors lead to a relatively small l_b , so that an efficient heating of the upper atmosphere becomes possible.

6.2. Thermal Conduction and Radiative Losses

If the twisted magnetic tube were thermally insulated, it would quickly heat up and remain filled with a thermal plasma that would steadily conduct the current with no further dissipation. Losses of the dissipated energy are therefore crucial in the regulation of the state of the circuit. In our numerical experiment we simply allowed the released energy to sink through the anode and cathode boundaries, assuming that it is radiated away outside our boundaries. Here we discuss a possible mechanism of the energy loss.

We expect the energy released in the corona to be deposited in an optically thin atmospheric layer by collisionless processes (such as beam instability). This layer is not able to cool radiatively,

and the deposited heat will be conducted to deeper and denser layers that can radiate the heat away by bremsstrahlung (Thompson & Beloborodov 2005). The radiation flux emitted at that depth is $F_\gamma \sim h\epsilon_{\text{ff}}$ where h is a characteristic scale-height and ϵ_{ff} is the free-free emissivity. Plasma with temperature T_e and density n_e has the emissivity

$$\epsilon_{\text{ff}} = \left(\frac{2}{\pi}\right)^{3/2} \alpha \theta_e^{1/2} n_e^2 \sigma_{\text{T}} m_e c^3, \quad \theta_e \equiv \frac{k_{\text{B}} T_e}{m_e c^2}, \quad (50)$$

where $\alpha = e^2/\hbar c = 1/137$ is the fine structure constant. The characteristic scale-height on which density and temperature change in the layer is the hydrostatic scale-height, so $h = k_{\text{B}} T_e / m_i g$ (we assume here $T_e < T_i$ since the collisionless dissipation heats mostly electrons. Then the emitted radiation flux is

$$F_\gamma = h\epsilon_{\text{ff}} = \left(\frac{2}{\pi}\right)^{3/2} \alpha \frac{m_e}{m_i} \theta_e^{3/2} \frac{c^2}{g} n_e^2 \sigma_{\text{T}} m_e c^3. \quad (51)$$

The radiation carries away a significant fraction of the energy flux from the corona when $F_\gamma \sim F = n_c \gamma_b m_e c^2$, where $\gamma_b = e\Phi_e / m_e c^2 \simeq \gamma_{\text{res}}$. This gives one relation between temperature $\theta_e = k_{\text{B}} T_e / m_e c^2$ and Thomson optical depth $\tau_{\text{T}} = h\sigma_{\text{T}} n_e$ at which the heat flux is converted to radiation,

$$\theta_e^{-1/2} \tau_{\text{T}}^2 \simeq \frac{\tau_c \gamma_b}{\alpha} \frac{m_e}{m_i} \frac{c^2}{g R_{\text{NS}}}, \quad (52)$$

where

$$\tau_c \equiv R_{\text{NS}} \sigma_{\text{T}} n_c \sim 0.01 - 0.1. \quad (53)$$

Equation (52) is not sufficient to determine θ_e and τ_{T} of the emitting layer because the mechanism of heat transport to this layer has not been specified yet. A second relation is needed, which is the equation of thermal conductivity (Thompson & Beloborodov 2005). It relates the heat flux $F_c \sim F \sim F_\gamma$ to the temperature gradient: $F_c = \kappa dT_e/dz$ where $\kappa = n_e v_e \ell k_{\text{B}}$, $v_e = (k_{\text{B}} T_e / m_e)^{1/2}$, and ℓ is the mean free path of electrons. In the absence of plasma turbulence, the mean free path is determined by Coulomb collisions,

$$\ell_{\text{Coul}} = \frac{\theta_e^2}{n_e \sigma_{\text{T}}}. \quad (54)$$

If strong plasma turbulence develops with energy density above the thermal level, $U_{\text{turb}} = (\delta E_{\parallel})^2 / 8\pi \gg k_{\text{B}} T_e / \lambda_{\text{De}}^3$, the fluctuating electric field suppresses the mean free path. It is then given by

$$\ell \simeq \lambda_{\text{De}} \left(\frac{U_{\text{turb}}}{n_e k_{\text{B}} T_e} \right)^{-1}. \quad (55)$$

(We here assumed that the turbulence develops at frequencies $\omega \sim \omega_{Pe}$.) We will keep ℓ as a parameter in our estimates. It is bounded from above and below by $\lambda_{\text{De}} < \ell < \ell_{\text{Coul}}$.

Estimating $dT_e/dz \sim T_e/h$, one finds

$$F_c = n_e v_e \ell \frac{k_{\text{B}} T}{h} = n_e v_e \ell g m_i, \quad (56)$$

$$\theta_e^{-3} \tau_T^2 \simeq \frac{1}{\alpha} \left(\frac{\ell}{\ell_{\text{Coul}}} \right). \quad (57)$$

Combining equations (52) and (57), one finds the temperature of the radiating layer,

$$\begin{aligned} \theta_e &\simeq \left(\tau_c \gamma_b \frac{m_e}{m_i} \frac{c^2}{g R_{\text{NS}}} \frac{\ell_{\text{Coul}}}{\ell} \right)^{2/5}, \\ k_B T_e &\sim 200 \left(\frac{\tau_c}{0.1} \right)^{2/5} \left(\frac{\gamma_b}{10^3} \right)^{2/5} \left(\frac{\ell}{\ell_{\text{Coul}}} \right)^{-2/5} \text{ keV}. \end{aligned} \quad (58)$$

If $\ell < \ell_{\text{Coul}}$ (suppressing heat conduction) the emission temperature will grow above 200 keV. The growth, however, will be quickly stopped at $\theta_e \sim 1$ because the hot layer starts to generate e^\pm pairs which can short out the circuit (see § 6.4).

6.3. Anomalous Resistivity and Hydrostatic Equilibrium

In addition to the heating by the relativistic beam that comes from the corona, the atmosphere may experience a significant anomalous heating in response to the strong electric current. This type of heating is known to occur in astrophysical and laboratory plasmas when the drift speed of the current-carrying electrons, v_d , exceeds the sound speed $c_s = (k_B T_e / m_i)^{1/2}$ (e.g. Bernstein & Kulsrud 1961). If the electron current can be described as a shift of a Maxwellian distribution with respect to the ions in velocity space, $\Delta v_e = v_d$, a positive gradient $df_e/dv_e > 0$ appears in the electron distribution function viewed from the rest-frame of the ion component. The positive gradient exists at $v_e < v_d$ and will amplify slow plasma modes with phase speed along the magnetic field $\omega/k_\parallel < v_d$. The dispersion relation of ion-sound waves gives $\omega/k_\parallel = c_s (1 + k^2 \lambda_{De}^2)^{-1/2}$ and they are easily amplified when $v_d > c_s$. The excited ion-sound turbulence creates the anomalous resistivity and heating.

With an increasing level of turbulence, $U_{\text{turb}}/n_e k_B T_e$, the mean free path of the electrons ℓ decreases according to equation (55). This implies a higher resistivity and a lower thermal conductivity. Thus, a reduced ℓ leads to a strong anomalous heating and the suppression of heat conduction out of the layer. It is then possible that the layer is overheated, loses hydrostatic balance, and expands in a runaway manner. We now estimate the critical ℓ for this to happen. We neglect the radiative losses in this estimate.

The ohmic heating rate per unit area of the layer is

$$F_{\text{Ohm}} \simeq h \frac{j^2}{\sigma}, \quad (59)$$

where $h = k_B T_e / m_i g$,

$$\sigma = \frac{n_e e^2 \ell}{m_e v_e}, \quad (60)$$

is electrical conductivity, and $v_e = (k_B T_e / m_e)^{1/2}$ is electron thermal speed. The conductive heat loss F_c is given by equation (56), and we find

$$\frac{F_{\text{Ohm}}}{F_c} = \left(\frac{m_e}{m_i} \right)^2 \left(\frac{c^2}{g R_{\text{NS}}} \right)^2 \frac{\tau_c^2}{\theta_e^3} \left(\frac{\ell}{\ell_{\text{Coul}}} \right)^{-2}, \quad (61)$$

Hence the layer must be overheated if

$$\frac{\ell}{\ell_{\text{Coul}}} < 2 \times 10^{-3} \theta_e^{-3/2} \tau_c. \quad (62)$$

Here $\tau_c = \sigma_T R_{\text{NS}} j / c e \sim 10^{-1} - 10^{-2}$ (§ 6.2), and the temperature is limited by pair creation to $\theta_e \lesssim 1$ (see § 6.4 below). One can see that the ohmic overheating requires a high level of plasma turbulence, when the mean-free path is strongly reduced compared to the Coulomb value. This level is achievable in principle because it is still below the upper limit $U_{\text{turb}} / n_e k_B T_e \sim 1$ that corresponds to the minimum $\ell \sim \lambda_{\text{De}}$. Indeed,

$$\frac{\lambda_{\text{De}}}{\ell_{\text{Coul}}} \simeq \frac{4}{3} \pi^{1/2} \left(\frac{n_e r_e^3}{\theta_e} \right)^{1/2} = \left(\frac{2}{3} \right)^{1/2} \frac{\tau_T^{1/2}}{\theta_e} \left(\frac{g r_e}{c^2} \frac{m_i}{m_e} \right)^{1/2} \simeq 2 \times 10^{-7} \frac{\tau_T^{1/2}}{\theta_e}. \quad (63)$$

Note that anomalous heating becomes interesting only when the thermal heat flux is strongly suppressed. In other words, F_{Ohm} may compete with F_c and overheat the layer only when F_c is small. One can derive from the above formulae,

$$\frac{F_{\text{Ohm}}}{F_c} \simeq \left(\frac{F_c}{4 \times 10^{22} \tau_c \theta_e \text{ erg s}^{-1} \text{ cm}^{-2}} \right)^{-2}. \quad (64)$$

Substituting $\tau_c \sim 10^{-1} - 10^{-2}$ and $\theta_e \lesssim 1$ one finds that the maximum energy flux one could possibly get from the ohmically-heated layer is $F_c \sim 10^{21} \text{ erg s}^{-1} \text{ cm}^{-2}$. Even if the layer covers the whole star with area $4\pi R_{\text{NS}}^2 \simeq 10^{13} \text{ cm}^2$, its total power would not exceed $10^{34} \text{ erg s}^{-1}$. This is two orders of magnitude smaller than the observed luminosity of the corona, and hence the anomalous heating of the atmosphere is unlikely to generate the observed activity.

Note that the marginally stable state $F_{\text{Ohm}} = F_c$ has the electrostatic potential drop across the layer $e\delta\Phi_e \sim k_B T_e$ (it equals the energy gained by an electron crossing the layer). Since T_e is limited by pair creation, the maximum potential drop that can be sustained by the layer is $\sim m_e c^2$. This is at least 2 orders of magnitude lower than the voltage $\gamma_{\text{res}} m_e c^2$ that is developed in the corona with e^\pm discharges. Therefore, if the turbulence in the transition layer reaches the level required for runaway heating, the plasma may be supplied to the corona at a much lower voltage, and therefore at a much lower dissipation rate.

Pair creation in the atmosphere (see § 6.4 below) would tend to reduce its mean molecular weight and increase h . When the expressions for F_{Ohm} and F_c are modified to include the pair density, $n_e \rightarrow n_e + n_\pm$, one finds that the critical value of ℓ/ℓ_{Coul} for runaway heating (eq. 62) increases as $1 + n_\pm/n_e$. The pair density is unlikely to exceed a critical value $n_* \sim n_c(h/\ell)$ at

which the diffusive flux of hot e^\pm out of the atmosphere dominates the corona and shortens out the electric circuit. One finds the relation

$$\frac{F_{\text{Ohm}}}{F_c} = \left(\frac{n_*}{n_e + n_\pm} \right)^2 \frac{1}{\theta_e}. \quad (65)$$

At sufficiently high $\theta_e \sim 1$, the pair density may approach the maximum value $n_\pm \sim n_*$. If the atmosphere enters the regime $n_\pm \sim n_*$ and $n_* > n_e$, then Ohmic heating would be suppressed according to equation (65). Perhaps a cyclic overheating with strong pair enrichment would occur.

The effects discussed in this and previous sections indicate the possibility of an alternative way of forming the corona, through heating and pair creation in the atmosphere. This would require a high level of turbulence in the atmospheric plasma, and it is unclear whether this level is reached. Observations of the high-energy tail of the X-ray spectrum may help to constrain the composition and temperature of the transition layer of magnetars.

6.4. Heated Atmospheric Layer as a Possible Source of e^\pm

6.4.1. Channels of Pair Creation

The dominant channels of thermal pair creation in a hot atmosphere involve an electron-ion collision. There are three such channels which we summarize below.

1. An e^\pm pair can be created directly in a collision between an ion and an energetic electron (or positron), $e^- + Z \rightarrow e^- + e^- + e^+$. This reaction is possible when the kinetic energy of the incident electron exceeds a threshold

$$E_{e,\text{thr}} = 2m_e c^2, \quad (66)$$

as both e^- and e^+ can be created in the lowest Landau state. When the temperature $k_B T_e \ll 2m_e c^2$, the reaction occurs in the high-energy tail of the electron distribution.

2. A bremsstrahlung photon can be emitted in an electron-ion collision, almost always in the ordinary polarization mode. The threshold energy for conversion of the O-mode photon to a pair is given by

$$E_{\gamma,\text{thr}} = \frac{2m_e c^2}{\sin \theta_{kB}}, \quad (67)$$

where θ_{kB} is the angle of photon propagation with respect to the magnetic field. (O-mode photons can convert to a pair with both particles in the lowest Landau state; e.g. Daugherty & Harding 1983.) The threshold for pair creation is $E'_\gamma > 2m_e c^2$ in the frame where photon propagates perpendicular to \mathbf{B} , and is larger by a factor $1/\sin \theta_{kB}$ in the lab frame.

This second channel of pair creation is similar to the first one, where a virtual photon converts directly to a pair during the electron-ion collision. The emission of a real bremsstrahlung photon

makes the process two-step and increases its threshold from $2m_e c^2$ to $2m_e c^2 / \sin \theta_{kB}$. The cross-section for bremsstrahlung emission of a \sim MeV photon by an electron of energy $\sim 1 - 2$ MeV is (Berestetskii, Lifshitz & Pitaevskii 1982)

$$\sigma_{\text{bremss}} = 0.3 Z^2 \alpha \sigma_T. \quad (68)$$

By contrast, the cross-section for direct $e^+ -$ production is smaller by an additional factor of α . In the absence of the magnetic field, both processes involve a momentum transfer $Q \sim m_e c$ transverse to the direction of the incident electron. Since this value of Q is smaller than the momentum $p_\perp = 2^{1/2}(B/B_{\text{QED}})^{1/2} m_e c$ of the first Landau excitation, both cross sections will be modified in the presence of the magnetic field. The corresponding calculations have not yet been carried out and the exact cross sections are not known.

Note that bremsstrahlung emission is preferentially beamed along \mathbf{B} , in the direction of the incident electron, so θ_{kB} may be small. Then the threshold is substantially higher than $2m_e c^2 \simeq 1$ MeV. If the photon propagates away from the emission site where \mathbf{B} has a different direction, the threshold may be reduced (θ_{kB} increases). Gravitational bending of the photon trajectory may also help the propagating photon to build up θ_{kB} . Then non-local pair creation will take place.

3. An electron can be side-scattered into the first Landau state by the Coulomb interaction with an ion. The excited electron rapidly emits an energetic photon in a dipole transition to the Landau ground state, and the photon converts to a pair. This channel requires the initial electron to have a minimum total energy

$$E_{e,\text{thr}} = E_B = \left[2 \left(\frac{B}{B_{\text{QED}}} \right) + 1 \right]^{1/2} m_e c^2 \simeq 6.7 B_{15}^{1/2} m_e c^2. \quad (69)$$

The side-scattering into the first Landau state involves a perpendicular momentum transfer $p_\perp = 2^{1/2}(B/B_{\text{QED}})^{1/2}$, and the corresponding Coulomb cross section is

$$\sigma_{\text{Coul}}(0 \rightarrow 1) \simeq \frac{4\pi Z^2 e^4}{(p_\perp c)^2} = \frac{3Z^2}{4} \left(\frac{B}{B_{\text{QED}}} \right)^{-1} \sigma_T. \quad (70)$$

For typical $B \sim (10 - 100)B_{\text{QED}}$, it is larger than the bremsstrahlung cross section by a factor ~ 10 (cf. eq. 68).

The energy of the de-excitation photon, $E_\gamma < E_B$, depends on its emission angle θ_{kB} with respect to the magnetic field. This dependence appears because Landau energy E_B exceeds $m_e c^2$ in the super-QED field and the de-exciting electron can experience a significant recoil. The released energy E_B is then shared between the emitted photon and the electron: $E_B = E_\gamma + E_e$.

The dependence $E_\gamma(\theta_{kB})$ is found from momentum and energy conservation: $E_\gamma \cos \theta_{kB} = c p_e$ and $E_\gamma + (c^2 p_e^2 + m_e^2 c^4)^{1/2} = E_B$, where p_e is the recoil momentum of the electron and it is taken into account that the electron can recoil only along \mathbf{B} . Eliminating p_e , one finds

$$E_\gamma(\theta_{kB}) = \frac{E_B}{\sin^2 \theta_{kB}} \left[1 - \left(1 - \sin^2 \theta_{kB} + \frac{m_e^2 c^4}{E_B^2} \sin^2 \theta_{kB} \right)^{1/2} \right]. \quad (71)$$

In the super-critical field, $B \gg B_{\text{QED}}$, this simplifies to

$$E_\gamma(\theta_{kB}) = E_B \frac{(1 - \cos \theta_{kB})}{\sin^2 \theta_{kB}}. \quad (72)$$

The de-excitation photon has the maximum energy $E_\gamma = E_B$ when it is emitted at $\theta_{kB} = \pi/2$ (no recoil) and the minimum energy $E_\gamma = E_B/2$ when $\theta_{kB} = 0$ (maximum recoil).

De-excitation photons are emitted in the O or E mode: the gyrational motion of the excited electron overlaps both linear polarization states. An O-mode photon will immediately convert to an e^\pm pair if it satisfies the threshold condition (67) (which is satisfied in a large range of θ_{kB} when $B \gg B_{\text{QED}}$). An E-mode photon with $E_\gamma < E_B$ cannot convert to a pair. It will, however, split in two daughter photons, at least one of which will be in O-mode (Adler et al. 1970) and can convert to a pair if above the threshold.¹²

6.4.2. Feeding the Corona with Atmospheric Pairs

The rate of pair creation in the atmosphere may be roughly estimated as the rate of electron-ion collisions above the threshold E_{thr} ,

$$\dot{n}_+ \sim n_i n_e(E_e > E_{\text{thr}}) \sigma c, \quad (73)$$

where σ and E_{thr} are the cross section and the threshold energy of the relevant channel, and

$$\frac{n_e(E_e > E_{\text{thr}})}{n_e} \simeq \frac{E_{\text{thr}}}{(T_e m_e c^2 / 2\pi)^{1/2}} \exp \left[-\frac{E_{\text{thr}}}{k_B T_e} \right] \quad (74)$$

is the density of 1-D electrons that have energy $E_e > E_{\text{thr}}$. Atmospheric pair production is able to feed the coronal current j_B if

$$\dot{N}_+ = h \dot{n}_+ > \frac{j_B}{e}, \quad (75)$$

or, equivalently,

$$\frac{n_e(E_e > E_{\text{thr}})}{n_e} \tau_T n_i \left(\frac{\sigma}{\sigma_T} \right) > n_c, \quad (76)$$

where $\tau_T = \sigma_T n_e h$. This condition may be rewritten using $\tau_c = R_{\text{NS}} \sigma_T n_c$ and $h = \theta_e (m_e/m_i)(c^2/g)$,

$$\theta_e \tau_T^2 \frac{n_e(E_e > E_{\text{thr}})}{n_e} > \left(\frac{\sigma}{\sigma_T} \right)^{-1} \left(\frac{R_{\text{NS}} g}{c^2} \right) \frac{m_i}{m_e} \tau_c. \quad (77)$$

¹²All three components of the momentum are conserved in the splitting process. Splitting is therefore allowed kinematically only for the mode with the smaller index of refraction n . In a super-QED magnetic field, n_O receives a (positive) correction $\propto \alpha(B/B_{\text{QED}})$ from vacuum polarization; whereas the correction to n_E is $\propto \alpha(B/B_{\text{QED}})^0$. Splitting of the O-mode is therefore kinematically forbidden even in the regime of moderately strong photon dispersion. See Baring & Harding (2001) for a treatment of pair cascades in the open-field region of radio pulsars with surface magnetic fields near B_{QED} , in which the effect of relaxing this kinematic selection rule is considered.

The thermal pair production may take place in the optically thin region $\tau_T < 1$. Using $\tau_c \sim 0.01 - 0.1$, one can show that a high $\theta_e \gtrsim 1/2$ is required. If the condition (77) is met at some depth τ_T , the atmospheric pairs will dominate the charge supply to the coronal circuit. The created pairs have kinetic energies $\sim k_B T_e$, comparable to $\sim m_e \Phi_g$, so e^\pm may overflow the gravitational barrier and maintain the current.

6.4.3. Numerical Models

In order to see how atmospheric pair production could affect the circuit, we have done a few numerical simulations using the following toy model. We assume that the atmosphere responds to the heat flux from the corona by producing e^\pm pairs. Therefore, in addition to the ion-electron atmosphere, we now maintain a thermal e^\pm atmosphere. Its density at each boundary is regulated in the experiment so that it is proportional to the flux of lost energy through the boundary.

If the supplied pairs were cold, the circuit would be in the same regime as in their absence. The fact that positrons are now available in the atmosphere to carry the current instead of ions does not lead to any significant reduction of the voltage across the circuit: it still evolves to the state with $e\Phi_e \simeq \gamma_{\text{res}} m_e c^2$, in which energetic e^\pm are supplied via the resonant-scattering channel. We have checked this by running the models with cold e^\pm atmospheres. With a very large $\gamma_{\text{res}} > \zeta^{-1}$ the circuit would evolve to the linear-accelerator state described in § 4.2.

The key property of atmospheric pairs is, however, that they are hot enough to feed the current thermally (cf. § 4.1). Their expected kinetic energy is comparable to the height of the gravitational barrier (§ 6.3) and a significant fraction of the supplied e^\pm can overflow the barrier. Therefore, the required current j_B can be conducted at a small voltage $e\Phi_e < \gamma_{\text{res}} m_e c^2$.

We have checked that the thermally-driven regime is indeed established in our experiment with a realistic $k_B T_\pm = 0.5 m_e c^2$. The established voltage then depends on the efficiency of pair supply in response to the energy flux from the corona. We define this efficiency as the fraction of the escaping energy that is returned in the form of e^\pm (kinetic plus rest-energy) and denote it by ξ . We find that the voltage across the circuit adjusts so that the flux of produced energy is just enough for the boundary to supply a minimum number ~ 1 of pairs per accelerated particle escaping the corona. Thus, the voltage is related to ξ roughly as $e\Phi_e \sim \xi^{-1} m_e c^2$.

For example, a maximum possible efficiency $\xi \sim 1$ reduces the voltage of the circuit to $e\Phi_e \sim m_e c^2$, which is just enough to create mildly relativistic pairs with rate $\dot{N}_+ \sim j_B/e$. The voltage was found to fluctuate significantly, but it did not get high enough to initiate the resonant channel of e^\pm production ($\gamma_{\text{res}} = m_i/m_e = 10$ in the simulation). The ion current was small, $j_i/j_B \simeq 10^{-2}$.

When ξ is reduced, a higher voltage is required in the circuit to get one pair per energetic particle escaping the corona, and the voltage follows the relation $e\Phi_e \sim \xi^{-1} m_e c^2$. This estimate is applicable as long as $\xi \gtrsim \gamma_{\text{res}}^{-1}$, so that $e\Phi_e < \gamma_{\text{res}} m_e c^2$. A further reduction of ξ does not lead

to an increase of voltage: then the circuit is mainly fed by pairs created via the resonant channel, and voltage is maintained at $e\Phi_e \sim \gamma_{\text{res}} m_e c^2$ as described in § 5. The thermal pair creation in the atmosphere then has a negligible effect on the circuit.

We have also studied one modification of this experiment by allowing only the anode to supply pairs with efficiency $\xi = 1/2$. The e^\pm atmosphere created by the anode filled the whole tube, and conducted the current. Ions lifted from the anode surface contributed a small fraction to the current $j_i/j_B \simeq 3 \times 10^{-2}$. The established voltage was ~ 5 times higher than in the model with pair supply at both ends. However, the circuit was able to operate without igniting the resonant pair creation (which we checked by setting $\gamma_{\text{res}} = \infty$). This shows that the thermally-driven regime can operate even when pair creation takes place at one footpoint of the magnetic tube.

In summary, the current may be fed by atmospheric e^\pm if $e\Phi_e/m_e c^2 > \xi^{-1}$. We expect that the surface pair production will dominate over resonant channel if

$$\xi > \frac{1}{\gamma_{\text{res}}}. \quad (78)$$

The exact numerical coefficient in this condition may be found experimentally; it increases if one of the surfaces (anode or cathode) dominates the pair supply.

7. CRUST EXCAVATION AND FORMATION OF A LIGHT-ELEMENT SURFACE LAYER

7.1. Mass Transfer in the Coronal Circuit

The existence of an ion current in the magnetosphere implies the transfer of mass from the anode footpoint of a magnetic line to its cathode footpoint. The rate of transfer may be easily estimated for the idealized configuration of a twisted dipole (§ 2),

$$\dot{M} \sim m_p \frac{j_i}{e} 4\pi R_{\text{NS}}^2 \sim \left(\frac{j_i}{j}\right) \frac{m_p c}{e} \varepsilon_j B R_{\text{NS}} \sim 10^{17} \left(\frac{j_i}{j}\right) \varepsilon_j B_{15} \text{ g s}^{-1}. \quad (79)$$

Here the dimensionless coefficient $\varepsilon_j \equiv \Delta\phi \sin^2 \theta$ measures the strength of the twist in the dipole magnetosphere (see eq. [1]). During the active life of a magnetar, $t \sim 10^4$ yr, a significant mass is transferred through the magnetosphere,

$$\Delta M \sim 3 \times 10^{28} \left(\frac{j_i}{j}\right) \varepsilon_j B_{15} \text{ g}. \quad (80)$$

It is much larger than the mass of the stellar atmosphere, and the atmosphere is quickly removed from the anode part of the stellar surface.

There is, however, a mechanism which can re-generate the atmosphere and regulate its column density. A thin atmosphere is unable to stop the energetic particle flowing from the corona and

these particles will hit the crust and knock out new ions. In a steady state, the atmosphere column density can adjust so that the rate of ion supply equals the rate of their transfer through the corona. Then the rate of crust excavation at the anode footprints is proportional to the ion current through the corona.

Excavation depends on the chemical composition of the uppermost crust of the neutron star. If it is made of light elements, the atmosphere is easily re-generated by simple knock out of ions from the surface. If it is made of carbon, oxygen, or any heavier elements, the ions are condensed into long molecular chains in a $\sim 10^{15}$ G magnetic field (Neuhauser, Koonin, & Langanke 1987; Lieb, Solovej, & Yngvason 1992; see Thompson et al. 2000 for estimates of the chain binding energy in the case of $\sim 10^{15}$ G magnetic fields). The knock out of light elements by the beam is still possible in this case because of spallation reactions. We discuss the excavation process in more detail below.

7.2. Excavation of Hydrogen and Helium Layers

Light elements — hydrogen and helium — may be present only above a certain depth in the crust. A strong upper bound on the column of hydrogen is obtained by balancing the Fermi energy of the degenerate electrons under hydrostatic pressure with the threshold for electron captures on protons, $E_{Fe} = m_e c^2 [(p_{Fe}/m_e c)^2 + 1]^{1/2} \sim 1.3$ MeV. At higher densities, free protons are rapidly consumed by electron captures $e^- + {}^1\text{H} \rightarrow n + \nu$. The maximum depth of a helium layer is limited by the triple-alpha reaction $3\alpha \rightarrow {}^{12}\text{C}$, which is very temperature- and density-dependent. The interior of a magnetar probably sustains a temperature of $\sim 2 \times 10^8$ K at an age of $\sim 10^3 - 10^4$ yr (e.g. Arras, Cumming, & Thompson 2004). In the presence of a light-element layer at the stellar surface, the crust temperature remains close to the central temperature where $\rho > 10^6$ g cm $^{-3}$ (e.g. Potekhin et al. 2003). At such densities and temperatures helium cannot be present (its lifetime would be only $\sim 10^{-3} (Y\rho_6)^{-2}$ yr). Only an upper layer of density $\rho < 10^5$ g cm $^{-3}$, where temperature is below $\sim 1 \times 10^8$ K, will survive helium burning.

The maximal layer of light elements will be drained rapidly from the anode surface and deposited at the cathode surface in the presence of a magnetic twist. The timescale for its removal can be estimated as follows. The column mass density Σ of ions (Z, A) is related to the pressure P through the equation of hydrostatic equilibrium,

$$\Sigma g = P = \frac{e B_{\text{NS}}}{2\pi\hbar^2} \frac{p_{Fe}^2}{2\pi}. \quad (81)$$

Here it is taken into account that the pressure is dominated by degenerate one-dimensional electrons (electrons are confined to their lowest Landau state in the density range of interest: $E_{Fe} < E_B$). The excavation time down to a depth with a Fermi momentum p_{Fe} is

$$t_{\text{exc}} = \frac{\Sigma}{A m_p j_i / e} = 0.3 \frac{Z/A}{\varepsilon_j} \left(\frac{j_i}{j} \right)^{-1} \left(\frac{p_{Fe}}{m_e c} \right)^2 \frac{R_{\text{NS},6}}{g_{14}} \text{ yr}. \quad (82)$$

Substituting $j_i/j \sim 0.1$ and $\varepsilon_j \sim 0.1$ shows that the excavation time of the maximal hydrogen layer ($E_{Fe} \simeq 1.3$ MeV or $p_{Fe} \simeq 1.2$ MeV/c) is much shorter than the active $\sim 10^4$ -yr lifetime of a magnetar. Taking a more realistic maximum density $\rho \sim 10^5$ g cm $^{-3}$, one has $p_{Fe}/m_e c \simeq 6 \times 10^{-3} \rho_5 B_{15}^{-1}$, and the excavation time is hours or days. It can therefore be shorter than the timescale for hydrogen consumption as a result of diffusion to a deeper layer of carbon (Chang et al. 2004).

We conclude that the anode surface of the star should be solid and made of heavier elements — carbon or iron, which form molecular chains. Nevertheless, it is possible for a gaseous atmosphere of light elements to be maintained above such a condensed, heavy-element surface. The particles accelerated in the corona impinge on the surface with energies high enough to knock out free protons and α -particles from the heavy nuclei. In addition, a flux of heavy nuclei may be maintained by a modest flux of hard X-ray photons that photodissociate atoms from the end of the molecular chains. Given an ionization energy E_I , the hard X-ray luminosity that is needed to maintain an upward flux $\dot{N}_Z = \varepsilon_Z j/e$ of nuclei of charge Z from the anode surface is $L_X = 10^{32} (\varepsilon_Z/0.1) (\varepsilon_j/0.1) (E_I/100 \text{ keV}) B_{15} R_{\text{NS},6} \text{ erg s}^{-1}$.

7.3. Beam Stopping and Spallation of Nuclei in a Solid Crust

When the beam enters the crust, it is stopped by two-body collisions, and collective processes become negligible. In particular, the growth length of beam instability l_b (eq. [46]) is much larger than the mean free path to two-body collisions (their ratio scales as $n_e^{5/6}$ and is large in condensed matter because n_e is large). The stopping length of the electron beam is then mainly determined by the cross section for Coulomb scattering off the nuclei, which involves excitation to Landau states $n > 0$.

Consider a downward-moving electron with an energy $\gamma m_e c^2$ much greater than that of the first Landau level E_B (eq. [69]). The electron side scatters off an ion of charge Ze into Landau level $n > 1$ with a cross section

$$\sigma_{\text{Coul}}(0 \rightarrow n) \sim \frac{\sigma_{\text{Coul}}(0 \rightarrow 1)}{n(n-1)} \sim \frac{Z^2}{n(n-1)} \left(\frac{B}{B_{\text{QED}}} \right)^{-1} \sigma_{\text{T}}, \quad (83)$$

where $\sigma_{\text{Coul}}(0 \rightarrow 1)$ is given by equation (70) and we have made use of the fact that $p_{\perp}^2 = 2n(B/B_{\text{QED}})(m_e c)^2$ in Landau level n . (See Kotov & Kelner 1985 for a closely related discussion of Landau excitations by fast-moving particles in sub-QED magnetic fields.) The scattered electron continues to move along the magnetic line with a new Lorentz factor γ_{\parallel} that is found from the energy conservation,

$$\gamma m_e c^2 = \gamma_{\parallel} \left[2n \left(\frac{B}{B_{\text{QED}}} \right) + 1 \right]^{1/2} m_e c^2, \quad (84)$$

where the recoil of the nucleus has been neglected. Excitation to the first level $n = 1$ has the largest cross section, and hence this transition is most frequent. The probability of excitation to levels

$n' \geq n$ is $\sim \frac{1}{n}$. One may neglect these high-level excitations in the estimates below.

The excited electron loses energy very quickly by a series of electric dipole transitions in which the Landau level decreases by 1. The photon emitted in each transition takes away energy $E'_\gamma \sim (2n)^{-1/2} E_B$ when measured in the frame with Lorentz factor γ_\parallel . As discussed in § 6.3, the energy of a de-excitation photon is reduced by the electron recoil and depends on the emission angle. It can be emitted in either polarization state, and only the O-mode photon can convert directly to a pair. An E-mode de-excitation photon cannot create a pair directly off the magnetic field. It can, however, produce e^\pm by hitting a nucleus; or it can split and create an O-mode photon that is able to produce a pair.

The e^\pm produced by the de-excitation photons have energies $E_\gamma \sim \gamma_\parallel E_B$ in the lab frame. They can again side-scatter and produce more such photons and more pairs. Thus, a pair cascade develops as a beam with initial $\gamma = \gamma_0$ propagates into the crust, giving more e^\pm with lower Lorentz factors $\gamma < \gamma_0$.

In a condensed surface layer, the E-mode de-excitation photons will interact with an ion more rapidly than they split.¹³ The most frequent outcome of this interaction is the conversion of the photon to a pair in the Coulomb field of the nucleus. Less frequently, the photon can knock out a neutron, proton, or alpha particle. Knockout requires a minimum photon energy of $\sim 15 - 20$ MeV, and its cross section typically peaks at $\sim 20 - 30$ MeV (e.g. Dietrich & Berman 1988). The cross section for pair creation is

$$\frac{\sigma_{e^+e^-}^Z}{\sigma_T} = \frac{7}{6\pi} Z^2 \alpha \left[\ln \left(\frac{2E_\gamma}{m_e c^2} \right) - \frac{109}{42} \right], \quad (85)$$

which is $\sigma_{e^+e^-}^Z \simeq 3.2 Z^2$ mb when the photon has an energy $E_\gamma = 25$ MeV. For comparison the cross section for proton knockout from oxygen is

$$\sigma(\gamma, {}^{16}\text{O} \rightarrow p, {}^{15}\text{N}) \simeq 12 \text{ mb} \quad (86)$$

at $E_\gamma \simeq 25$ MeV. This cross section scales approximately in proportion to Z , and so we take

$$\sigma(\gamma, Z \rightarrow p, Z - 1) = 1.5 Z \text{ mb} \quad (87)$$

for proton knockout. The cross section for neutron knockout is similar but slightly larger.

We can now estimate the number of protons knocked out per incident electron. We will assume in this estimate an idealized surface layer that is composed of ions of a single charge Z . First we

¹³For example, the mean free path for splitting is 0.03 cm for an E-mode photon of energy $2m_e c^2 / \sin \theta$ that propagates perpendicular to the magnetic field (Baring 2000). This compares with a mean free path for nuclear pair creation of $2 \times 10^{-5} B_{15}^{-6/5}$ cm in a condensed carbon layer with a density of $1 \times 10^7 B_{15}^{6/5}$ g cm⁻³ (as deduced from a simple Wigner-Seitz model; see Lai 2001). One sees that splitting is slower in the condensed phase, but would be faster in a gaseous atmosphere composed of carbon atoms.

note that the side-scattering to the first Landau level $n = 1$ is most frequent. Then the scattering electron (or positron) with energy $E_e = \gamma m_e c^2$ gives a de-excitation photon with $E_\gamma \sim E_e$, and a significant fraction of E_e is shared between two daughter particles. Therefore, we can roughly estimate the number of generations in the cascade down to an energy of $\sim 25 \text{ MeV} \simeq 50 m_e c^2$ as $\log_2(\gamma_0/50) \sim 5$. The number of $\sim 25 \text{ MeV}$ photons created per incoming electron is about $\gamma_0/50$. A large fraction of these photons are in the E-mode and hit a nucleus, yielding a proton with a probability $\sigma(\gamma, Z \rightarrow p, Z-1)/\sigma_{e^+e^-}^Z$. The yield of protons per incident primary electron is therefore

$$N_p \simeq \left(\frac{\gamma_0}{50}\right) \frac{\sigma(\gamma, Z \rightarrow p, Z-1)}{\sigma_{e^+e^-}^Z} \sim 0.1 \left(\frac{\gamma_0}{10^3}\right) \left(\frac{Z}{26}\right)^{-1}. \quad (88)$$

Coulomb scattering of a relativistic electron (or positron) occurs at a Thomson depth

$$\tau_T(0 \rightarrow n \geq 1) \sim \frac{Z\sigma_T}{\sigma_{\text{Coul}}} \sim \frac{1}{Z} \left(\frac{B}{B_{\text{QED}}}\right) \simeq \frac{20}{Z} B_{15}. \quad (89)$$

Note that the cascade develops at a significant depth that buries the created positrons — they annihilate in the crust and cannot escape back through the surface. The relativistic cascade is strongly beamed into the star, and noticeable backscattering may occur only after the last stage of the cascade that gives e^\pm with $\gamma \sim E_B/2m_e c^2 \sim 3B_{15}^{1/2}$, after $\log_2(\gamma_0 m_e c^2/E_B) \sim 8$ generations. Even the O-mode branch of the cascade, which involves immediate pair creation off the magnetic field, ends at a large $\tau_T \gtrsim 100Z^{-1}B_{15}$. This layer is optically thick to positron annihilation. Therefore, the anode surface can supply positive charges only by emitting ions.

The depth at which ion spallation occurs is controlled by the free path of the E-mode photons produced in the cascade,

$$\tau_T(\gamma \rightarrow e^+e^-) \sim \log_2\left(\frac{\gamma_0}{50}\right) \frac{Z\sigma_T}{\sigma_{e^+e^-}^Z} = \frac{10^3}{Z}. \quad (90)$$

The knocked-out protons diffuse through the spallation layer $\tau_T \sim 10^3 Z^{-1}$ on a short timescale, much shorter than the excavation time of this layer and, at the temperature $k_B T \sim 0.5 \text{ keV}$, the free protons in the crust are quickly sublimated to the atmosphere.¹⁴ The flux of knock-out protons is likely to be the main supplier of ions for the atmosphere and corona, especially if the yield N_p is sufficient to feed the required ion current j_i . Excavation of the crust is driven by spallation followed immediately by sublimation of the light-element spallation products to the atmosphere.

Our preferred circuit model has voltage $e\Phi_e \sim 1 \text{ GeV}$ and ion current $j_i \sim 0.1j$ (see § 5). If the gaseous atmosphere does not significantly decelerate the particles flowing from the corona, they will impact the solid crust with $\gamma_0 \sim 10^3$. The estimated proton yield $N_p \sim 0.1$ is then marginally sufficient to feed the ion current $j_i \sim 0.1j$.

¹⁴Protons have a binding energy of a few keV at the surface and are sublimated to the atmosphere much more easily than the heavy elements that are locked in molecular chains.

This suggests two possible modes in which the circuit can operate:

1. The knock-out yield N_p for the characteristic Lorentz factor in the circuit $e\Phi_e/m_e c^2 \sim \gamma_{\text{res}}$ exceeds the ion fraction j_i/j of the current. This implies that the column density of the atmosphere will grow until it is able to damp the relativistic beam from the corona and reduce the crustal excavation rate. The steady-state column density of the atmosphere is determined by its efficiency of stopping the relativistic e^\pm . If collisionless processes do not decelerate the relativistic beam in the atmosphere, but just form a plateau in its distribution function (§ 6.1), then a sufficiently thick atmosphere must be accumulated to decelerate the beam through direct two-body collisions.

Direct collisions initiate a cascade in the atmosphere which is similar to that in the crust: the beam particles side-scatter off the atmospheric ions and emit photons which convert to e^\pm . The crust excavation rate will be reduced if the atmospheric cascade extends down to a Lorentz factor ~ 50 before it reaches the solid surface. This requires $\sim \log_2(\gamma_{\text{res}}/50) \sim 5$ generations of pair-creation, and then the optical depth to side-scattering should be ~ 5 . Thus, the electron column density of the atmosphere will be regulated to the value

$$N_{e,\text{atm}} \sim \frac{Z_{\text{atm}} \log_2(\gamma_{\text{res}}/50)}{\sigma_{\text{Coul}}} \sim 100 \left(\frac{B_{15}}{Z_{\text{atm}}} \right) \sigma_{\text{T}}^{-1}, \quad (91)$$

where we have made use of eq. (89). Z_{atm} is the nuclear charge of the atmospheric ions; one can take $Z_{\text{atm}} = 1$ for a hydrogen atmosphere.

2. The atmosphere is completely removed from the anode surface and j_i/j in the circuit is regulated by the proton knock-out yield N_p so that $j_i/j = N_p/(1 + N_p)$. The circuit solution can be expected to be similar to that obtained in §5 since, in either case, the current is mainly maintained by the e^\pm produced in the corona. In the absence of a dense atmosphere near the anode, the magnetospheric electric field will be screened by the solid surface.

The thickness of the plasma layer that is accumulated near the cathode surface is limited by burning processes such as electron capture or capture on heavy ions through the penetration of a diffusive tail to greater depths (Chang, Arras, & Bildsten 2004).

8. DISCUSSION

8.1. Comparison with Solar Corona

The corona of a magnetar may be viewed as a collection of closed current-carrying flux tubes with footpoints anchored in a relatively cold stellar surface. As in the Solar corona, a current is created by the twisting motions of the footpoints. Another similarity with the Solar corona is the important interaction of the coronal plasma with a dense atmospheric layer on the stellar surface where the plasma becomes collisional and can efficiently radiate the energy flux received from the corona.

However, the magnetar corona is distinguished from the Solar corona in a few important respects. The differences in the behavior of the magnetic field are as follows.

1. The footpoints of magnetic lines of the Solar corona are constantly pushed and twisted because the outer envelope of the Sun is convective and in constant motion. In addition, magnetic flux tubes are observed to emerge from the Solar convection zone with a twist already implanted in them. By contrast, the neutron star’s rigid crust is subject only to rare and sporadic yielding events (starquakes). Because the crust is stably stratified, the transfer of a toroidal magnetic field to the exterior occurs through a differential rotation of the crustal material along the gravitational equipotential surfaces.

2. The magnetic twists have long lifetimes between starquakes, and their evolution differs from the evolution of twists in the Solar corona. Once a current $\mathbf{j} = (c/4\pi)\nabla \times \mathbf{B}$ is created in the magnetosphere of a neutron star, it lives a long time because the net current $I \sim R_{\text{NS}}^2 j$ is enormous and maintained by its self-induction. The gradual decay of the current induces an e.m.f. along the magnetic field lines, which forces the plasma and electric field to self-organize into a quasi-steady electric circuit. The ease with which charges can be supplied by e^\pm production when the induced voltage exceeds $e\Phi_e \sim 1$ GeV implies a “bottleneck” for the decay of the twist (§§ 2 and 5).

3. The evolution of the magnetic field between the starquakes involves a gradual release of the twist energy through Joule dissipation and migration of the twist toward the magnetic polar axis. The latter process causes a gradual flaring of the poloidal field lines. Explosive magnetic reconnection similar to Solar flares is likely to be triggered by starquakes, but not during the following slow-dissipation stage.

4. — The external magnetic field of a magnetar is likely to have less small-scale structure compared with the Solar corona. The small-scale braiding of magnetic lines followed by reconnection and dissipation is one of the possible mechanisms for the heating of the Solar corona (Parker 1979). Precisely what creates this structure is unclear: it could be driven by the hydrodynamic turbulence that is excited at the top of the Solar convection zone or by the Taylor relaxation of a helical magnetic field (e.g. Diamond & Malkov 2003). In magnetars, the small-scale structure of magnetic field can be expected to dissipate quickly after the starquakes if it is created in these events. The dissipation timescale is longest for the large-scale twists expected from large-scale motions of the crust. Indirect evidence that small-scale instabilities are less important comes from the observed distribution of energies of SGR bursts: the cumulative energy in bursts $E^2 dN/dE \sim E^{0.4}$ is weighted toward the largest events (Cheng et al. 1996; Gogus et al. 2001). By contrast, several recent measurements of the distribution of Solar flare energies suggest a power-law $dN/dE = E^k$ with $k < -2$, and are therefore consistent with the basic picture of coronal heating by ‘nano-flares’ (Walsh & Ireland 2003).

Let us also note a few differences in the behavior of plasma in the magnetar corona and the Solar corona.

5. — The rapid cooling of the transverse motion of charged particles in the ultra-strong magnetic

field of magnetars makes the particle distribution functions one-dimensional. This reduces the number of relevant plasma modes in the corona.

6. — The coronal plasma of magnetars is continually lost to the surface and re-generated. By contrast, the Solar corona is in hydrostatic equilibrium. Its density n is much higher than the minimum needed to maintain the current, and the mean drift speed j/en of the coronal currents is much below the electron and ion thermal speeds. So, the *mean* current does not experience a strong anomalous resistivity. Strong plasma turbulence is expected in localized current sheets and can develop explosively, giving rise to the Solar flares. In the magnetar corona, a strong turbulence is maintained routinely, everywhere where current flows. The very mechanism of the current supply involves a strongly non-linear phenomenon — e^\pm discharge.

7. — The magnetar corona is dominated by relativistic e^\pm pairs. As indicated by our numerical experiments, ions lifted from the surface contribute a modest fraction, perhaps $\sim 10\%$, to the charge flow.

8.2. Magnetospheric Circuit as a Double-layer Problem

From the plasma physics point of view, there is an interesting connection between the magnetospheric circuit and the double-layer problem that was first studied by Langmuir (1929) and later by many authors (for reviews see Radau 1989; Block 1978). The magnetospheric current flows along a magnetic tube with footpoints on a cold conductor and is subject to the boundary condition $E \simeq 0$ at the footpoints. We argued that the tube curvature is not essential to understanding many features of the circuit, and studied the charge flow in a straight tube where gravity is replaced by a force $m\mathbf{g}$ that attracts plasma to the anode and cathode boundaries. The longitudinal electric field must develop between the two boundaries because of gravity. This is a significant difference from the normally invoked mechanisms for double-layer formation (such as current-driven instability). In our case, the gravitational potential traps the thermal particles at the footpoints of magnetic field lines and impedes the flow of the current that is required by the self-induction of the twisted magnetic field.

Thus, perfect conditions for double-layer formation are created. And indeed, our numerical experiment showed the formation of a huge relativistic double layer between the footpoints, of size $L \sim R_{\text{NS}}$. This result is obtained if the current can be maintained only by particles lifted from the anode and cathode surfaces. It could have dramatic consequences for the magnetar physics because of the huge dissipation rate in the double layer: the energy of magnetic twist would be quickly released in a powerful burst.

However, there is one more ingredient in the problem, which again makes the magnetar circuit different from the previously studied double layers: new charges (e^\pm) can be created by accelerated particles in the tube. This process qualitatively changes the problem because voltage is now limited by e^\pm discharge (§ 5). As a result, the circuit enters the new state of self-organized criticality where

voltage repeatedly builds up and is screened by the e^\pm creation. This allows the current to flow and maintain the required $\nabla \times \mathbf{B}$.

8.3. Observational Implications

Two important observational implications of the magnetospheric twist were already pointed out by TLK, based on the force-free model of a twisted dipole:

1. The poloidal field lines are inflated compared with a pure dipole, so that a larger magnetic flux connects the star to its light cylinder R_{lc} . This implies a higher spin-down torque. Thus, the twisting leads to a higher spindown rate \dot{P} .

2. The minimum particle density needed to maintain the currents, $n_c = j/ec$, is high enough to make the magnetosphere semi-opaque. The main source of opacity is resonant cyclotron scattering. If the magnetic field lines are twisted through an angle $\Delta\phi \sim 1$, the optical depth to scattering happens to be $\sim n/n_c$ (independent of r , B , and nature of the flowing charges). This must strongly modify the observed radiation from the star — its spectrum and pulse profile.

TLK also pointed out that if the magnetospheric current is carried by ions and electrons lifted from the stellar surface, one expects a dissipation rate comparable to the observed persistent luminosity of magnetars.

Further implications of the one-dimensional plasma model developed in the present paper are as follows.

3. The density of the plasma corona is found to be close to its minimum $n_c = j/ec$ as conjectured by TLK. It is largely made of e^\pm pairs rather than electron-ion plasma. This suggests that the optical depth of the corona is determined mostly by the cyclotron resonance of e^\pm . All species of particles (e^- , e^+ , and even ions) flow with relativistic bulk speeds and large temperatures $\sim e\Phi_e$. The cyclotron resonance is very broad, which will have important implications for radiative transfer through the corona. Note, however, that our calculations focused on the inner corona $r \sim R_{NS}$ where most of the energy release occurs. At larger radii $r \sim (10 - 20)R_{NS}$, where electron cyclotron energy is in the keV range, e^\pm feel a strong radiative drag force and can decelerate to a small velocity. We defer a detailed analysis of this part of the corona to another paper.

4. The voltage $e\Phi_e \simeq \gamma_{res}m_e c^2 \sim 1$ GeV along the twisted magnetic lines of the corona is regulated by the threshold for e^\pm discharge, and its exact value depends on B and the spectrum of target photons involved in e^\pm creation, especially on its high-energy tail at 10 – 300 keV (§ 5). By coincidence, the mean electric field developed along the magnetic lines, $E \sim \Phi_e/R_{NS}$, is marginally sufficient to lift ions from the anode footpoint. Therefore, in addition to e^\pm pairs, some ions are present in the corona. Their abundance depends on the exact Φ_e and is $\simeq 10\%$ for $e\Phi_e = 1$ GeV (see Fig. 10). The coronal ions may produce interesting features in the magnetar spectrum and likely to play a key role in the low-frequency emission (§ 8.4.2).

5. The rate of energy dissipation in the twisted magnetosphere is given by $L_{\text{diss}} = I\Phi_e$ where I is the net current through the corona. The current may be estimated as

$$I \sim j_B a^2 \sim \frac{c}{4\pi} \Delta\phi \frac{B}{R_{\text{NS}}} a^2, \quad (92)$$

where a is the size of a twisted region on the stellar surface and $\Delta\phi = |\nabla \times \mathbf{B}|(B/R_{\text{NS}})^{-1} \lesssim 1$ characterizes the strength of the twist. The calculated value of $e\Phi_e$ is comparable to 1 GeV, and implies

$$L_{\text{diss}} = I\Phi_e \sim 10^{37} \Delta\phi \left(\frac{B}{10^{15} \text{ G}} \right) \left(\frac{a}{R_{\text{NS}}} \right)^2 \left(\frac{e\Phi_e}{\text{GeV}} \right) \text{ erg s}^{-1}. \quad (93)$$

The typical luminosity observed by INTEGRAL is $L_{\text{diss}} \sim 10^{36} \text{ erg s}^{-1}$ around 100 keV. It is consistent with a partially twisted magnetosphere, $a \sim 0.3R_{\text{NS}}$, or a global moderate twist with $\Delta\phi (e\Phi_e/\text{GeV}) \sim 0.1$. (Larger dissipation rates and larger twists are not yet excluded by the data: e.g. the output at 1 MeV is presently unknown.) More precise formulae may be obtained for concrete magnetic configurations. In the simplest case of a twisted dipole (TLK), one can use equation (1) and find I by integrating $\mathbf{j} \cdot d\mathbf{S}$ over one hemisphere of the star. This gives $I = \frac{1}{8} \Delta\phi c B_{\text{pole}} R_{\text{NS}}$ and $L_{\text{diss}} = 1.2 \times 10^{37} \Delta\phi B_{\text{pole},15} R_{\text{NS},6} \Phi_{e,\text{GeV}}$.

6. Once created, a magnetospheric twist has a relatively long but finite lifetime. The energy stored in the magnetic twist is $\mathcal{E}_{\text{twist}} \sim (I^2/c^2) R_{\text{NS}}$. This energy dissipates in a time

$$t_{\text{decay}} = \frac{\mathcal{E}_{\text{twist}}}{L_{\text{diss}}} \simeq \frac{IR_{\text{NS}}}{c^2 \Phi_e} = \frac{R_{\text{NS}} L_{\text{diss}}}{c^2 \Phi_e^2} \simeq 3 \left(\frac{L_{\text{diss}}}{10^{36} \text{ ergs s}^{-1}} \right) \left(\frac{e\Phi_e}{\text{GeV}} \right)^{-2} \text{ yr}. \quad (94)$$

The exact numerical coefficient in this equation again depends on the concrete magnetic configuration. For example, the energy stored in the global twist of a dipole is $\mathcal{E}_{\text{twist}} = 0.17(\Delta\phi)^2 E_{\text{dipole}}$ (TLK), where $E_{\text{dipole}} = \frac{1}{12} B_{\text{pole}}^2 R_{\text{NS}}^3$ is the energy of a normal dipole. In this case, one finds $t_{\text{decay}} = 0.8 (R_{\text{NS}}/c^2) L_{\text{diss}}/\Phi_e^2$.

The characteristic timescale of decay is determined by voltage Φ_e and the corona luminosity L_{diss} . Note that a stronger twist (brighter corona) lives longer. Given a measured luminosity and its decay time, one may infer Φ_e and compare it with the theoretically expected value. Since Φ_e does not change as the twist decays in our model, one can solve equation (94) for $\mathcal{E}_{\text{twist}}(t)$ and $L_{\text{diss}}(t) = -d\mathcal{E}_{\text{twist}}/dt$. This gives

$$L_{\text{diss}}(t) = 5 \times 10^{35} \left(\frac{e\Phi_e}{\text{GeV}} \right)^{-2} (t_0 - t) \text{ erg s}^{-1}, \quad (95)$$

where time t is expressed in years. The final decay of the twist should occur at a well-defined time $t_0 = t + t_{\text{decay}}$. The finite time of decay implies that the emission called “persistent” in this paper is not, strictly speaking, persistent. If the time between large-scale starquakes is longer than the decay time of the twist, the magnetar should be seen to enter a quiescent state and the observed luminosity should then be dominated by the surface blackbody emission.

7. The voltage Φ_e implies a certain effective resistivity $\mathcal{R} = \Phi_e/I$ of the corona. This resistivity leads to spreading of the electric current *across* the magnetic lines. Equivalently, the magnetic helicity is redistributed within the magnetosphere. This spreading is described by the induction equation $\partial \mathbf{B}/\partial t = -c \nabla \times \mathbf{E}$. The magnitude of $\nabla \times \mathbf{E}$ depends on the gradient of E_{\parallel} transverse to the twisted magnetic field lines. Our model of the magnetospheric voltage implies that Φ_e has a gradient on a lengthscale $\sim R_{\text{NS}}$, so that $\partial B_{\text{twist}}/\partial t \sim c E_{\parallel}/R_{\text{NS}}$. The characteristic spreading time of the twist $B_{\text{twist}} = \Delta\phi B (a/R_{\text{NS}})$ is $t_{\text{spread}} \sim B_{\text{twist}} (\partial B_{\text{twist}}/\partial t)^{-1}$ and can be roughly estimated as

$$t_{\text{spread}} \sim \frac{\Delta\phi B}{E_{\parallel}} \frac{R_{\text{NS}}}{c} \left(\frac{a}{R_{\text{NS}}} \right) \sim 300 \Delta\phi \left(\frac{B}{10^{15} \text{ G}} \right) \left(\frac{e\Phi_e}{\text{GeV}} \right)^{-1} \left(\frac{a}{R_{\text{NS}}} \right) \text{ yr.} \quad (96)$$

If a twisting event happens near the magnetic equator, it initially does not affect the extended magnetic lines with $R_{\text{max}} \sim R_{\text{lc}}$. Its impact on spindown may appear with a delay as long as t_{spread} . Although the exact numerical coefficient in equation (96) is unknown, the rough estimate suggests a timescale that is comparable to the decay time (eq. [94]): their ratio is $\propto (a/R_{\text{NS}})^{-1}$. The relative magnitude depends sensitively on geometrical factors; it is possible that starquakes occurring far from the poles will have little effect on the spindown, but further investigation is needed.

8. Even a small ion current implies a large transfer of mass through the magnetosphere over the $\sim 10^4$ -yr active lifetime of a magnetar. Essentially all the hydrogen and helium which could be stored at the surface is rapidly transferred from the anode surface to the cathode surface, thereby exposing heavier elements (e.g. carbon) that are strongly bound in molecular chains. A continuing flux of protons and alpha particles can, nonetheless, be maintained in the circuit. The bombarding relativistic electrons from the corona cause the gradual disruption of ions just below the solid surface. They trigger a cascade of e^{\pm} pairs and gamma-rays that knock out nucleons and α -particles from the heavier nuclei. This process re-generates the light-element atmosphere on the surface and regulates its column density (§ 7). As a result, the Thomson depth of the atmosphere equilibrates to a value ~ 100 . The chemical composition of the upper crust (carbon or heavier elements) and its light-element atmosphere affect radiative transfer and the emerging spectrum of the star’s radiation (e.g. Zavlin & Pavlov 2002).

9. Our study of the transition region in § 6 suggests that the energy dissipated in the corona is radiated away below it in two forms (see also Thompson & Beloborodov 2005). First, the high-energy radiation with a hard spectrum possibly extending up to ~ 1 MeV. This radiation is powered by collisionless dissipation of the coronal beam in the transition region. Second, a blackbody radiation component that is caused by thermalization of the remaining energy of the beam when it enters dense atmospheric layers and then the crust. Two-body collisions and development of a pair cascade are responsible for this thermalization. Our first estimate gives comparable luminosities in the high-energy and blackbody components. Further investigation of the transition region may show that the collisionless dissipation is more efficient and less energy is left for the blackbody component. This would be in a better agreement with observations of SGR 1806-20 which show that the high-energy component can be more luminous than the blackbody component (e.g. Mereghetti et al.

2005; Molkov et al. 2005).

Note also that the rest-energy flux of the positrons impacting the surface is only a small fraction $\sim m_e c^2 / e \Phi_e$ of the total dissipation rate in the circuit. Even if these positrons annihilated at $\tau_T \sim 1$, the energy flux at ~ 0.5 MeV in annihilation radiation would be small compared with the bremsstrahlung emission.

8.4. Emission from the Magnetar Corona

8.4.1. Hard X-ray Emission

The radiative output from the magnetar corona is observed to peak above 100 keV (Kuiper, Hermsen & Mendez 2004; Mereghetti et al. 2005; Molkov et al. 2005; den Hartog et al. 2006). It is likely fed by the inner parts of the corona: in the model investigated in this paper, one expects that the bulk of the coronal current is concentrated fairly close to the star, at radii $\lesssim 2R_{\text{NS}}$. Currents in the outer region $r \gg R_{\text{NS}}$ (even if it is strongly twisted) flow through a small polar cap on the star and therefore are small. For example, in the twisted-dipole configuration, the maximum current which can flow beyond a radius R scales as $\Delta\phi/R^2$.

Emission produced in the inner corona cannot extend above ~ 1 MeV, regardless the mechanism of emission, because photons with energy $\gtrsim 1$ MeV cannot escape the ultra-strong magnetic field. There are two possible linear polarizations of photons in strongly magnetized vacuum: *E*-mode (electric vector perpendicular to \mathbf{B}) and *O*-mode (electric vector has a component along \mathbf{B}). An *E*-mode photon cannot escape because it splits into two photons. An *O*-mode photon propagating at angle θ with respect to \mathbf{B} cannot escape when its energy $E_\gamma > 2m_e c^2 / \sin \theta$ because it converts to a pair. Therefore, the spectrum escaping the inner corona must cut off at or below 1 MeV. The available RXTE and INTEGRAL data show that the cutoff must be above 100 keV. The existence of such a cutoff may be indicated by COMPTEL upper limits for AXP 4U 0142+61 (den Hartog et al. 2006).

The possible mechanisms of emission are strongly constrained. The corona has a low density $n \sim n_c = j_B / ec \lesssim B(4\pi e R_{\text{NS}})^{-1} \sim 10^{17} B_{15} \text{ cm}^{-3}$ and its particles practically do not collide with each other, so two-body radiative processes are negligible. The only available emission process in the corona is upscattering of surface X-rays. The scattering can occur resonantly (excitation to the first Landau level followed by de-excitation) or non-resonantly (Compton scattering). The scattering, however, cannot explain the observed 100-keV emission:

1. *Resonant upscattering by electrons (or positrons)* with Lorentz factor γ_e gives high-energy photons with energy $\sim \gamma_e \hbar e B / m_e c \gg 1$ MeV (§ 5.1), which cannot escape. They either split (if *E*-mode) or convert to pairs (if *O*-mode). Each splitting event gives two daughter photons, and at most one of them is again an *E*-mode photon which will split again. One can deduce that an upscattering event followed by repeated splitting could give at best two *O*-mode photons of energy

$E_\gamma < 1$ MeV that can avoid the conversion to e^\pm and escape, and the probability of this particular branch is small, $p \ll 1$. Even with $p = 1$, the number of escaping photons would not be sufficient to explain the observed emission. The voltage along the magnetic lines adjusts so that the coronal particles experience ~ 1 resonant scattering before they are lost to the surface, while the observed emission requires the production of $10^3 - 10^4$ 100-keV photons per particle.

2. *Resonant upscattering by ions* with Lorentz factors γ_i gives photons of energy $\gamma_i eB/m_p c$ which is too low to explain the 100-keV emission (ions are mildly relativistic in the circuit with \sim GeV voltage, $\gamma_i \sim 1$).

3. *Compton scattering* is strongly suppressed for *E*-mode photons because the electron can move only along **B**. The cross section of O-mode scattering by electron with Lorentz factor γ_e is $\sim \sigma_T/\gamma_e^2$.¹⁵ This may be seen by transforming the photon to the rest frame of the relativistic electron. Then the photon propagates at angle $\sin\theta' \sim 1/\gamma_e$ with respect to the magnetic field and its electric vector is nearly perpendicular to **B**, i.e. the photon becomes mostly E-mode. Viewing it as a classical wave that shakes the 1D electron, one finds the cross section of scattering $\sigma = \sigma_T \sin^2\theta' = \sigma_T/\gamma_e^2$. The corresponding optical depth of the corona is $\tau = n_e R_{\text{NS}} \sigma = \tau_c/\gamma_e^2$. The upscattered photon is boosted in energy by γ_e^2 and the net Compton amplification factor of O-mode radiation passing through the corona is $\tau\gamma_e^2 = \tau_c$, i.e. does not depend on γ_e . Since $\tau_c = \sigma_T R_{\text{NS}} n_e$ is small, $\sim 0.1 - 0.01$, one concludes that the energy losses of the corona by Compton scattering are a small fraction of the surface O-mode luminosity.

A promising location for the source of observed 20 – 100 keV emission is the transition region between the corona and the thermal photosphere (see Thompson & Beloborodov 2005 and § 6). The transition region can radiate away (through bremsstrahlung) a significant fraction of the energy dissipated in the corona. Its temperature is $k_B T \sim 100(\ell/\ell_{\text{Coul}})^{-2/5}$ keV (eq. [58]), where $\ell/\ell_{\text{Coul}} < 1$ is a numerical factor that parameterizes the suppression of thermal conductivity by plasma turbulence. This suppression is likely to be significant, and the emission temperature may be above 100 keV. The emitted hard X-ray spectrum is well approximated as single-temperature optically thin bremsstrahlung (Thompson & Beloborodov 2005). Therefore, its photon index below the exponential cutoff is close to -1 , in agreement with magnetar spectra observed with INTEGRAL and RXTE.

The observed pulsed fraction increases toward the high-energy end of the magnetar spectrum and approaches 100% at 100 keV (Kuiper et al. 2004). If the hard X-rays are produced by one or two twisted spots on the stellar surface, the large pulsed fraction implies that the spots almost disappear during some phase of rotation. Then they should not be too far from each other and, in particular, cannot be antipodal because a large fraction of the stellar surface is visible to observer due to the gravitational bending of light: $S_{\text{vis}}/4\pi R_{\text{NS}}^2 = (2 - 4GM/c^2 R_{\text{NS}})^{-1} \simeq 3/4$ (Beloborodov

¹⁵This assumes Thomson regime of scattering, $\gamma_e \hbar \omega \ll m_e c^2$. At larger energies, the electron recoil becomes important (Klein-Nishina regime) and the cross section is reduced.

2002). The decreasing pulsed fraction at smaller energies may be explained by contamination of the strongly pulsating component by another less pulsed and softer component of the magnetospheric emission (see § 8.4.2).

Hard X-ray emission may also be produced at about 100 km above the star surface (Thompson & Beloborodov 2005). The magnetic field is about 10^{11} G in this region, and the keV photons flowing from the star encounter a cyclotron resonance and interact efficiently with the current-carrying electrons. Therefore, the electrons experience an outward radiative pressure and cannot close the circuit unless an additional electric field develops that helps them flow back to the star. We show in the accompanying paper that a positron injected in the region where $\hbar\omega_{c,e}$ sits below the blackbody peak will undergo a runaway acceleration and upscatters keV photons to a characteristic energy $E_\gamma \simeq (3\pi/8)\alpha^{-1}m_e c^2$, where $\alpha = \frac{1}{137}$ is the fine structure constant. Such a photon is immediately converted to an e^\pm pair in the magnetic field, and the created pairs emit a synchrotron spectrum consistent with the observed 20-100 keV emission.

8.4.2. 2-10 keV Emission

A promising emission mechanism for the observed soft X-ray tail of the blackbody component is resonant upscattering of keV photons (blackbody surface radiation) by the current-carrying particles in the magnetosphere (TLK). This scattering occurs over a continuum of frequencies, with an optical depth ~ 1 . Electrons (and positrons) resonantly scatter the blackbody photons at a distance $r_{\text{res}} = 180 (B_{\text{pole},15} R_{\text{NS},6})^{1/3} (\hbar\omega/1 \text{ keV})^{-1/3}$ km from a neutron star with a polar magnetic field B_{pole} . Both electrons and positrons feel a strong drag force in this region (Thompson & Beloborodov 2005). The emergent X-ray spectrum and pulse profile are established in this outer zone.

Ions flowing through the inner magnetosphere can also upscatter the thermal X-rays emitted from the surface. The ions are mildly relativistic and their cyclotron resonance near the star is $6B_{15}$ keV – just in the 2 – 10 keV band. On the other hand, the ion current may be suppressed (see Fig. 10), which would make the scattering optical depth small. The ion density in the magnetosphere is expected to be much higher during the first $10^3 - 10^5$ seconds following an SGR flare. Then the X-ray luminosity from the temporarily heated surface of the star exceeds the Eddington luminosity at the ion-cyclotron resonance and lifts ions from the surface (e.g. Ibrahim et al. 2001). We defer a detailed study of X-ray upscattering in the corona to a future work.

8.4.3. Optical and Infrared Emission

The observed infrared (K -band) and optical luminosities of magnetars are $\sim 10^{32}$ erg/s (Hulleman et al. 2004), which is far above the Rayleigh-Jeans tail of the surface blackbody radiation. The inferred brightness temperature is $\sim 10^{13}$ K if the radiation is emitted from the surface of the

star. Three principle emission mechanisms may then be considered.

1. Coherent plasma emission. Eichler, Gedalin, & Lyubarsky (2002) proposed that the optical emission is generated as O-mode radiation at a frequency $2\omega_{Pe}$. Such a mechanism would have to work inside the atmospheric layer where density is high enough that $2\omega_{Pe}$ lies in the optical band (the plasma frequency in the corona is 2 orders of magnitude lower). The plasma frequency in a hydrostatic layer of temperature $T_e = \theta_e(m_e c^2/k_B)$ and Thomson depth τ_T is $\hbar\omega_{Pe} = 0.65 (\tau_T/\theta_e)^{1/2} g_{14}^{1/2}$ eV. A potential difficulty with this mechanism is that the brightness temperature of the low-frequency O-mode photons is limited to a value $k_B T_b \sim m_e c^2/\tau_T$ by induced scattering in the higher layers of the transition layer (where n_e is lower and the radiation lies significantly above the local plasma frequency). The corresponding upper limit for K-band luminosity is

$$\omega L_\omega = \frac{k_B T_b \omega^3}{8\pi^2 c^2} 4\pi R_{NS}^2 = 8 \times 10^{29} \left[\frac{k_B T_b(\omega)}{10 m_e c^2} \right] \left(\frac{\omega}{\omega_{K\text{-band}}} \right)^3 \text{ erg s}^{-1}. \quad (97)$$

This may be in conflict with the observed flux in 4U 0142+61 (Hulleman et al. 2004). Note also that the low-frequency tail of the plasma emission from the transition layer may also be upscattered into the optical-IR range by relativistic electrons with Lorentz factors $\gamma_e \gtrsim 10$.

2. Non-thermal synchrotron emission from electrons with high γ_e . This mechanism could work only far from the star, $r \gtrsim 200 R_{NS} \gamma_e^{2/3}$, where the minimum energy of the synchrotron photons, $\sim \gamma_e^2 \hbar e B / m_e c$, is below the optical band ($B < 10^8 \gamma_e^{-2}$ G). The magnetic lines extending to large r form a small cap on the stellar surface and carry a tiny fraction of the total magnetospheric current, $f \sim (r/R_{NS})^{-2} \sim 3 \times 10^{-5} \gamma_e^{-4/3}$. If the voltage maintained along the extended lines is comparable to 1 GeV, energy dissipation rate in the region is only $10^{30} \gamma_e^{-4/3} \text{ erg s}^{-1}$, orders of magnitude smaller than the observed optical-IR luminosity. Therefore this mechanism appears to be unlikely.
3. Ion cyclotron emission from radii $\sim 20 R_{NS}$, where the ion cyclotron frequency is in the optical band. The observed flux then implies ion temperatures of $\sim 10^{11}$ K. Such temperatures are indeed achieved in the corona as we discussed above. This mechanism also requires a sufficient number of ions in the corona. Our results show that the ion population is sensitive to the ratio of voltage $e\Phi_e$ to the ion gravitational energy (Fig. 10). The ion population is suppressed if this ratio is below unity — then pairs strongly dominate the corona. The detailed analysis of electric circuit on extended field lines and cyclotron emission is deferred to a future work.

The ions will act as a filter for the radio and microwave radiation that is emitted just above the star. The radiation reaching $r \gtrsim 50 R_{NS}$ will be partially absorbed by the ions at their cyclotron resonance. The perpendicular energy of the heated ions increases as they approach the star, due to the standard mirroring effect. Their cyclotron cooling and transit times are comparable at a radius $\sim 200 (v_i/c)^{-1/5} R_{NS,6}^{6/5} B_{\text{pole},15}^{2/5} \text{ km}$, where the cyclotron energy of the ions is $\simeq 0.5 B_{\text{pole},15}^{-1/5} (v_i/c)^{3/5} R_{NS,6}^{-3/5} \text{ eV}$, in the optical-IR range.

4. Curvature emission by pairs in the inner magnetosphere can extend into the optical-IR range. Charges moving on field lines with a curvature radius $R_C \lesssim R_{\text{NS}}$ will emit radiation with frequency

$$\nu_C \sim \gamma_e^3 \frac{c}{2\pi R_C}, \quad (98)$$

which is in the K-band ($\nu = 10^{14}$ Hz) or optical when $\gamma_e m_e c^2 \gtrsim \text{GeV}$. As in models of pulsar radio emission, bunching of the radiating charges is required to produce the observed luminosity. This bunching can be a result of soliton formation in the 1-D plasma (e.g. Asseo, Pelletier, & Sol 1990). The radio luminosity of a normal pulsar can approach $\sim 10^{-2}$ of its spindown power, and it is not implausible that the observed fraction $\sim 10^{-4}$ of the power dissipated in the corona of a magnetar is radiated in optical-IR photons by the same coherent mechanism.

There are indications of charge bunching on the Debye scale in our numerical experiment. Although this detail of the experiment is difficult to scale to the real corona of magnetars, it supports the possibility of coherent curvature radiation. Suppose a fraction f of the net flow of particles through the corona $\dot{N}_e = I/e \sim 10^{39} L_{\text{diss}36} (e\Phi_e/\text{GeV})^{-1} \text{ s}^{-1}$ is carried by bunches of \mathcal{N} electrons (or positrons). The power emitted by one bunch is $\dot{E} = (2/3)(\mathcal{N}e)^2 \gamma_e^4 c/R_C^2$, and the total coherent luminosity produced by the corona is given by

$$L \approx f \mathcal{N} \dot{N}_e \frac{e^2}{R_C} \gamma_e^4. \quad (99)$$

Using the relation $\nu_C \sim (c/2\pi R_C) \gamma_e^3$ for curvature radiation, we find the number of charges per bunch that is required to explain the observed luminosity $L \sim 10^{32} \text{ erg s}^{-1}$,

$$\mathcal{N} \sim 10^4 f^{-1} L_{32} \nu_{C,14}^{-4/3}. \quad (100)$$

This is much smaller than the number of charges per Debye sphere, $\mathcal{N}_D \sim (n_e r_e^3)^{-1/2} \sim 10^{11}$, which sets a scale for the maximum possible \mathcal{N} . Thus, a very weak bunching of charges can generate a significant power in coherent curvature radiation in the magnetar corona. This level of bunching is very small compared with what is needed to explain the radio emission of radio pulsars.

For example, one can compare with the Crab pulsar. The total flux of e^\pm pairs from the pulsar, $\dot{N}_e \sim 10^{39} \text{ s}^{-1}$, is comparable to the flux in a magnetar corona. The pulsar e^\pm flow is concentrated on the open field lines, and its density is enhanced by a factor $R_{\text{lc}}/R_{\text{NS}} \sim 10^2$. The curvature radius of the open field lines near the star is $R_C \sim 10 R_{\text{NS}}$. These differences are, however, modest compared with the much larger bunching efficiency that is implied by the observed brightness of the radio emission from the Crab pulsar. Supplying its luminosity $L \sim 10^{31} \text{ erg s}^{-1}$ at $\nu \sim 10^8 \text{ Hz}$ would require $\gamma_e \sim 60$ and $\mathcal{N} \sim 10^{11} f^{-1}$.

The dispersion relation for the IR-optical radiation in the corona becomes dominated by plasma rather than by vacuum polarization in the ultra-strong magnetic field. The curvature radiation

is, generally, a superposition of all possible polarization modes (see Arons & Barnard 1986 for a detailed description of the normal modes of a strongly magnetized plasma). Emission of the superluminal O-mode will occur if the bunch size (measured in its rest frame) is smaller than the plasma skin depth. The O-mode photons are most susceptible to stimulated downscattering in frequency by the e^\pm . This process is described by an optical depth $\tau_{\text{ind}} = \tau(kT'_b/m_e c^2)$ (e.g. Levich & Sunyaev 1970), where τ is the optical depth to spontaneous Compton scattering and $T'_b = T_b \gamma_e$ is the brightness temperature in the rest frame of the scattering e^\pm . The O-mode photons avoid Bose-condensation if $\tau_{\text{ind}} < 1$. Using $\tau = \tau_c/\gamma_e^2$ (see § 8.4.1), we find $\tau_{\text{ind}} = \tau_c(kT'_b/m_e c^2)\gamma_e^{-1}$, so T_b is bounded by $kT_b < \gamma_e m_e c^2/\tau_c$. With $\gamma_e \sim 10^3$ and $\tau_c \sim 0.01 - 0.1$ expected in the corona, this upper limit is consistent with the observed infrared and optical luminosity of magnetars. The E-mode also comprises a fraction of the curvature emission when the magnetic field lines are twisted (Luo & Melrose 1995). Its stimulated scattering is negligible because the cross section of spontaneous scattering of E-mode photons of frequency ν is suppressed compared to σ_T by a factor $\sim (2\pi\gamma_e\nu m_e c/eB)^2 \sim 10^{-8} B_{15}^{-2} \gamma_{e3}^2 (h\nu/\text{eV})^2$. Finally, curvature emission in the subluminal Alfvén mode is possible, but this mode is ducted along the magnetic field lines and has a frequency below the ambient plasma frequency (Arons & Barnard 1986).

Note that the spectrum of curvature emission is expected to cut off at frequencies above ν_C that corresponds to the maximum Lorentz factor (a few γ_{res}) of e^\pm in the corona. This cutoff may be observable in the optical or infrared band (cf. Hulleman et al. 2004).

8.5. Evolution Following Bursts of Activity

Bursts of magnetar activity are associated with starquakes — sudden crust deformations that release the internal magnetic helicity of the star and impart an additional twist to the magnetosphere. The increased twist causes observable changes.

The increase of the twist should lead to a larger luminosity from the corona since the luminosity is simply proportional to the net current flowing through the magnetosphere. Between bursts, the magnetospheric currents persistently dissipate and the corona disappears after the time t_{decay} (eqs. [94] and [95]). If there were no bursts during a long time $t > t_{\text{decay}}$ the magnetar should enter the quiescent state with no coronal emission. The soft X-ray emission has been observed to decay on a timescale of a few years (e.g. Gotthelf & Halpern 2005). The decay of the high-energy component would be especially important to study since it probes directly the postburst evolution of the corona.

During periods of high activity, when bursts occur frequently, the growth of the twist may be faster than its decay. The twist may grow to the point of a global instability. When the magnetic lines achieve a twist angle $\Delta\phi \gtrsim 1$ the magnetosphere becomes unstable and relaxes to a smaller twist angle. A huge release of energy must then occur, producing a giant flare. It is possible that the 27 December 2004 giant flare from SGR 1806-20 was produced in this way — a prolonged

period of unusually high activity preceded the flare. If the flare indeed released the external twist energy, then the current through the magnetosphere should have decreased after the flare, and the coronal luminosity now should be smaller than it was prior to the flare. See Lyutikov (2005) for a recent critical discussion of the location of the trigger in SGR flares.

A possible way to probe the twist evolution is to measure the history of spindown rate \dot{P} of the magnetar. The existing data confirm the theoretical expectations: the spin-down of SGRs was observed to accelerate months to years following periods of activity (Kouveliotou et al. 1998, 1999; Woods et al. 2002). A similar effect was also observed following more gradual, sub-Eddington flux enhancement in Anomalous X-ray Pulsars (Gavriil & Kaspi 2004). This “hysteresis” behavior of the spindown rate probably represents the delay with which magnetic helicity is redistributed from the inner to outer closed magnetic field lines.

Since the density of the plasma corona is proportional to the current that flows through it, changes in the twist also lead to changes in the coronal opacity. The opacity should increase following bursts of activity and affect the X-ray pulse profile and spectrum. Such changes, which persist for months to years, have been observed following large X-ray outbursts from two SGRs (Woods et al. 2001a).

8.6. Further Developments

1. We focused in this paper on the inner magnetosphere, that is, on field lines that do not extend beyond a radius $R_{\max} \sim 2R_{\text{NS}}$. This portion of the magnetosphere is expected to retain most of the toroidal field energy, and to dominate the non-thermal output of the star. The study of the outer region may, however, reveal some qualitative differences in the circuit behavior because plasma in the outer region is subject to strong “cyclotron drag.” The X-rays emitted from the stellar surface and transition layer must interact strongly with electrons and positrons at a radius of $\sim 30 - 100$ km. The resonant frequency $eB/m_e c$ at such radii falls into the X-ray band and e^\pm may be decelerated to $\gamma_e \simeq \gamma_{\text{res}} \sim 1$. This drag will cause a local change of the electric field in the circuit (TLK; Thompson & Beloborodov 2005). At yet larger radii, beyond ~ 200 km from the star, ions may populate higher Landau levels $n > 0$. Then a new degree of freedom appears in the problem: the transverse motion of the ions.

2. Like the solar transition region, the transition layer at the base of a magnetar corona may respond to the coronal dissipation by increasing the supply of plasma. In particular, pair creation in the transition layer needs further investigation because pairs may feed the coronal current (§ 6.4). The state of this layer and its effect on the corona is determined by the level of plasma turbulence (see §§ 6.2 and 6.3). This layer may partially insulate the star from the hot corona because plasma turbulence suppresses thermal conduction. By trapping the generated heat, the layer may overheat and expand to the corona.

3. The transition layer also plays a crucial role in the energy balance of the corona because

it produces radiation that can escape the magnetar. A significant part of the released energy is emitted in the hard X-ray band. The rest of the released energy is deposited in an optically thick surface layer and reprocessed into blackbody radiation with $k_B T \lesssim 1$ keV. An accurate calculation of the ratio of the two emission components (hard X-ray to blackbody) that are fed by the corona remains to be done.

4. The role of transverse waves in the corona, which were suppressed in our numerical experiment, will need to be studied. The waves produce a three-dimensional pattern of magnetic-field fluctuations $\delta(\nabla \times B) \neq 0$ and their study will require a 3-D (or at least 2-D) simulations.

5. Our plasma model of the corona may be generalized to include the effects of rotation. This can be done by changing the neutrality condition $\rho = 0$ to $\rho = \rho_{co}$. Note that ρ_{co} may be easily maintained by a small polarization of the current-carrying plasma because $\rho_{co} \ll en_c$ (see eq. [2]). The rotation can be taken into account by adding an extra source term $4\pi\rho_{co}$ to the Poisson equation (cf. eq. 24),

$$\frac{dE_{\parallel}}{dl} = 4\pi(\rho - \rho_{co}). \quad (101)$$

Then E_{\parallel} vanishes if $\rho = \rho_{co}$ along the magnetic line, so that ρ_{co} is the new equilibrium charge density.

6. It is important to understand the resistive redistribution of the twist in the magnetosphere, in particular its spreading toward the open field lines, because it is a promising source of torque variability in active magnetars (TLK). This would require the construction of a global, time-dependent model of the currents in the magnetosphere.

We thank A. Frolov, P. Goldreich, A. Gruzinov, M. Medvedev, and M. Ruderman for discussions. AMB is supported by NASA ATP and an Alfred P. Sloan Fellowship. CT is supported by the Natural Sciences and Engineering Research Council of Canada.

REFERENCES

- Adler, S. L., Bahcall, J. N., Callan, C. G., & Rosenbluth, M. N. 1970, *Phys. Rev. Lett.*, 25, 1061
- Arons, J., & Barnard, J. J. 1986, *ApJ*, 302, 120
- Arras, P., Cumming, A., & Thompson, C. 2004, *ApJ*, 608, L49
- Asseo, E., Pelletier, G., & Sol, H. 1990, *MNRAS*, 247, 529
- Bak, P., Tang, C., & Wiesenfeld, K. 1987, *Phys. Rev. Lett.*, 59, 381
- Baring, M. G. 2000, *Phys. Rev. D*, 62, 016003
- Baring, M. G., & Harding, A. K. 2001, *ApJ*, 547, 929
- Beloborodov, A. M. 2002, *ApJ*, 566, L85
- Berestetskii, V. B., Lifshitz, E. M., & Pitaevskii, L. P. 1982, *Quantum Electrodynamics*, Oxford: Pergamon Press.
- Bernstein, I. & Kulsrud, R. M. 1961, *Phys. Fluids*, 4, 1037
- Block, L. P. 1978, *Ap&SS*, 55, 59
- Braithwaite, J., & Spruit, H. C. 2004, *Nature*, 431, 819
- Braithwaite, J., & Spruit, H. C. 2006, *A&A*, in press ([astro-ph/0510287](#))
- Canuto, V., Lodenguai, J., & Ruderman, M. 1971, *Phys. Rev. D*, 3, 2303
- Carlqvist, P. 1982, *Ap&SS*, 87, 21
- Chang, P., Arras, P., & Bildsten, L. 2004, *ApJ*, 616, L147
- Cheng, B., Epstein, R. I., Guyer, R. A., & Young, C. 1996, *Nature*, 382, 518
- Daugherty, J. K., & Harding, A. K. 1983, *ApJ*, 273, 761
- De Luca, A., Caraveo, P. A., Mereghetti, S., Negroni, M., & Bignami, G. F. 2005, *ApJ*, 623, 1051
- den Hartog, P. R., Hermsen, W., Kuiper, L., Vink, J., in 't Zand, J. J. M., & Collmar, W. 2006, *A&A*, in press ([astro-ph/0601644](#))
- Diamond, P. H., & Malkov, M. 2003, *Physics of Plasmas*, 10, 2322
- Dietrich, S. S., & Berman, B. L. 1988, *Atomic Data and Nuclear Data Tables*, 38, 199
- Eichler, D., Gedalin, M., & Lyubarsky, Y. 2002, *ApJ*, 578, L121

- Gavriil, F. P., & Kaspi, V. M. 2004, *ApJ*, 609, L67
- Godfrey, B. B., Shanahan, W. R., & Thode, L. E. 1975, *Physics of Fluids*, 18, 346
- Göğüş, E., Kouveliotou, C., Woods, P. M., Thompson, C., Duncan, R. C., & Briggs, M. S. 2001, *ApJ*, 558, 2
- Goldreich, P., & Julian, W. H. 1969, *ApJ*, 157, 869
- Gotthelf, E. V., & Halpern, J. P. 2005, *ApJ*, 632, 1075
- Harding, A. K., & Muslimov, A. G. 2002, *ApJ*, 568, 862
- Hibschman, J. A., & Arons, J. 2001, *ApJ*, 554, 624
- Herold, H. 1979, *Phys. Rev. D*, 19, 2868
- Hulleman, F., van Kerkwijk, M. H., & Kulkarni, S. R. 2004, *A&A*, 416, 1037
- Hurley, K., et al. 2005, *Nature*, 434, 1098
- Ibrahim, A. I., et al. 2001, *ApJ*, 558, 237
- Kaspi, V. M., Gavriil, F. P., Woods, P. M., Jensen, J. B., Roberts, M. S. E., & Chakrabarty, D. 2003, *ApJ*, 588, L93
- Kotov, Y. D., & Kelner, S. R. 1985, *Sov. Astron. Lett.*, 11, 392
- Kouveliotou, C., et al. 1998, *Nature*, 393, 235
- Kouveliotou, C., et al. 1999, *ApJ*, 510, L115
- Kuiper, L., Hermsen, W., & Mendez, M. 2004, *ApJ*, 613, 1173
- Lai, D. 2001, *Reviews of Modern Physics*, 73, 629
- Landau, L. D., & Lifshitz, E. M. 1975, *Classical Theory of Fields*, Oxford: Pergamon Press.
- Langmuir, I., 1929, *Phys. Rev.*, 33, 954
- Levich, E. V., & Sunyaev, R. A. 1970, *Astrophys. Lett.*, 7, 69
- Lieb, E. H., Solovej, J. P., & Yngvason, J. 1992, *Phys. Rev. Lett.*, 69, 749
- Luo, Q., & Melrose, D. B. 1995, *MNRAS*, 276, 372
- Lyutikov, M., 2005, preprint ([astro-ph/0511711](#))
- Marsden, D., & White, N. E. 2001, *ApJ*, 551, L155

- Mereghetti, S., Götz, D., Mirabel, I. F., & Hurley, K. 2005, *A&A*, 433, L9
- Molkov, S., Hurley, K., Sunyaev, R., Shtykovsky, P., Revnivtsev, M., & Kouveliotou, C. 2005, *A&A*, 433, L13
- Neuhauser, D., Koonin, S. E., & Langanke, K. 1987, *Phys. Rev. A*, 36, 4163
- Parker, E. N. 1979, Oxford, Clarendon Press; New York, Oxford University Press, 1979, 858 p.
- Potekhin, A. Y., Yakovlev, D. G., Chabrier, G., & Gnedin, O. Y. 2003, *ApJ*, 594, 404
- Raadu, M. A. 1989, *Phys. Rep.*, 178, 25
- Ruderman, M. A., & Sutherland, P. G. 1975, *ApJ*, 196, 51
- Tang, X. Z., & Boozer, A. H. 2005, *Physical Review Letters*, 94, 225004
- Taylor, J. B. 1986, *Reviews of Modern Physics*, 58, 741
- Thompson, C., & Beloborodov, A. M. 2005, *ApJ*, 634, 565
- Thompson, C., & Duncan, R. C. 1996, *ApJ*, 473, 322
- Thompson, C., & Duncan, R. C. 2001, *ApJ*, 561, 980
- Thompson, C., Duncan, R. C., Woods, P. M., Kouveliotou, C., Finger, M. H., & van Paradijs, J. 2000, *ApJ*, 543, 340
- Thompson, C., Lyutikov, M., & Kulkarni, S. R. 2002, *ApJ*, 574, 332
- Woods, P. M., Kouveliotou, C., Göğüş, E., Finger, M. H., Swank, J., Smith, D. A., Hurley, K., & Thompson, C. 2001, *ApJ*, 552, 748
- Woods, P. M., Kouveliotou, C., Göğüş, E., Finger, M. H., Swank, J., Markwardt, C. B., Hurley, K., & van der Klis, M. 2002, *ApJ*, 576, 381
- Walsh, R. W., & Ireland, J. 2003, *Astron. Astrophys. Rev.*, 12, 1
- Woods, P. M., & Thompson, C. 2006, in “Compact Stellar X-ray Sources,” eds. W. H. G. Lewin and M. van der Klis, Cambridge University Press, astro-ph/0406133
- Zavlin, V. E., & Pavlov, G. G. 2002, *Neutron Stars, Pulsars, and Supernova Remnants*, 263

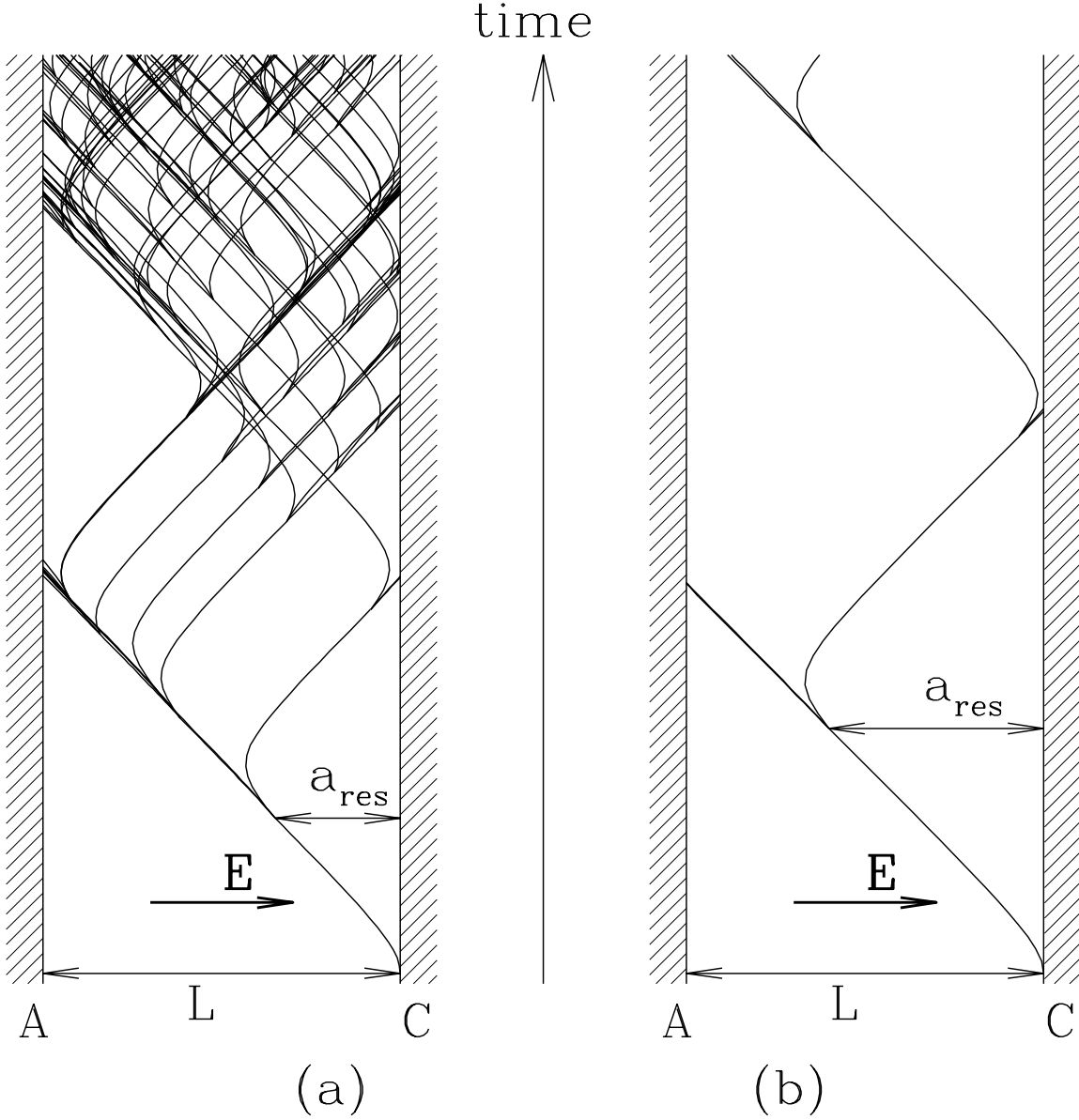


Fig. 5.— Spacetime diagrams illustrating the critical character of the e^\pm breakdown and formation of avalanches. The toy model used in this illustration is described in the text; $e\Phi_e = eEL = 11m_e c^2$ is assumed. The figure shows worldlines of particles (starting with one seed electron at cathode). (a) $a_{\text{res}}/L = 0.35$ (supercritical case). (b) $a_{\text{res}}/L = 0.6$ (critical case).

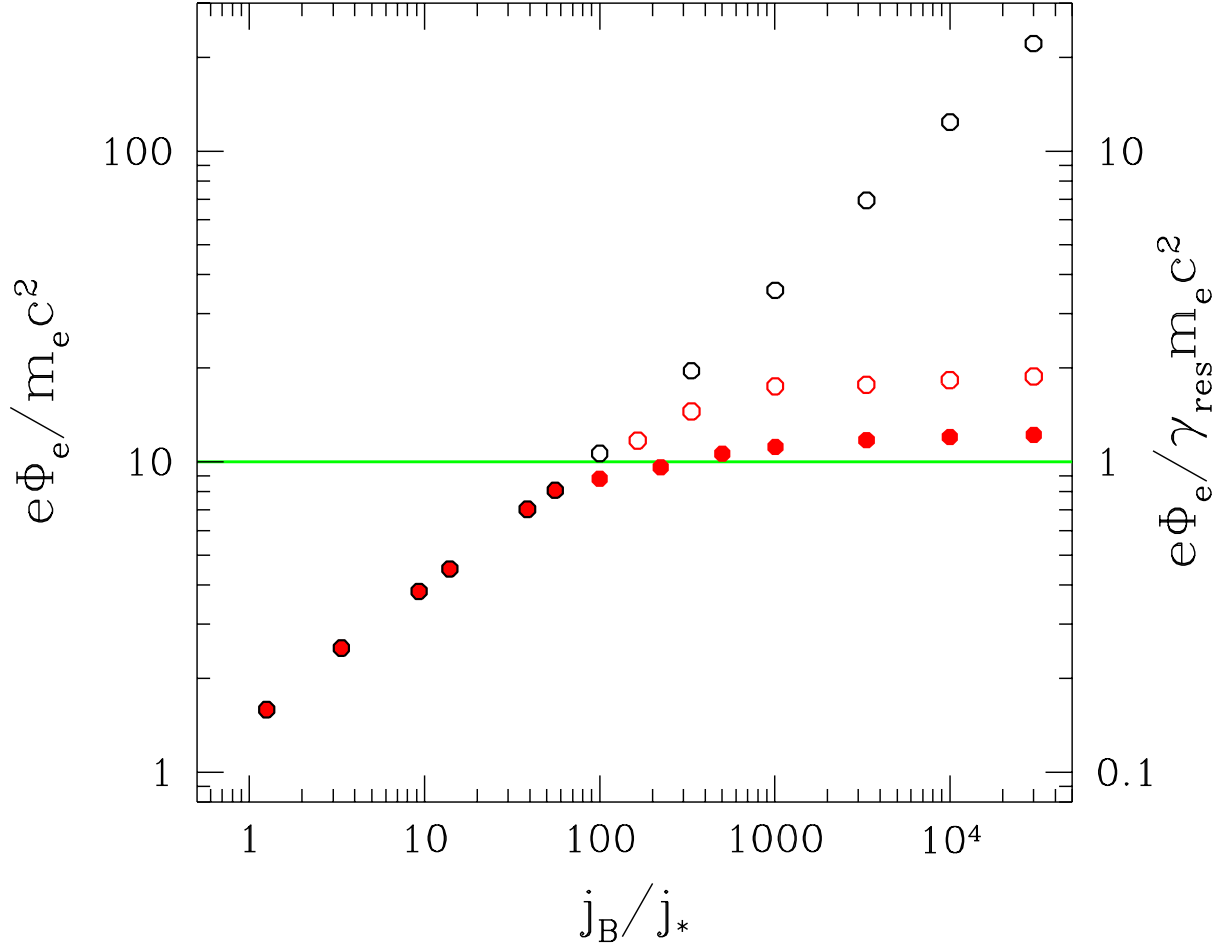


Fig. 6.— Voltage vs. current for circuits with (red circles) and without (black circles) e^\pm creation. Model A of pair production is represented by filled red circles and Model B by open red circles; both models have the resonant Lorentz factor $\gamma_{\text{res}} = 10$. Each point in the figure represents the result of one experiment and shows the time-averaged voltage Φ_e . The current is expressed in units of j_* (see the text).

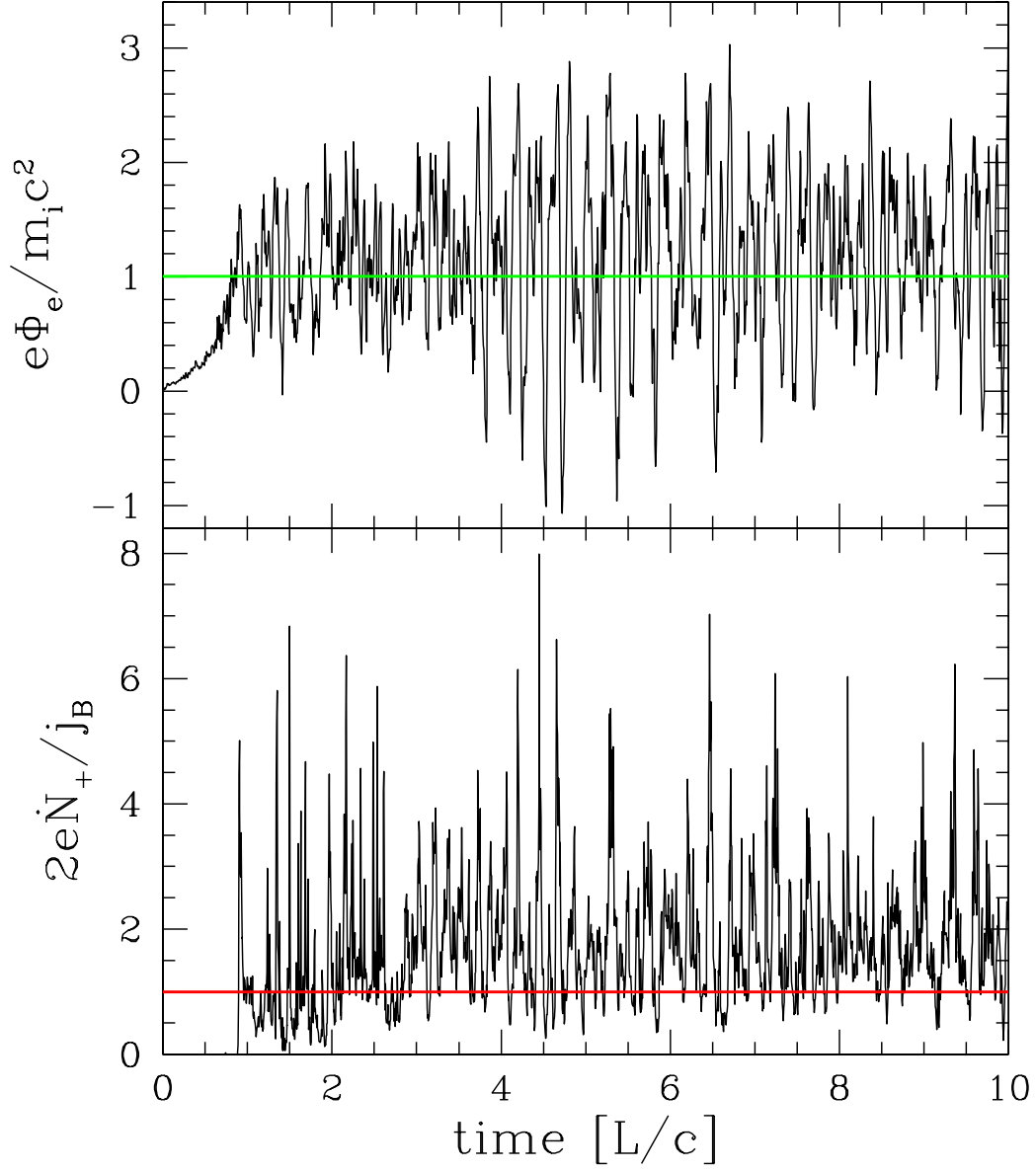


Fig. 7.— Relaxation of the circuit during the first 10 light-crossing times. The circuit parameters are: $m_i = 10m_e$, $j = 10^4 j_*$, $\gamma_{\text{res}} = m_i/m_e$. Model A is used for pair production (infinite window above γ_{res} with free path $l = 0$). A quasi-steady fluctuating state is established after a few L/c .

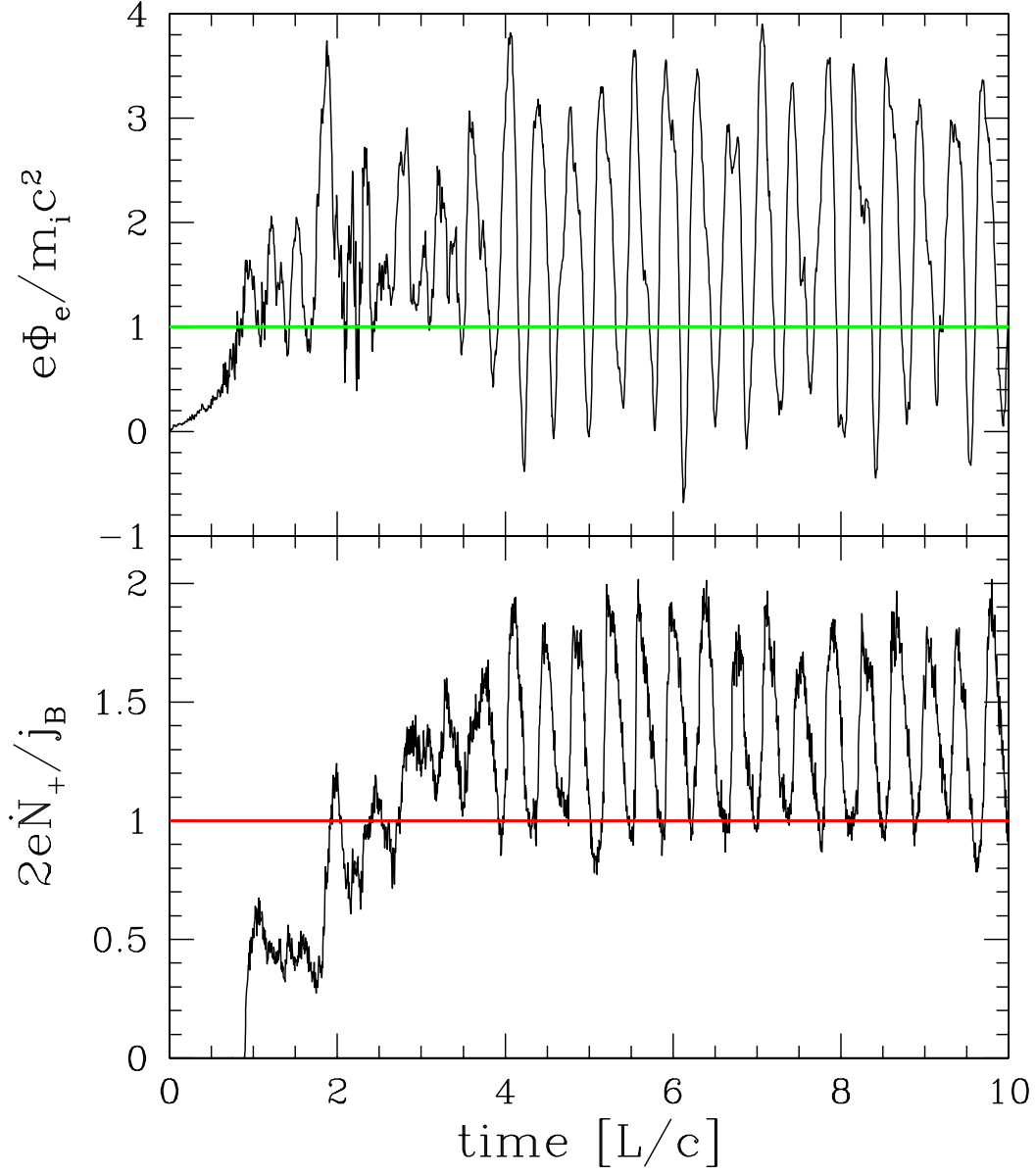


Fig. 8.— Same as Fig. 7, but Model B is used for pair production: narrow window $\gamma_{\text{res}} < \gamma_e < 2\gamma_{\text{res}}$ with free path $l = L/3$.

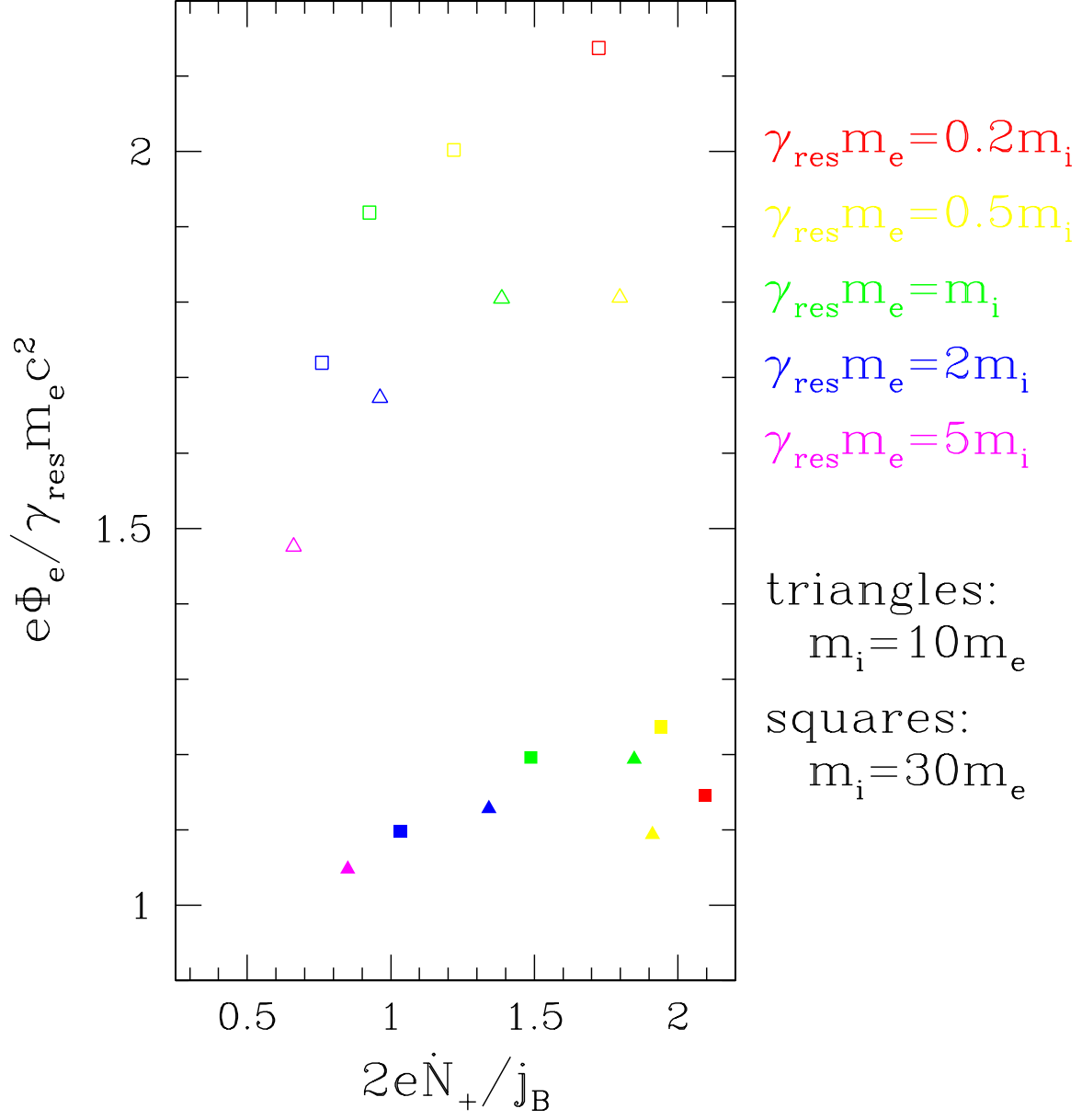


Fig. 9.— Circuits with $m_i/m_e = 10, 30$ and various values of γ_{res} ranging from $m_i/5m_e$ to $5m_i/m_e$. Here $\bar{\Phi}_e$ is the time-averaged voltage and $2\dot{N}_+$ is the time-averaged rate of e^\pm creation in the circuit. Model A of pair production is shown by open symbols, and Model B by filled symbols.

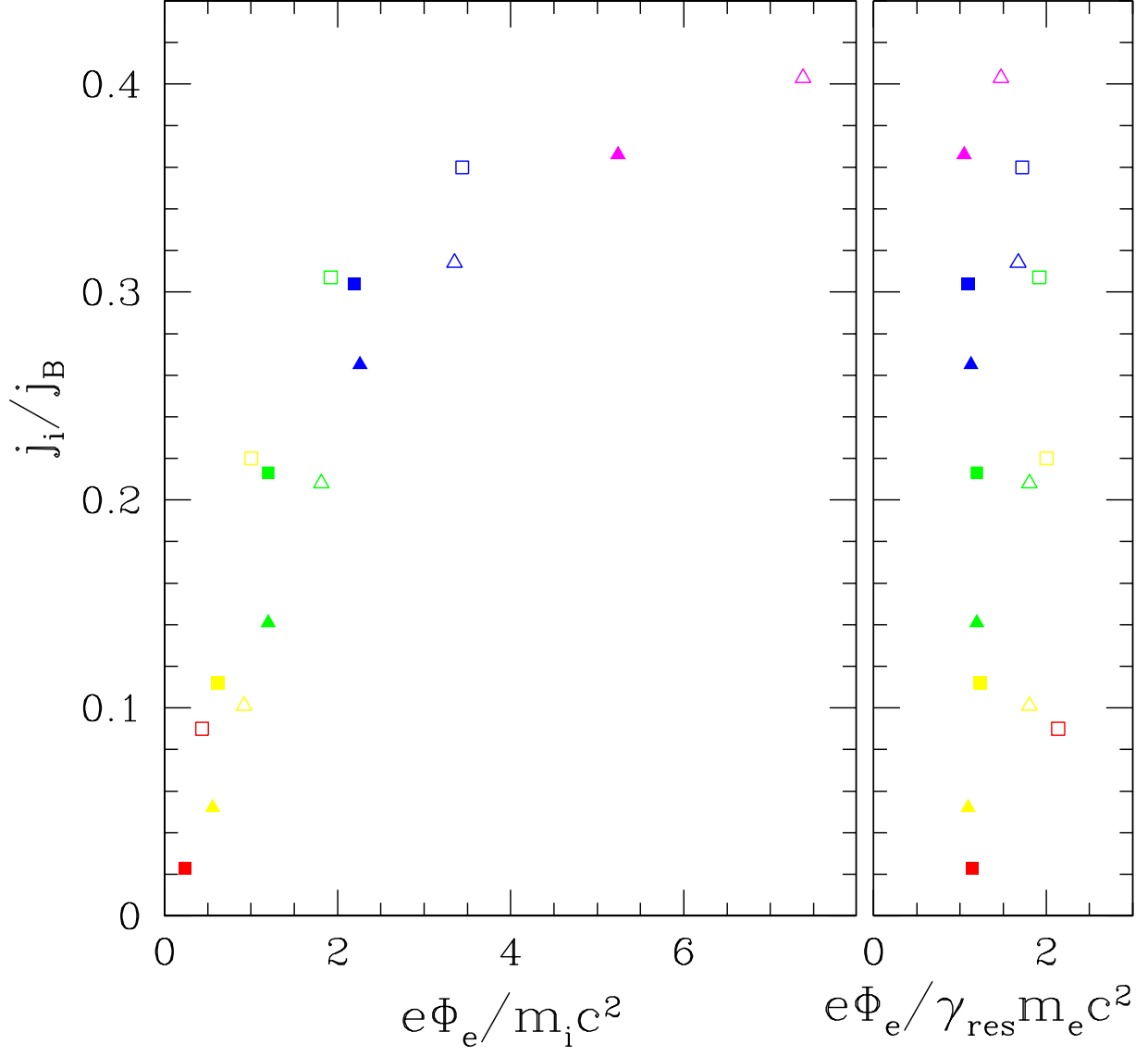


Fig. 10.— Fraction of the electric current carried by ions vs. voltage, for the same set of models as in Fig. 9. Colors have the same meanings. In the left panel voltage is taken in units of $m_i c^2$, and in the right panel in units of $\gamma_{res} m_e c^2$.

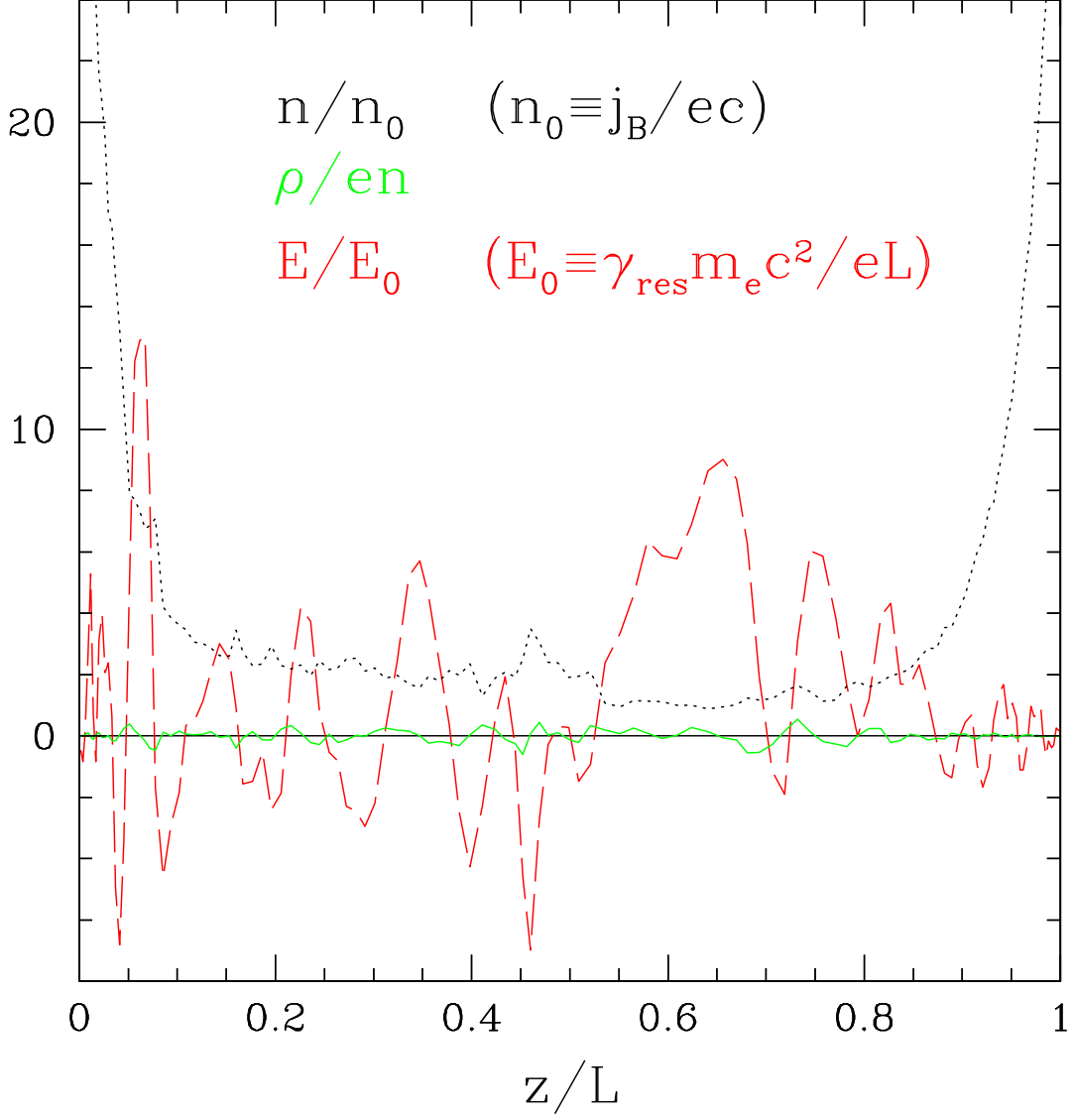


Fig. 11.— Snapshot of the circuit with $\gamma_{res} = m_i/m_e = 10$ and $j_B = 10^4 j_*$ ($\lambda_D/L = 10^{-2}$). Model A is assumed for e^\pm creation. The three curves show particle density $n = n_i + n_e + n_p$ (dotted), charge density $\rho = e(n_i - n_e + n_p)$ (solid), and electric field E (long-dash).

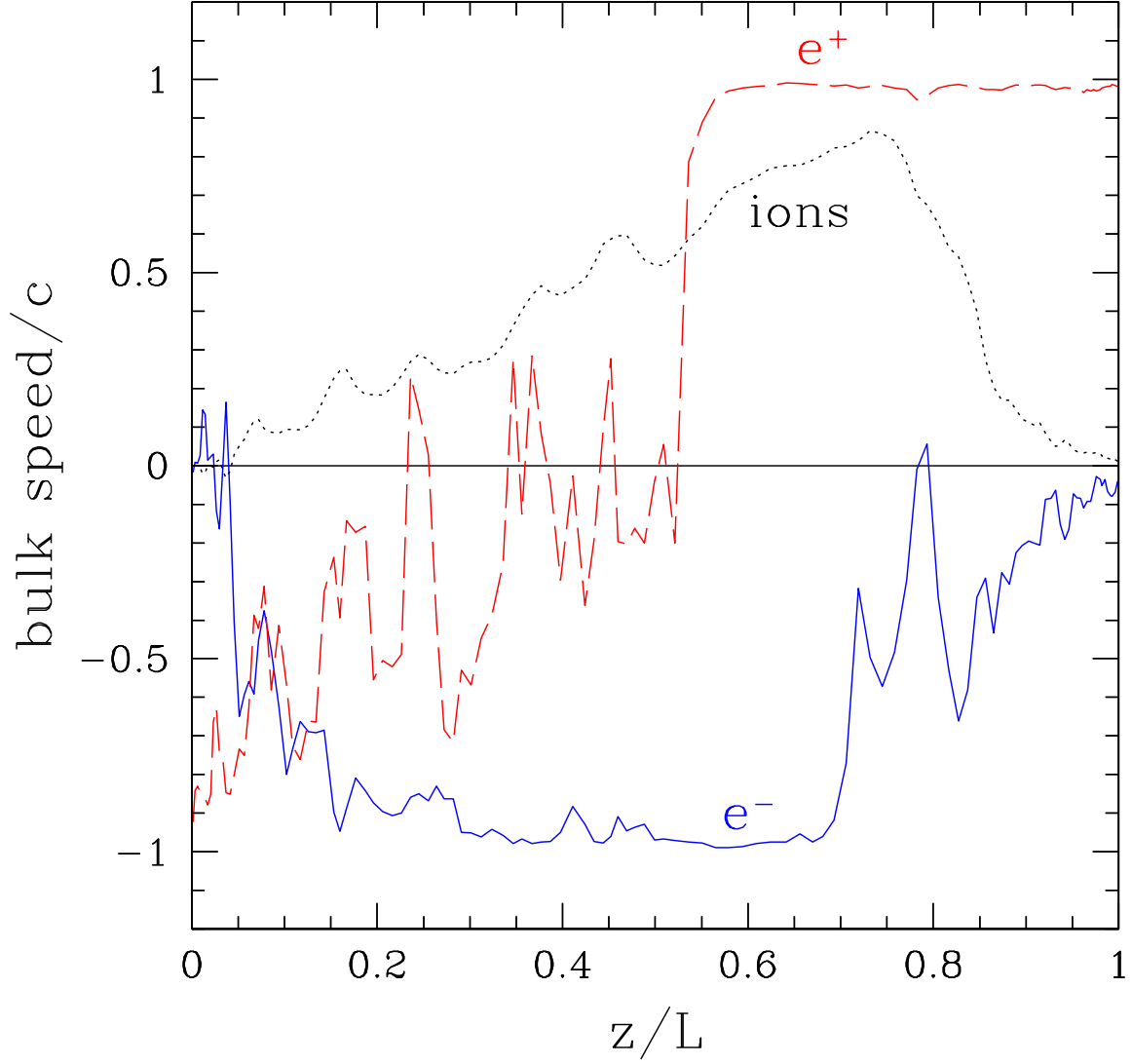


Fig. 12.— Mean velocities of ions, electrons, and positrons as a function of position in the circuit. The mean velocities v_X are related to densities n_X of the three species $X = i, e, p$ by $v_X = j_X / \bar{v}_x$ where j_X is the current carried by species X . The snapshot is taken of the same model and the same time as Fig. 11.

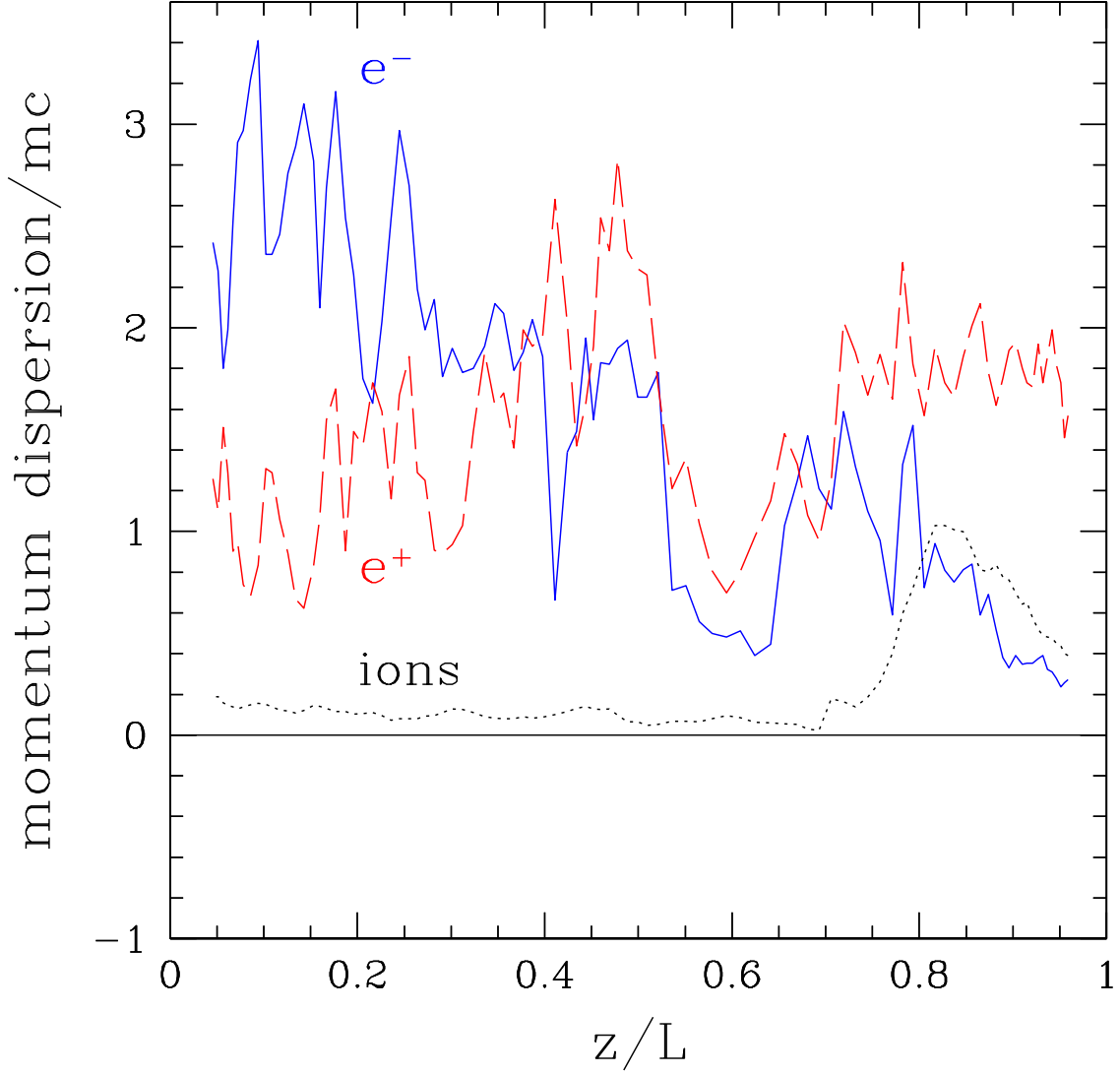


Fig. 13.— Dispersion of momentum (around the mean bulk momentum) for ions, electrons, and positrons as a function of position in the circuit. The snapshot is taken of the same model at the same time as in Fig. 11. Only the corona is shown ($h < z < L - h$) and the surface layers of height $h = 0.04L$ are excluded from the figure.

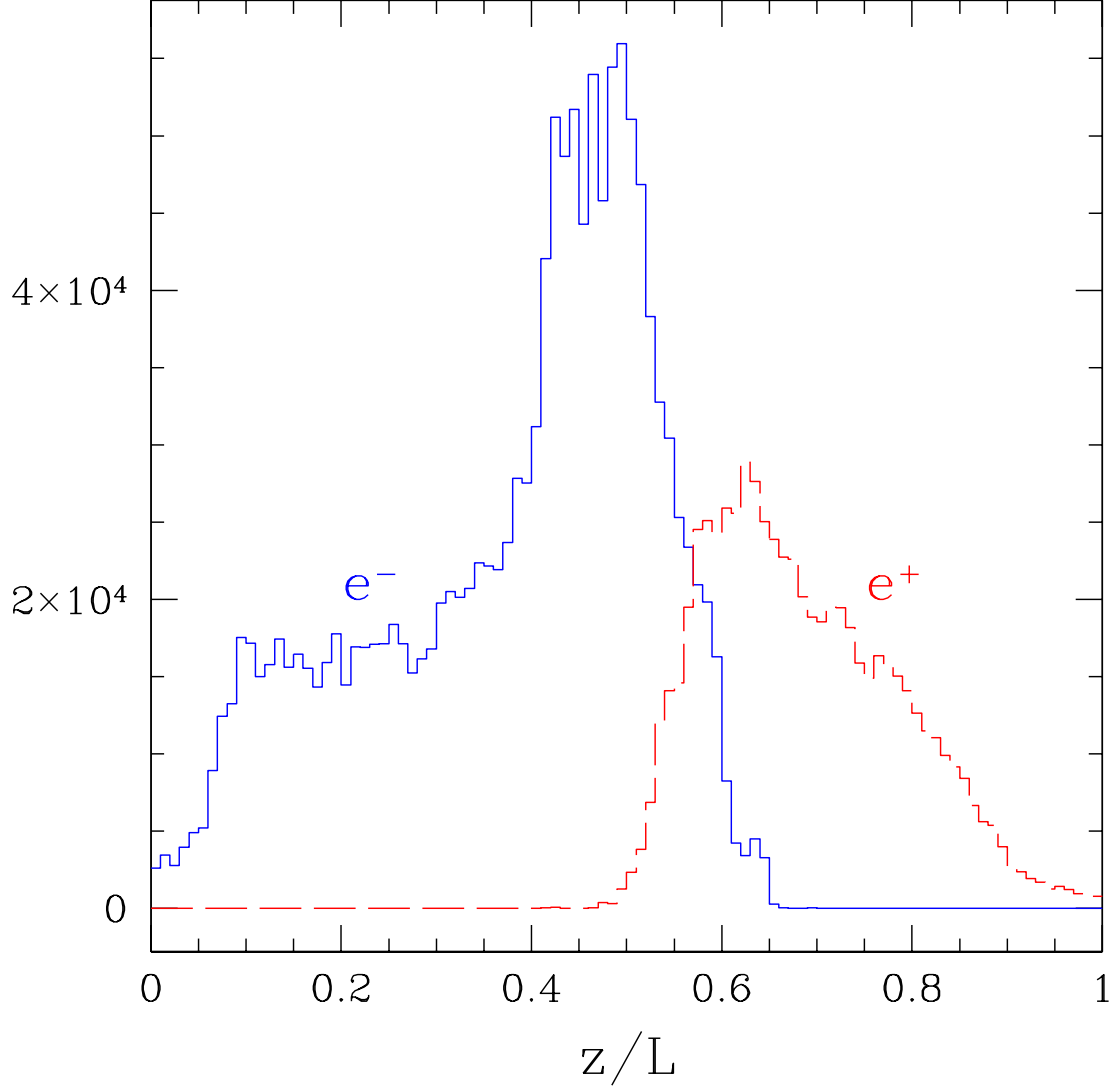


Fig. 14.— Distribution of pair-creation events at $10 < ct/L < 20$ over z . The circuit model is the same as in Figs. 7 and 11-13. The figure shows separately pair creation by accelerated e^- and e^+ (solid and long-dashed curves, respectively).